

**Universität  
Rostock**



Traditio et Innovatio

# **Efficient DFT-Based Calculation of Exciton Coupling in Molecular Aggregates**

**Master-Arbeit**

**von Per-Arno Plötz, geb. am 24. August 1986 in Eutin**

**Betreuer und 1. Prüfer : Prof. Dr. O. Kühn, Universität Rostock**

**2. Prüfer: Dr. S. Bokarev, Universität Rostock**

**Rostock, den 26. August 2013**

- redaktionell überarbeitete Fassung -



## Abstract

Calculating the energies of and the couplings between electronic transitions on aggregated molecules is the problem being faced when simulating excitation energy transfers in nanomaterials like artificial and natural light harvesting systems. A method is developed to calculate the parameters of the Frenkel exciton Hamiltonian with high efficiency using time-dependent density functional based tight-binding (TD-DFTB). In this vein it is possible to describe the electronic structure of the monomers and the exciton coupling in the aggregate in a consistent way by defining the transition densities in a TD-DFTB manner. This overcomes discrepancies between different levels of approximations applied to the excitation spectra of the monomers and the aggregates' excitations. At the same time the method does not suffer from charge transfer problems between the monomers and is able to include effects of intra- as well as intermolecular vibrations. The computational effort is manageable even for complex organic aggregates, since a TD-DFTB calculation has to be done only for the isolated monomers. The method is evaluated by means of a formaldehyde oxime dimer and is compared with standard TD-DFTB. Here it has shown its applicability for not too small intermolecular distances. Furthermore it is tested and applied to a dimer of perylene bisimide dyes. The ease of calculating coupling strengths enables us to systematically analyse the possible aggregation structures.



# Zusammenfassung

Die Berechnung von Anregungsenergien ist ebenso wie die Berechnung der Kopplungen zwischen elektronischen Anregungen ein Schlüssel zur Simulation des Exzitonenergietransfers in molekularen Aggregaten, unter anderem in künstlichen wie auch natürlichen Lichtsammelkomplexen. Um eben diese Frenkel-Exzitonparameter zu berechnen, wird eine neue, hoch effiziente Methode entwickelt, die auf der *time-dependent density functional based tight-binding* (TD-DFTB) Methode aufbaut. Auf diese Weise ist es möglich, unter Vermeidung inkonsistenter Näherungen in der Beschreibung von Anregung der Monomere und des Aggregats, sowohl die elektronische Struktur der Moleküle als auch die Exzitonenkopplung konsistent zu TD-DFTB zu beschreiben. Gleichzeitig vermeidet diese Methode problematische Ladungstransferprozesse und kann prinzipiell auch intra- und intermolekulare Vibrationen berücksichtigen. Dabei ist der rechnerische Aufwand gering, da sie auf Größen der TD-DFTB Rechnung für das isolierte Monomer beruht. Diese neue Methode wird anhand eines Formaldoxim-Dimers getestet und mit herkömmlicher TD-DFTB verglichen, was ihre Anwendbarkeit für nicht zu kleine Abstände zeigt. Weitere Vergleiche können anhand von Perylenbisimid-Dimeren angestellt werden. Es ist damit gangbar die möglichen Aggregationsstrukturen dieses Chromophors systematisch zu untersuchen.



# Contents

<b>Table of Contents</b>	<b>v</b>
<b>List of Figures</b>	<b>ix</b>
<b>Nomenclature</b>	<b>xiii</b>
<b>1. Introduction</b>	<b>2</b>
<b>2. Theory of Frenkel Excitons</b>	<b>5</b>
2.1. Excitation Energy Transfer . . . . .	5
2.2. Frenkel Excitons . . . . .	7
2.3. Calculating Coupling Parameters . . . . .	10
2.3.1. Dipole-Dipole Coupling . . . . .	11
2.3.2. Extended Dipole Moment . . . . .	13
2.3.3. Atomic-Centred Charges . . . . .	14
2.3.4. Transition Density Cube Method . . . . .	15
2.3.5. Electronic Coupling Matrix Elements . . . . .	15
2.3.6. Molecular Dynamic Issues . . . . .	16
2.3.7. Supermolecule . . . . .	16
2.4. Density-Functional Based Tight-Binding . . . . .	17
2.4.1. Theory . . . . .	17
2.4.2. Forces . . . . .	25
2.4.3. Time-dependent DFTB . . . . .	25
2.4.4. Parametrisation . . . . .	27
2.5. Coulomb Coupling within the DFTB-Scheme . . . . .	29
2.5.1. Coulomb Coupling by Mulliken Transition Charges . . . . .	29
2.5.2. Coupled System Formulation . . . . .	31
2.6. Computational Details . . . . .	34

---

<b>3. Results</b>	<b>36</b>
3.1. Formaldehyde Oxime Dimer . . . . .	36
3.1.1. Dependence of the Coupling Strength on the Distance . . . . .	37
3.1.2. Dependence of the Coupling Strength on the Angle . . . . .	40
3.2. Perylene Bisimide Dye . . . . .	42
3.2.1. Geometry of Monomer and Dimer . . . . .	43
3.2.2. Electronic Structure of the PBI Monomer . . . . .	43
3.2.3. Electronic Structure of the PBI Dimer . . . . .	46
3.2.4. Coupling Strength in Dependence on the Dimer Configuration . . . . .	46
3.2.5. Coulomb Coupling by the TBFE Approach . . . . .	48
3.2.6. Aggregation Structure . . . . .	55
<b>4. Conclusion</b>	<b>59</b>
<b>A. Derivations</b>	<b>63</b>
A.1. Coulomb Interactions of Two Slater-Type Orbitals . . . . .	63
A.2. Limit for $\gamma_{\alpha\alpha}$ . . . . .	65
<b>B. Program Source Code</b>	<b>66</b>
B.1. Extract of Modified Linear Response Calculation . . . . .	66
B.2. Calculating the Coupling Strength . . . . .	69
<b>C. TDDFTB<sup>+</sup> Inputs</b>	<b>78</b>
C.1. Electronic Transitions . . . . .	78
C.2. Annealing MD . . . . .	79
C.3. NG-Branch Input . . . . .	81
<b>Bibliography</b>	<b>xv</b>
<b>Declaration of Primary Authorship</b>	<b>xxiv</b>



# List of Figures

2.1. EET in HOMO-LUMO representation . . . . .	6
2.2. Dexter transfer in HOMO-LUMO representation; left singlet-singlet transfer; right triplet-triplet transfer . . . . .	7
2.3. Configurations of H- and J-dimers in point-dipole approximation (adapted from [24]) . . . . .	13
2.4. Slater-Koster overlap integral of two p-orbitals . . . . .	28
3.1. Formaldehyde oxime monomer (N-methylidenehydroxylamine, CAS num- ber: 75-17-2 ) and the orientation of the transition dipole vector $\vec{d}$ . . . . .	36
3.2. Varying the distance (orthogonal to transition dipole moment) . . . . .	37
3.3. Varying the tilt angle $\theta$ (tilt axis perpendicular to transition dipole moment, the distance between the monomer in the calculation is larger compared to the distance indicated in this picture) . . . . .	37
3.4. From left to right: 1) Mulliken Transition charges for the $S_0 \rightarrow S_1$ transition; the colors indicate the sign and the radii the absolute value of $q_\alpha^{0,1}$ 2) HOMO- 1 3) LUMO; the HOMO-1 $\rightarrow$ LUMO is the main contribution to the $S_0 \rightarrow S_1$ transition . . . . .	38
3.5. TD-DFTB based methods to calculate the coupling strength of the formalde- hyde oxime (values are calculated with a stepsize of 0.5 Å, for a better viewing the lines result from a fitting procedure) . . . . .	38
3.6. TBFE compared to various DFT based methods (values are calculated with a stepsize of 0.5 Å, for a better viewing the lines result from a fitting procedure) 40	

---

3.7. TD-DFTB based methods to calculate the coupling of the formaldehyde oxime for different tilt angles $\theta$ (values are calculated with a stepsize of $2.5^\circ$ , for a better viewing the lines result from a fitting procedure) . . . . .	41
3.8. TBFE compared to various DFT based methods for different tilt angles $\theta$ (values are calculated with a stepsize of $0.5 \text{ \AA}$ , for a better viewing the lines result from a fitting procedure) . . . . .	42
3.9. Molecular structure of PBI-1[80] . . . . .	43
3.10. Molecular structure in its dissected form [81], the groups R and R' are replace by H . . . . .	43
3.11. Geometry optimisation with DFTB (blue) and DFT/B3LYP (red) . . . . .	44
3.12. HOMO and LUMO obtained by TD-DFT and TD-DFTB . . . . .	45
3.13. Excitation scheme for a PBI-1 dimer (TD-DFTB supermolecule calculation), energies in eV . . . . .	47
3.14. PBI-core with axes . . . . .	48
3.15. Scan of the deformed dimer in x- and y-direction . . . . .	49
3.16. Scan of the deformed dimer in x- and y-direction, $z=1 \text{ \AA}$ . . . . .	50
3.17. Scan of the deformed dimer in x- and y-direction, $z=2 \text{ \AA}$ . . . . .	51
3.18. Scan of the deformed dimer in x- and z-direction . . . . .	52
3.19. Scan of the deformed dimer in x-direction and turning around the z-axis . .	53
3.20. Mulliken transition charges of PBI-1 monomer, radii are proportional to the absolute value . . . . .	54
3.21. Scan of the deformed dimer, coupled-system method, from top to bottom: 1) scan in x- and y-direction 2) same as before with $z = 1 \text{ \AA}$ 3) same as before with $z = 1 \text{ \AA}$ 4) scan in x- and z-direction 5) scan in x-direction and turning around the z-axis . . . . .	56
3.22. Illustration of the different types of PBI-1 dimers; the shifted dimer (left) is the basic component of the aggregate; the planar dimer (right) energetically preferred but cannot form longer chains . . . . .	57

---

3.23. Top: planar dimer; bottom: shifted dimer; left: complete structure; right: framework without side groups . . . . .	57
3.24. Tetramer structure; left: including all groups; right: framework without side groups . . . . .	57



# Nomenclature

$J$	Coulomb coupling
$m, n$	monomer indices
$\vec{d}_{mad}$	transition dipole moment for $a \rightarrow d$
$\vec{X}_m$	center of mass of monomer $m$
$\vec{X}$	$= \vec{X}_m - \vec{X}_n$
$\vec{r}_m$	set of electronic coordinates in monomer $m$
$\alpha, \beta, \gamma$	atomic indices
$\vec{R}_\alpha$	spatial coordinate of nucleus $\alpha$
$\vec{R}_m$	set of $\vec{R}_\alpha$ with $\alpha \in m$
$\varphi_{ma}(\vec{r}_m; \vec{R}_m)$	adiabatic electronic state $a$ of monomer $m$ (indices $a, b$ )
$\rho(\vec{r})$	electronic probability density function

Unless otherwise stated, atomic units are used throughout this thesis ( $|e| = a_0 = m_e = \hbar = 1/4\pi\epsilon_0 = 1$ ).





# Chapter 1.

## Introduction

The process of relocating an excitation on a molecule over its surrounding is called excitation energy transfer (EET). Due to a Coulomb interaction a deexcitation in the donor may cause an excitation in the acceptor. These processes play an important role in light-harvesting systems, artificial [1] as well as natural [2], for example in the pigment-protein complexes of photosynthetic antennae [3, 4]. Moreover is the EET in metallic quantum dots [5, 6] and organic semiconductors [7] of huge interest. The latter have promising features for applications in photovoltaics [8, 9]. For a detailed description the knowledge of the Coulomb coupling is essential. This parameter connects the monomeric chromophore spectra with the spectra of aggregates in solution and therefore, it is vital for describing the collective excitation of an assembly of molecules.

Depending on the sign of the coupling parameter these aggregates can form either J- or H-aggregates which were observed spectroscopically for the first time independently by Jelley [10] and Scheibe et al. [11] (J-aggregates are occasionally also called Scheibe-aggregates). They discovered a concentration-dependent shift in the absorption maximum of pseudoisocyanine chloride in water, which was in contradiction to the Beer-Lambert law but could be explained by a reversible aggregation [12]. The absorption band was red-shifted compared to the monomer, which is the major spectroscopic property of J-aggregates. This bathochromic (from the ancient greek βαθύς, deep) shift comes along with a shifted fluorescence band. The absorption spectra of H-aggregates are blue-shifted, they show no or a minimal fluorescence. They are named after this hypsochromic shift (ὕψος, height).

These spectroscopic properties are explainable in the point-dipole model of a dimer (see Section 2.3.1). For a parallel-oriented molecules with a translation vector perpendicular to the transition dipole moment (see Figure 2.3) two possible transitions exist with different transition energies resulting in a level splitting. Due to the Coulomb repulsion the transi-



tion with parallel transition dipole moments is energetically higher than the monomeric transition and the antiparallel transition (blue-shifted absorption). The latter has in the ideal case no total transition dipole moment ( $\vec{d}_m + \vec{d}_n = 0$ ) and is therefore forbidden. Any population from the higher level may undergo a nonradiative relaxation to the lower one. Here it cannot contribute to the fluorescence and must relax non-radiately, thus, explaining the described properties of an H-aggregate. Associated to such a configuration is a positive value of  $J$ .

A J-aggregate configuration can be characterised by a parallel configuration of the dipole moments and translation vector. In this case the transition including two parallel dipole moments is energetically below the transition with antiparallel transition dipole moments. Since the latter is spectroscopically forbidden (or has for a non-ideal configuration a very low oscillator strength) the absorption spectrum is red-shifted and a fluorescence from this state can be observed. The spectra were later described by Franck and Teller with Frenkel's exciton theory [13].

This reversible aggregation is driven by non-covalent bonds, which include Van der Waals forces,  $\pi$ - $\pi$  stacking and H-Bonds. It is a dynamical process between accumulation and dissolution, the equilibrium is influenced by the solvent and the concentration.

Since the calculation of the coupling as key parameter in EET is very demanding, several approximations have to be introduced to model these supermolecular structures and to estimate the Coulomb coupling. Very often these approximations are not congruent with the remaining description of the system. This work tries to develop a method to calculate the Coulomb coupling within the time-dependent density functional based tight-binding (TD-DFTB) description of the aggregate. This technique is characterised by specific approximations which strongly reduce the calculation effort compared to conventional density functional theory (DFT) without an extensive loss of accuracy. Such a feasible tool may help to enlarge the set of systems where simulations of the EET can be carried out.

In addition to a better description of natural processes in light-harvesting systems a more precise way of modelling these interactions may help to describe and develop nanoscale optical devices [14, 15] and other devices with molecular sizes.

One system which is subject of recent scientific work are aggregates of perylene bisimides (PBI). These self organising dyes feature a high quantum efficiency, thermal- and photostability [16] and are used, e.g. as lacquers. There is a large number of PBI derivatives, most of them assemble as H-aggregates [17] offering only a small amount of fluorescence. In contrast to these the PBI-1 derivative shows a typical absorption spectrum of J-aggregates and is fluorescent. Because of its high exciton mobility [18] and the related possibilities of offering an efficient energy transport they are of special interest in recent research.

This thesis is organised in the following way. The first part after this introduction deals with the theory of Frenkel excitons. It underlines the significance of the coupling strength and presents important methods how this may be calculated. The next part lays out the TD-DFTB theory. This is used to develop a new method to calculate the Coulomb coupling. At the end of the first part a brief overview of the computational implementation is given. In the second part this method is evaluated with a formaldehyde oxime dimer and is finally applied to PBI aggregates.

## Chapter 2.

# Theory of Frenkel Excitons

This chapter presents the basic theory of exciton coupling within the Frenkel exciton picture. It explains the different methods to calculate the Coulomb coupling before the TD-DFTB methods is described. Using this, a Frenkel exciton formulation is developed which leads to the calculation of the Coulomb coupling consistent within TD-DFTB.

### 2.1. Excitation Energy Transfer

A molecule which is brought into an excited state by absorbing light (amongst others) may transfer its energy to a neighbouring atom. Such a donor (D) acceptor (A) process is described in a reaction formula (with \* marking the excitation) as



The excited acceptor can alternatively take the role as a donor in the next EET step, leading to a migration of the exciton. If A and D are identical molecules, the process is named homogeneous, if not, it is named heterogeneous. Especially in the homogeneous case the excitation can be delocalised over several monomers (Wannier-Mott exciton) which would mean a large separation of the electron and the hole. In contrast, excitons which are located on one or a few molecules are named Frenkel excitons (electron and hole stay at the same monomer), these are mainly treated in this work. The former are typically found in highly ordered molecular crystals while a loose assembly of molecules tends to form the

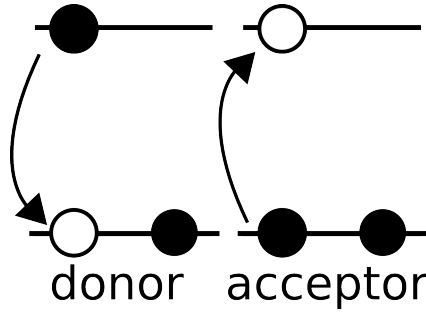


Figure 2.1.: EET in HOMO-LUMO representation

latter. Figure 2.1 shows an EET in the HOMO-LUMO representation.

Since it is a deexcitation similar to a spontaneous photon emission of the donor the process may be seen as a fluorescence resonant energy transfer (FRET), resonant because of the necessity to have close excitation levels in donor and acceptor. This process was explained for the first time by Th. Förster [19] (therefore, also Förster resonant energy transfer). In his interpretation of the phenomenon he did not assume a photon mediated process. Instead it is described without radiation but in a direct dipole-dipole interaction. The oscillation during the deexcitation in the donor stimulates an oscillation in the acceptor which is excited in this way. The transfer rate constant  $k_T$  for a FRET with a distance  $X$  between donor and acceptor is [20]

$$k_T = k_D \left( \frac{R_0}{X} \right)^6. \quad (2.2)$$

Here,  $k_D$  represents the emission rate constant of the excited free donor. The Förster radius  $R_0$  is set to be equal to the value of  $X$  which fulfils the condition  $k_T = k_D$ . This means,  $R_0$  is the distance in which 50% of the energy is transferred. This process differs from a radiation-driven process because of the  $\frac{1}{X^6}$  proportionality. A process involving a real photon would be proportional to  $\frac{1}{X^2}$ .

At distances with a sufficient overlap of the wave functions of the donor and the acceptor the EET can be affected via the Dexter electron transfer [21]. In this process the excited electron skips directly to the acceptor as well as an electron in the HOMO is transferred as well. The total spin of the donor acceptor system is conserved and the rate constant is given by [22]

$$k_{\text{Dex}} \sim \exp \left( -\frac{2X}{L} \right), \quad (2.3)$$

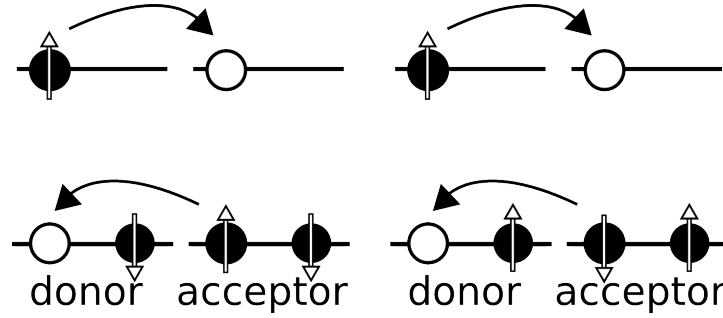


**Figure 2.2.:** Dexter transfer in HOMO-LUMO representation; left singlet-singlet transfer; right triplet-triplet transfer

with  $L$  being the "effective average Bohr radius" [21] which is connected to the sum of the Van der Waals radii of the donor and acceptor. This process is illustrated in Figure 2.2. It shows the two possibilities for the transfer which are the singlet-singlet and the triplet-triplet transfer.

## 2.2. Frenkel Excitons

Analysing the excitons in aggregated systems the Frenkel exciton description is used. In this section a derivation is presented following Ref. [23]. For an aggregation of molecules the Hamiltonian can be constructed as

$$H_{\text{agg}} = \sum_m H_m + \frac{1}{2} \sum_{m,n} V_{mn}. \quad (2.4)$$

Here,  $V_{mn}$  describes all kinds of intermolecular interactions, including the electron-electron interaction ( $V_{mn}^{\text{(el-el)}}$ ), the repulsion of the nuclei  $V_{mn}^{\text{(nuc-nuc)}}$  and the electron-nuclei coupling  $V_{mn}^{\text{(el-nuc)}}$ . The first sum of Eq. (2.4) represents the intramolecular contributions.  $H_m$  itself is the Hamiltonian for monomer  $m$  which is separable into the nuclear kinetic energy operator  $T_m$  and the electronic Hamiltonian  $H_m^{(\text{el})}$ , given as

$$H_m = T_m + H_m^{(\text{el})}. \quad (2.5)$$

Staying restricted to Frenkel excitons, the electrons and holes will remain localised and the aggregate Hamiltonian can be expanded into the adiabatic electronic states of the particular monomers  $\varphi_{ma_m}(\vec{r}_m; \vec{R}_m)$  (With  $\vec{r}_m$  for the electronic coordinates of molecule  $m$

and  $\vec{R}_m$  for the nuclear coordinates.) They can be obtained by solving

$$H_m^{(\text{el})}(\vec{R}_m)\varphi_{ma_m}(\vec{r}_m; \vec{R}_m) = U_{ma_m}(\vec{R}_m)\varphi_{ma_m}(\vec{r}_m; \vec{R}_m). \quad (2.6)$$

Here,  $U_{ma_m}(\vec{R}_m) = E_{ma_m}(\vec{R}_m) + V_{nuc-nuc}(\vec{R}_m)$  is the sum of electronic energy eigenvalue and the nucleus-nucleus potential and represents the single-molecule PES of molecule  $m$  in state  $a_m$ . These monomer states are used to define the Hartree product

$$\phi_A^{(\text{HP})}(\vec{r}; \vec{R}) = \prod_m \varphi_{ma_m}(\vec{r}_m; \vec{R}_m). \quad (2.7)$$

For a compact formulation  $A$  includes all quantum numbers  $a_m$  and  $\vec{r}$  ( $\vec{R}$ ) includes the set of monomer coordinates  $\vec{r}_m$  ( $\vec{R}_m$ ). An antisymmetric wave function is obtained by

$$\phi_A^{(\text{AS})}(\vec{r}; \vec{R}) = \frac{1}{\sqrt{N_p!}} \sum_{\text{perm}} (-1)^p \mathcal{P} [\phi_A^{(\text{HP})}(\vec{r}; \vec{R})]. \quad (2.8)$$

$\mathcal{P}$  creates one of  $N_p$  permutations of the electronic coordinates of different molecules (counted by  $p$ ). The total wave function  $|\psi\rangle$  can be expanded into these antisymmetric wave functions

$$|\psi\rangle = \sum_A c_A |\phi_A^{(\text{AS})}\rangle. \quad (2.9)$$

Inserted into the Schrödinger equation

$$H_{\text{agg}} |\psi\rangle = E |\psi\rangle, \quad (2.10)$$

this leads by multiplying with  $\langle\psi|$  to

$$\sum_B \left( \langle\phi_A^{(\text{AS})}| H_{\text{agg}} |\phi_B^{(\text{AS})}\rangle - E \langle\phi_A^{(\text{AS})}| \phi_B^{(\text{AS})}\rangle \right) = 0. \quad (2.11)$$

The Hamiltonian matrix will be

$$\langle\phi_A^{(\text{AS})}| H_{\text{agg}} |\phi_B^{(\text{AS})}\rangle = \sum_m \langle\phi_A^{(\text{AS})}| H_m |\phi_B^{(\text{AS})}\rangle + \frac{1}{2} \sum_{mn} \langle\phi_A^{(\text{AS})}| V_{mn} |\phi_B^{(\text{AS})}\rangle. \quad (2.12)$$

Picking a pair of  $m$  and  $n$  out of the second sum the elements will only differ from zero if the permutation is restricted to electronic states on the molecules  $m$  and  $n$ . Any other permutation will lead to a multiplication by zero. In the restricted case the part of the

electron-electron interaction can be simplified to

$$\begin{aligned}
\langle \phi_{a_m a_n}^{(AS)} | V_{mn}^{(el-el)} | \phi_{b_m b_n}^{(AS)} \rangle &= \int d\vec{r}_m d\vec{r}_n \frac{1}{\sqrt{N_p!}} \sum_{\text{perm}} (-1)^p \mathcal{P} \varphi_{ma_m}^*(\vec{r}_m; \vec{R}_m) \varphi_{na_n}^*(\vec{r}_n; \vec{R}_n) \\
&\quad \times V^{(el-el)} \frac{1}{\sqrt{N_p!}} \sum_{\text{perm}} (-1)^p \mathcal{P} \phi_{nb_n}(\vec{r}_n; \vec{R}_n) \phi_{mb_m}(\vec{r}_m; \vec{R}_m) \\
&= \int d\vec{r}_m d\vec{r}_n \varphi_{ma_m}^*(\vec{r}_m; \vec{R}_m) \varphi_{na_n}^*(\vec{r}_n; \vec{R}_n) V^{(el-el)} \phi_{nb_n}(\vec{r}_n; \vec{R}_n) \phi_{mb_m}(\vec{r}_m; \vec{R}_m) \\
&\quad - \int d\vec{r}_m d\vec{r}_n \varphi_{ma_m}^*(\vec{r}_n; \vec{R}_n) \varphi_{na_n}^*(\vec{r}_m; \vec{R}_m) V^{(el-el)} \phi_{nb_n}(\vec{r}_n; \vec{R}_n) \phi_{mb_m}(\vec{r}_m; \vec{R}_m) \\
&\equiv J_{mn}^{(el-el)}(a_m a_n, b_n b_m) - K_{mn}^{(el-el)}(a_m a_n, b_n b_m).
\end{aligned} \tag{2.13}$$

The first integral is the direct Coulomb interaction and abbreviated by  $J_{mn}$ . The exchange part  $K_{mn}$  groups several contributions, accruing from the spatial overlap of the participating orbitals on molecules  $m$  and  $n$ . They can be neglected for sufficient large distances between the monomers, since the overlap decreases exponentially with the separation of the molecules. This assumption also implies the orthogonality of states on different monomers.

$$\langle \varphi_{ma_m} | \varphi_{na_n} \rangle = \delta_{ma_m, na_n} \tag{2.14}$$

This approximation allows the utilisation of the Hartree ansatz, since all terms of  $H_{\text{agg}}$  except  $V^{(el-el)}$  are independent of permutations in the electronic wave function. The states  $\phi_A^{(HP)}$  form an orthogonal basis, expanding the Hamiltonian into

$$H_{\text{agg}} = \sum_{A,B} \langle \phi_A^{(HP)} | H_{\text{agg}} | \phi_B^{(HP)} \rangle \cdot | \phi_A^{(HP)} \rangle \langle \phi_B^{(HP)} |. \tag{2.15}$$

The matrix elements are

$$\begin{aligned}
\langle \phi_A^{(HP)} | H_{\text{agg}} | \phi_B^{(HP)} \rangle &= \sum_m \langle \phi_A^{(HP)} | H_{\text{agg}} | \phi_B^{(HP)} \rangle + \frac{1}{2} \sum_{m,n} \langle \phi_A^{(HP)} | V_{mn} | \phi_B^{(HP)} \rangle \\
&= \sum_m \underbrace{\langle \varphi_{ma_m} | H_m | \varphi_{mb_m} \rangle}_{H_m(a_m b_m)} \prod_{k \neq m} \delta_{a_k, b_k} \\
&\quad + \frac{1}{2} \sum_{m,n} \underbrace{\langle \varphi_{ma_m} \varphi_{na_n} | V_{mn} | \varphi_{nb_n} \varphi_{mb_m} \rangle}_{J_{mn}(a_m a_n, b_n b_m)} \prod_{k \neq m, n} \delta_{a_k, b_k}.
\end{aligned} \tag{2.16}$$

With these one obtains the Hamiltonian for the aggregate in its compact form:

$$H_{\text{agg}} = \sum_m \sum_{a_m, b_m} H_m(a_m b_m) |\varphi_{ma_m}\rangle \langle \varphi_{mb_m}| + \frac{1}{2} \sum_{m,n} \sum_{a_m, a_n, b_n, b_m} J_{mn}(a_m a_n, b_n b_m) |\varphi_{ma_m} \varphi_{nb_n}\rangle \langle \varphi_{nb_n} \varphi_{mb_m}| \quad (2.17)$$

### 2.3. Calculating Coupling Parameters

Having derived the expression for the aggregate Hamiltonian and assuming that the monomer elements  $H_m(ab)$  are known, this section will present different ways to calculate the coupling elements  $J_{mn}(a_m a_n, b_n b_m)$  before the method within the TD-DFTB scheme is introduced in Section 2.5. The coupling matrix elements have to be extended by contributions of the interaction with the nuclei. The elements are defined as

$$\begin{aligned} J_{mn}(ab, cd) &= \int d\vec{r}_m d\vec{r}_n \varphi_{ma}^*(\vec{r}_m; \vec{R}_m) \varphi_{nb}^*(\vec{r}_n; \vec{R}_n) V \varphi_{nc}(\vec{r}_n; \vec{R}_n) \varphi_{md}(\vec{r}_m; \vec{R}_m) \\ &= \int d\vec{r}_m d\vec{r}_n \varphi_{ma}^*(\vec{r}_m) \varphi_{nb}^*(\vec{r}_n) V^{(\text{el-el})}(\vec{r}_m, \vec{r}_n) \varphi_{nc}(\vec{r}_n) \varphi_{md}(\vec{r}_m) \\ &\quad + \delta_{b,c} \int d\vec{r}_m \varphi_{ma}^*(\vec{r}_m) V^{(\text{el-nuc})}(\vec{r}_m, \vec{R}_n) \varphi_{md}(\vec{r}_m) \\ &\quad + \delta_{a,d} \int d\vec{r}_n \varphi_{nb}^*(\vec{r}_n) V^{(\text{nuc-el})}(\vec{R}_m, \vec{r}_n) \varphi_{nc}(\vec{r}_n) \\ &\quad + \delta_{a,d} \delta_{b,c} V_{mn}^{(\text{nuc-nuc})}(\vec{R}_m, \vec{R}_n). \end{aligned} \quad (2.18)$$

The nomenclature of the electronic states is modified in this formula, the indices are dropped out. In a statement like  $J_{mn}(ab, cd)$   $a$  and  $d$  are electronic states of monomer  $m$ ,  $b$  and  $c$  belong to monomer  $n$ . It should be recalled that  $\vec{r}_m$  is the compact notation for all electronic coordinates in molecule  $m$  ( $\vec{r}_{m_1}, \vec{r}_{m_2}, \dots$ ). Since  $\varphi_{ma}(\vec{r}_m)$  and its conjugated counterpart are antisymmetric the transition charge density may be defined as [23]

$$\rho_{ad}^{(m)}(\vec{x}) = N \int d\vec{r}_m \delta(\vec{x} - \vec{r}_{m_1}) \varphi_{ma}^*(\vec{r}_m) \varphi_{md}(\vec{r}_m), \quad (2.19)$$



with  $N$  being the number of electrons in molecule  $m$ . Covering only the electronic part, it is possible to define the molecular charge density including the nuclei:

$$n_{ad}^{(m)}(\vec{x}) = \rho_{ad}^{(m)}(\vec{x}) - \delta_{a,d} \sum_{\alpha \in m} Z_{\alpha} \delta(\vec{x} - \vec{R}_{\alpha}) \quad (2.20)$$

Here,  $Z_{\alpha}$  is the charge of nucleus  $\alpha$  in molecule  $m$ . With this formulation Eq. 2.18 simplifies to

$$\begin{aligned} J_{mn}(ab, cd) &= \int d\vec{x} \int d\vec{x}' \frac{\rho_{ad}^{(m)}(\vec{x}) \rho_{bc}^{(n)}(\vec{x}')}{|\vec{x} - \vec{x}'|} \\ &\quad - \delta_{b,c} \int d\vec{x} \sum_{\beta \in n} \frac{\rho_{ab}^{(m)}(\vec{x}) Z_{\beta}}{|\vec{x} - \vec{R}_{\beta}|} \\ &\quad - \delta_{a,d} \int d\vec{x}' \sum_{\alpha \in m} \frac{\rho_{bc}^{(n)}(\vec{x}') Z_{\alpha}}{|\vec{x}' - \vec{R}_{\alpha}|} \\ &\quad - \delta_{a,d} \delta_{b,c} V^{nuc-nuc} \\ &= \int d\vec{x} d\vec{x}' \frac{n_{ad}^{(m)}(\vec{x}) n_{bc}^{(n)}(\vec{x}')}{|\vec{x} - \vec{x}'|}. \end{aligned} \quad (2.21)$$

In practice this double integral is hard to evaluate. In most case it is principally impossible, since the wave function is only given on a grid. The following sections will summarise common approximations.

### 2.3.1. Dipole-Dipole Coupling

One of the crudest approximations is the dipole-dipole coupling [23]. The Coulomb interaction is developed into a multipole expansion. If the intermolecular distance is large enough, the transition dipole moment (second term) is sufficient to describe the Coulomb coupling. The center of mass coordinates for every molecule  $\vec{X}_m$  and their distance  $\vec{X}_{mn} = \vec{X}_m - \vec{X}_n$  is introduced. Both  $\vec{x}$  and  $\vec{x}'$  are expressed by coordinates originating at these centers ( $\vec{x} = \vec{x}_m + \vec{X}_m$ ,  $\vec{x}' = \vec{x}_n + \vec{X}_n$ ). This allows for the introduction of the relative coordinate  $\vec{x}_{mn} = \vec{x}_m - \vec{x}_n$ . The dominator in Eq. (2.21) is expanded into powers of  $\frac{x_{mn}}{X_{mn}}$ :

$$\begin{aligned} \frac{1}{|\vec{x} - \vec{x}'|} &= \frac{1}{|\vec{X}_{mn} + \vec{x}_{mn}|} \\ &= \frac{1}{X_{mn}} - \frac{\vec{x}_{mn} \vec{X}_{mn}}{X_{mn}^3} + \frac{1}{2} \left( -\frac{x_{mn}^2}{X_{mn}^3} + \frac{3(\vec{x}_{mn} \vec{X}_{mn})^2}{X_{mn}^5} \right) + \dots \end{aligned} \quad (2.22)$$

This implies for  $J_{mn}$

$$\begin{aligned}
 J_{mn}(ab, cd) &= \int d\vec{x}_m d\vec{x}_n n_{ad}(\vec{x}_m + \vec{X}_m) n_{bc}(\vec{x}_n + \vec{X}_n) \frac{1}{|\vec{x} - \vec{x}'|} \\
 &\approx \int d\vec{x}_m d\vec{x}_n n_{ad}(\vec{x}_m + \vec{X}_m) n_{bc}(\vec{x}_n + \vec{X}_n) \left( \frac{1}{X_{mn}} - \frac{\vec{x}_m \vec{X}_{mn}}{X_{mn}^3} - \frac{x_{mn}^2}{2X_{mn}^3} + \frac{3(\vec{x}_m \vec{X}_{mn})^2}{2X_{mn}^5} \right).
 \end{aligned} \tag{2.23}$$

Here, the total charge of the molecule is zero and remains zero in the case of a local excitation, which can be expressed as

$$\int d\vec{x} n_{ad}(\vec{x}) = 0. \tag{2.24}$$

All terms in Eq. (2.23) not containing  $\vec{x}_m$  and  $\vec{x}_n$  at once are zero, which leads to

$$J_{mn}(ab, cd) = \int d\vec{x}_m d\vec{x}_n n_{ad}(\vec{x}_m + \vec{X}_m) n_{bc}(\vec{x}_n + \vec{X}_n) \left( \frac{\vec{x}_m \vec{x}_n}{X_{mn}^3} - \frac{3(\vec{x}_m \vec{X}_{mn})(\vec{x}_n \vec{X}_{mn})}{X_{mn}^5} \right). \tag{2.25}$$

At this point the transition dipole moment is introduced. For an arbitrary  $\vec{X}_m$  it is defined for a transition from state  $a$  to  $d$ :

$$\vec{d}_{mad} = \int d\vec{r}_m n_{ad}(\vec{x}_m + \vec{X}_m) \vec{x}_m \tag{2.26}$$

Inserting  $\vec{d}_{mad}$  into Eq. (2.25) one obtains

$$J_{mn}(ab, cd) \approx \frac{\vec{d}_{mad} \vec{d}_{nbc}}{X_{mn}^3} - 3 \frac{(\vec{X}_{mn} \vec{d}_{mad})(\vec{X}_{mn} \vec{d}_{nbc})}{X_{mn}^5}. \tag{2.27}$$

In this picture it is easy to see the orientation dependency of the change between H- and J-aggregates which comes along with a change of sign of  $J$ . As it is shown in Figure 2.3 for a parallel alignment of the transition dipole moments the angle between these and the distance vector determines the character of the aggregate. Eq. (2.27) can be reformulated for a parallel alignment of equal dipole moments  $d$  into

$$J_{mn}(ab, cd) = \frac{d^2}{X_{mn}^3} (1 - 3 \cos^2 \alpha), \tag{2.28}$$

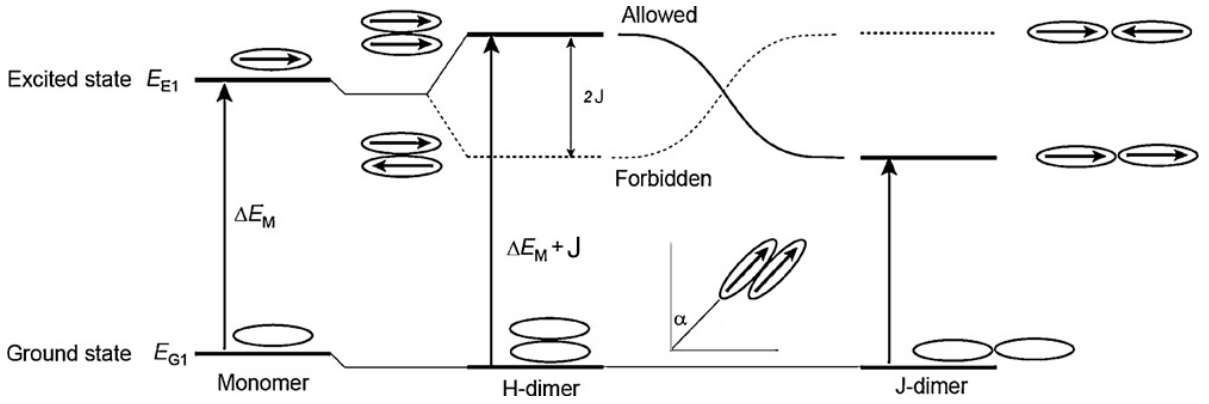


**Figure 2.3.:** Configurations of H- and J-dimers in point-dipole approximation (adapted from [24])

with  $\alpha$  being the angle between  $\vec{d}$  and  $\vec{X}_{mn}$ . Its root is

$$\begin{aligned} \alpha &= \arccos \sqrt{\frac{1}{3}} \\ &= 54.74^\circ. \end{aligned} \quad (2.29)$$

This angle is often called the magic angle since the coupling strength is zero at this configuration and the characteristics of the aggregate changes between that of an H- and a J-aggregate.

Since the numeric effort of the dipole-dipole approximation is the lowest of all methods, it is used in a wide range of applications [25, 26, 27].

### 2.3.2. Extended Dipole Moment

While Eq. (2.27) uses an infinitive small dipole extension (point dipoles) it can be upgraded to the extended dipole approximation (EDA) where the coupling is calculated by two point like transition charges per molecule ( $M, N$ ) [28]:

$$J_{mn}(ab, cd) = \sum_{M \in m}^2 \sum_{N \in n}^2 \frac{q_M^{ad} q_N^{bc}}{|\vec{R}_M - \vec{R}_N|} \quad (2.30)$$

The point charges are placed along the direction of the transition dipole. Their distance, the extension  $s$ , may be seen as a parameter determined by a fit to experimental results. The transition charges of the monomer must have the same absolute value and have to

fulfil the relation

$$q^{ad} = \pm \frac{d_{mad}}{s}. \quad (2.31)$$

In this way the extension of the involved molecules can be taken into account, which normally improves the dipole-dipole results.

### 2.3.3. Atomic-Centred Charges

The next extension to a more precise concept to calculate the Coulomb coupling is to define a distribution of atomic transition charges [29]  $q_\alpha^{ad}$  (on atomic site  $\alpha$ ). In this approximation the total coupling is the summation over all Coulomb interactions:

$$J_{mn}(ab, cd) = \sum_{\alpha \in m, \beta \in n} \frac{q_\alpha^{ad} q_\beta^{bc}}{|\vec{R}_\alpha - \vec{R}_\beta|} \quad (2.32)$$

The question which arises is how to partition a given transition density to the atomic sites. There are different methods used so far. If the monomer calculation has been performed using orthonormal basis functions the transition monomers can be derived from a configuration interaction singles (CIS) expansion [30, 31]

$$q_\alpha^{ad} = \sqrt{2} \sum_{v \in \alpha} \sum_l^{\text{unocc}} \sum_m^{\text{occ}} A_{ml}^{ad} c_l^v c_m^v, \quad (2.33)$$

whereas the index  $v$  runs over all atomic orbitals  $\chi_v$  belonging to atom  $\alpha$ ,  $c_l^v$  is the atomic orbital coefficient of the molecular orbital  $\phi_l = \sum_v c_l^v \chi_v$ .  $A_{ml}^{ad}$  is the CI coefficient of the transition from  $a$  to  $d$  from the CIS calculation corresponding to the excitation  $m \rightarrow l$ . If the basis set is not orthogonal, Eq. (2.33) is generalised by the Mulliken partitioning analysis [32] with the overlap matrix  $S_{v\mu} = \langle \chi_v | \chi_\mu \rangle$ :

$$q_\alpha^{ad} = \sqrt{2} \sum_{v \in \alpha} \sum_\mu \sum_l^{\text{unocc}} \sum_m^{\text{occ}} A_{ml}^{ad} c_l^v c_m^\mu S_{v\mu} \quad (2.34)$$

Another option to distribute the (transition) charges to the atomic sites is the stockholder method, where it is distributed by the fraction of the free atomic charges at each point of the molecule [29, 33]. The TrEsp (transition charge from electrostatic potential) uses the *ab-initio* electrostatic potential, obtained by *ab-initio* calculations to fit  $q_\alpha^{ad}$  [34].

### 2.3.4. Transition Density Cube Method

The transition density cube method does not situate the transition density elements on the atomic sites. Instead the transition density is partitioned into cubes on a three-dimensional grid of points [35] ( $\sigma$  is the spin variable).

$$q^{ad}(x, y, z) = V_{\delta} \int_z^{z+\delta_z} \int_y^{y+\delta_y} \int_x^{x+\delta_x} \int_{\sigma} \Psi_d(\vec{r}) \Psi_a(\vec{r}) d\sigma dx dy dz. \quad (2.35)$$

The cube element is given by the product of the step sizes along the coordinate axes ( $V_{\delta} = \delta_x \delta_y \delta_z$ ). Since the cube size is finite the sum of all  $q^{ad}$  may differ from zero. In this cases the residual charge is balanced by an equal addition on every cube [36].

### 2.3.5. Electronic Coupling Matrix Elements

Another possibility is to calculate the electronic coupling matrix elements in a Förster-Dexter type of approach [37]. The transition densities for the involved monomers are calculated separately by TD-DFT on an atomic centred grid of basis functions  $\phi_{\kappa}$ . The transition density for the transition ( $a, d$ ) in the molecule  $m$  is

$$\Psi_a^*(\vec{r}) \Psi_d(\vec{r}) = \sum_{\kappa\lambda} c_{a,\kappa}^* c_{d,\lambda} \phi_{\kappa}^*(\vec{r}) \phi_{\lambda}(\vec{r}). \quad (2.36)$$

At the end of this approach Eq. (2.13) is for the closed shell case reformulated in the Mulliken form

$$\langle \phi_{ab}^{(AS)} | V_{mn}^{(el-el)} | \phi_{dc}^{(AS)} \rangle = \sum_{\kappa\lambda \in m} \sum_{\mu\nu \in n} c_{a,\kappa}^* c_{d,\lambda} c_{b,\mu}^* c_{c,\nu} [2(\kappa\lambda|\mu\nu) - (\kappa\nu|\mu\lambda)]. \quad (2.37)$$

In this equation the abbreviated form for the Coulomb integrals is used

$$(\kappa\lambda|\mu\nu) = \iint \phi_{\kappa}^*(\vec{r}) \phi_{\lambda}(\vec{r}) \frac{1}{|\vec{r} - \vec{r}'|} \phi_{\mu}^*(\vec{r}') \phi_{\nu}(\vec{r}') d\vec{r} d\vec{r}'. \quad (2.38)$$

By summing the exchange part (second term of the sum in Eq. (2.37)) separately it is possible to specify  $K_{mn}^{(el-el)}(ab, cd)$ .

### 2.3.6. Molecular Dynamic Issues

Principally it is possible to include intra- as well as intermolecular vibrations in the presented methods to calculate the Frenkel exciton parameters. All changes of the molecular structure will influence the obtained values. For this purpose it needs a calculation for every structural propagation step. The effort of this differs from method to method. Including this in a description of Frenkel exciton parameters with all structural dependencies one needs to calculate the local transitions and the coupling for each time step along a MD trajectory. The calculation of the local transitions has to be done for each monomer including the influence of its surrounding in terms of the charge distribution. It can be expressed by transition couplings like  $J_{mn}(eg, gg)$  which indicate the interaction matrix element of a monomer  $n$  in the ground state  $g$  and an electronic transition on monomer  $m$  from the ground state to an excited state  $e$ .

### 2.3.7. Supermolecule

With every method that calculates the transition energies it is possible to calculate the coupling indirectly by the energy splitting of the coupled excitations and to use it as a reference. The advantage is that it is fully consistent to the monomer calculation. Despite the considerably grown effort, the drawback is the difficulty to identify the involved transitions. Sometimes it is possible by a structural symmetry to identify the excitation qualitatively by point group analysis. In other cases it is not possible to be restricted to Frenkel excitons. Nevertheless it is a benchmark calculation for all methods mentioned above.

At least DFT methods suffer from principal problems since conventional functionals provoke the delocalisation error. For large distances the repulsive interaction for the electrons is too large due to the Coulomb term and fractional charges are underestimated. Hybrid functionals may produce an error canceling of the delocalisation error [38]. Nevertheless charge transfer (CT) states are systemetically underestimated [39]. A method to overcome the problem is the subsystem formulation of TD-DFT [40].

The next section describes the TD-DFTB method. With this method it is possible to describe the propagation of the aggregate along a MD trajectory and the electronic excitation in a consistent way. The formulation of the coupling within this scheme, which is the missing element in a Frenkel exciton simulation, is developed in the succeeding section.

## 2.4. Density-Functional Based Tight-Binding

The density-functional based tight-binding method (DFTB) is an approximation to conventional density functional theory (DFT). It is based on the total energy expression, as obtained by the density functional theory. By approximations beyond those of DFT, DFTB offers a gain in calculation effort, since no integrals have to be calculated within run time. This fact allows to run calculations for much larger systems.

The DFTB method has been developed since 1995 [41] and is enhanced continuously. Besides a formulation in second order with self-consistent charge description (SCC-DFTB)[42] has been existent since 1998. Analogously to the time-dependent DFT (TD-DFT) it has been extended to time-dependent density-functional based tight-binding (TD-DFTB) [43], which allows for describing excited states. Since 2007 an assemblage of further extensions, including the third order energy expansion is known in literature as DFTB3 [44].

So far DFTB has been used in a wide field of applications like molecular electronic conduction[45], water clusters [46], electronic structure of quantum dots [47] and many more. It is implemented in the standalone codes DFTB<sup>+</sup> and hotbit as well as included, amongst others, in deMon, AMBER and Gaussian.

### 2.4.1. Theory

The main idea of DFTB is to consider the electronic density as a perturbed reference density. The reference density is the superposition of free neutral atomic densities. All deviations are formed by atomic centred charge fluctuations. With these assumptions it is possible to reformulate all expressions needed to calculate the final charge distribution in a manner where no demanding calculations have to be performed. The interaction of the charge distribution and their energies are determined via parametrised expressions. The set of parameters has to be built up beforehand by using a set of molecules. This last statement prevents to label the DFTB method purely *ab initio*.

### Zeroth Order DFTB

Starting point is the total energy expression as developed in DFT. For a system of  $M$  atomic cores and  $N$  electrons with the electronic probability density function  $\rho(\vec{r})$  [42]:

$$E = \sum_i^{\text{occ}} \langle \Psi_i | -\frac{\nabla^2}{2} + V_{\text{ext}}[\rho(\vec{r})] + \frac{1}{2} \int \frac{\rho(\vec{r}')}{|\vec{r} - \vec{r}'|} d\vec{r}' | \Psi_i \rangle + E_{\text{xc}}[\rho(\vec{r})] + \frac{1}{2} \sum_{\alpha, \beta}^M \frac{Z_\alpha Z_\beta}{|\vec{R}_\alpha - \vec{R}_\beta|} \quad (2.39)$$

The summation runs over all occupied Kohn-Sham eigenstates ( $\Psi_i$ ). Here and in the following the orbitals are either completely occupied or unoccupied. In a description for finite temperature every orbital would be weighted with its occupation  $f$  which would not change the principal conclusions presented in this chapter.

$E_{\text{xc}}$  in Eq. (2.39) denotes the exchange-correlation term. The last term gives the amount of repulsion between the nuclei. The basic idea of DFTB is to treat the electronic density as the sum of a reference density and the deviation to the factual density:

$$\rho(\vec{r}) = \rho_0(\vec{r}) + \delta\rho(\vec{r}) \quad (2.40)$$

The reference density itself is the superposition of free, neutral atoms. Thus Eq. (2.39) turns to

$$\begin{aligned} E = & \sum_i^{\text{occ}} \langle \Psi_i | \underbrace{-\frac{\nabla^2}{2} + V_{\text{ext}}[\rho_0(\vec{r})] + \int \frac{\rho_0(\vec{r}')}{|\vec{r} - \vec{r}'|} d\vec{r}' + V_{\text{xc}}[\rho_0(\vec{r})]}_{\hat{H}_0} | \Psi_i \rangle \\ & - \frac{1}{2} \iint \frac{\rho_0(\vec{r}')(\rho_0(\vec{r}) + \delta\rho(\vec{r}))}{|\vec{r} - \vec{r}'|} d\vec{r} d\vec{r}' - \int V_{\text{xc}}[\rho_0(\vec{r})](\rho_0(\vec{r}) + \delta\rho(\vec{r})) d\vec{r} \\ & + \frac{1}{2} \iint \frac{\delta\rho(\vec{r}')(\rho_0(\vec{r}) + \delta\rho(\vec{r}))}{|\vec{r} - \vec{r}'|} d\vec{r} d\vec{r}' + E_{\text{xc}}[\rho_0(\vec{r}) + \delta\rho(\vec{r})] + E_{\text{cc}}. \end{aligned} \quad (2.41)$$

The Coulomb interactions between the nuclei (last term in Eq. (2.39)) are combined to  $E_{\text{cc}}$ . After the expansion of the exchange-correlation energy at  $\rho_0$  the total energy may be



expressed as

$$\begin{aligned}
E = & \sum_i^{\text{occ}} \langle \Psi_i | \hat{H}_0 | \Psi_i \rangle - \frac{1}{2} \iint \frac{\rho_0(\vec{r}') \rho_0(\vec{r})}{|\vec{r} - \vec{r}'|} d\vec{r} d\vec{r}' + E_{\text{xc}}[\rho_0(\vec{r})] - \int V_{\text{xc}}[\rho_0(\vec{r})] \rho_0(\vec{r}) d\vec{r} + E_{\text{cc}} \\
& + \frac{1}{2} \iint \left( \frac{1}{|\vec{r} - \vec{r}'|} + \frac{\partial^2 E_{\text{xc}}}{\partial \rho(\vec{r}) \partial \rho(\vec{r}')} \Big|_{\rho_0(\vec{r})} \right) \delta \rho(\vec{r}) \delta \rho(\vec{r}').
\end{aligned} \tag{2.42}$$

In zeroth order of non SCC tight-binding theory the last term would be neglected and the Hamiltonian  $\hat{H}_0$  is calculated from the reference density. To keep the computational effort low, the frozen-core approximation can be applied. This implies that only valence orbitals are considered. Thus, all remaining terms in Eq. (2.42) depend on the reference density, respectively describe the repulsion of two atomic cores (including the core electrons) and the total energy within DFTB can be summarised to

$$E_0^{\text{TB}} = \sum_i^{\text{occ}} \langle \Psi_i | \hat{H}_0 | \Psi_i \rangle + E_{\text{rep}}. \tag{2.43}$$

The repulsive potential  $E_{\text{rep}}$  can be calculated pairwise and it only depends on the distance (and the species of the atoms). It is expressed as

$$E_{\text{rep}} = E_{\text{rep}}(\vec{R}_\alpha - \vec{R}_\beta). \tag{2.44}$$

With the help of the LCAO method (linear combination of atomic orbitals) the Kohn-Sham equations can be solved. The one-particle wave function  $\Psi_i$  is expanded into atomic (valence) orbitals:

$$\Psi_i(\vec{r}) = \sum_v c_{vi} \varphi_v(\vec{r} - \vec{R}_\alpha) \tag{2.45}$$

Applying the variation principle to Eq. (2.43) one obtains the following set of equations:

$$\sum_v^M c_{vi} (H_{\mu\nu}^0 - \varepsilon_i S_{\mu\nu}) = 0, \quad \forall \mu, i, \tag{2.46}$$

$$H_{\mu\nu}^0 = \langle \varphi_\mu | \hat{H}_0 | \varphi_\nu \rangle, \quad S_{\mu\nu} = \langle \varphi_\mu | \varphi_\nu \rangle, \quad \forall \mu \in \alpha, \nu \in \beta \tag{2.47}$$

Within the two-center approximation the matrix elements of the Hamiltonian become

$$H_{\mu\nu}^0 = \begin{cases} \epsilon^{\text{free neutral}}, & \text{if } \mu = \nu \\ \langle \varphi_\mu | \hat{T} + V_0^\alpha + V_0^\beta | \varphi_\nu \rangle, & \text{if } \mu \in \alpha \wedge \nu \in \beta \wedge \alpha \neq \beta \\ 0, & \text{else.} \end{cases} \quad (2.48)$$

The diagonal elements commensurate to the eigenvalues of the orbitals of the free neutral atoms. The nondiagonal elements differ only from zero, if both orbitals belong to different atoms. The potential in this case consists of the atomic potentials  $V_0^\alpha$  and  $V_0^\beta$ . Solving Eq. (2.46) Eq. (2.43) becomes

$$E_0^{\text{TB}} = \sum_i^{\text{occ}} \epsilon_i + E_{\text{rep}}. \quad (2.49)$$

In the calculation of the repulsive potential DFTB leaves a strictly formulated classification of *ab initio* methods. To calculate  $E_{\text{rep}}$  the first term in Eq. (2.49) is compared with DFT calculations. In doing so a set of molecules including the sought bond (or several equivalents) is manipulated systematically. The distance dependent repulsive potential for a certain pair of elements is obtained by the differences to DFTB without  $E_{\text{rep}}$ ,

$$E_{\text{rep}}(R) = \left\{ E_{\text{DFT}}(R) - \sum_i^{\text{occ}} n_i \epsilon_i(R) \right\} \Big|_{\text{reference system}}. \quad (2.50)$$

The set of molecules and the values of  $R$  that are included in the fit for this function is different in every parameter set. This level of DFTB works well for systems with a ground state density close to the reference density [48]. Since the reference density is the superposition of free atoms these systems are those whose electronegativities are close to each other. These are homo-nuclear systems and to a limited extent hydrocarbon systems.

### Self-Consistent DFTB in Second Order (SCC-DFTB)

If the electron density differs considerably from the reference density the SCC-DFTB level of approximation offers a more precise description of the electronic structure. This is especially the case for molecules governed by heteronuclear bonds with very different electronegativities. In this extension terms of second order in Eq. (2.42) are not neglected but included in the following derivation. The deviation to the reference density is split into components centred on the atomic sites and separated into radial function  $F_{ml}^\alpha$  and

spherical harmonics  $Y_{lm}$ :

$$\delta\rho(\vec{r}) = \sum_{\alpha} \delta\rho_{\alpha}(\vec{r}) \quad (2.51)$$

$$\delta\rho_{\alpha}(\vec{r}) = \sum_{l,m} K_{ml} F_{ml}^{\alpha} (|\vec{r} - \vec{R}_{\alpha}|) Y_{lm} \left( \frac{\vec{r} - \vec{R}_{\alpha}}{|\vec{r} - \vec{R}_{\alpha}|} \right) \quad (2.52)$$

The next approximation is to suppose that the major contribution is coming from the monopoles. Neglecting a possible contribution by higher order terms the expansion can be truncated after the monopole term. The deviation to the reference density on atom  $\alpha$  becomes

$$\delta\rho_{\alpha}(\vec{r}) \approx \Delta q_{\alpha} F_{00}^{\alpha} (|\vec{r} - \vec{R}_{\alpha}|) Y_{00}, \quad (2.53)$$

where the total charge is maintained,

$$\sum_{\alpha} \Delta q_{\alpha} = \int \delta\rho(\vec{r}) d\vec{r}. \quad (2.54)$$

The interaction of two such monopoles can be calculated from the Coulomb interaction and the exchange-correlation-energy [43]:

$$E_{\text{WW}} = \Delta q_{\alpha} \Delta q_{\beta} \underbrace{\iint \left( \frac{1}{|\vec{r} - \vec{r}'|} + \frac{\partial^2 E_{\text{xc}}}{\partial\rho(\vec{r})\partial\rho(\vec{r}')}\bigg|_{\rho_0} \right) F_{\alpha}(\vec{r}) F_{\beta}(\vec{r}') d\vec{r} d\vec{r}'}_{\gamma_{\alpha\beta}(R)} \quad (2.55)$$

For large distances ( $R = |\vec{R}_{\alpha} - \vec{R}_{\beta}| \rightarrow \infty$ ) the exchange-correlation term vanishes and Eq. (2.55) will be the Coulomb interaction between two point charges

$$\lim_{R \rightarrow \infty} \gamma_{\alpha\beta}(R) = \frac{1}{R} \quad (2.56)$$

For an interatomic distance between two identical atoms close to zero the integral in Eq. (2.55) describes the energy of an altered charge situated at atom  $\alpha$ , or in other words an electron-electron interaction on the same atom which can be approximated by

$$\lim_{R \rightarrow 0} \gamma_{\alpha\beta}(R) = \frac{\partial^2 E_{\alpha}}{\partial q_{\alpha}^2} = U_{\alpha}. \quad (2.57)$$

For this the homonuclear parameters are estimated by Pariser's observation [49]:

$$\gamma_{\alpha\alpha} \approx I_\alpha - A_\alpha \quad (2.58)$$

This means that it can be approximated by the difference between the ionisation potential  $I_\alpha$  and the electron affinity  $A_\alpha$ , which is at the same time two times the chemical hardness  $\eta_\alpha$  [50] or the Hubbard parameter  $U_\alpha$ :

$$\gamma_{\alpha\alpha} \approx I_\alpha - A_\alpha \approx 2\eta_\alpha \approx U_\alpha \quad (2.59)$$

The major advantage of DFTB is that the  $\gamma_{\alpha\beta}$  can be calculated beforehand for every combination of included elements. To achieve such a parametrisation it has to be interpolated for intermediate values of  $R$ . This can be done by the Klopman-Ohno approximation [51, 52]:

$$\gamma_{\alpha\beta}(R) = \sqrt{\frac{1}{R^2 + \frac{1}{4} \left( \frac{1}{U_\alpha} + \frac{1}{U_\beta} \right)^2}} \quad (2.60)$$

It was used in early DFTB versions, but has led to convergence problems. Alternatively an analytical expression can be derived [42]. It starts with assuming a charge density distribution represented by a Slater-type orbital

$$F_\alpha(\vec{r}) = \frac{\tau_\alpha^3}{8\pi} e^{-\tau_\alpha |\vec{r} - \vec{R}_\alpha|}. \quad (2.61)$$

The Coulomb interaction between two spheres of such a form is given by (for the derivation see A.1 in the appendix):

$$\gamma_{\alpha\beta}(R) = \iint \frac{1}{|\vec{r} - \vec{r}'|} \frac{\tau_\alpha^3}{8\pi} e^{-\tau_\alpha |\vec{r}' - \vec{R}_\alpha|} \frac{\tau_\beta^3}{8\pi} e^{-\tau_\beta |\vec{r} - \vec{R}_\beta|} d\vec{r} d\vec{r}' \quad (2.62)$$

$$= \frac{1}{R} - \left[ e^{-\tau_\alpha R} \left( \frac{\tau_\beta^4 \tau_\alpha}{2(\tau_\alpha^2 - \tau_\beta^2)^2} - \frac{\tau_\beta^6 - 3\tau_\beta^4 \tau_\alpha^2}{(\tau_\alpha^2 - \tau_\beta^2)^3 R} \right) + e^{-\tau_\beta R} \left( \frac{\tau_\alpha^4 \tau_\beta}{2(\tau_\beta^2 - \tau_\alpha^2)^2} - \frac{\tau_\alpha^6 - 3\tau_\alpha^4 \tau_\beta^2}{(\tau_\beta^2 - \tau_\alpha^2)^3 R} \right) \right]. \quad (2.63)$$

If  $\gamma_{\alpha\beta}$  is considered as a function of  $R$ ,  $\tau_\alpha$  and  $\tau_\beta$ , its special case  $\gamma_{\alpha\alpha}$  is given by

$$\gamma_{\alpha\alpha} = \lim_{R \rightarrow 0} \gamma(\tau_\alpha, \tau_\alpha, R) \quad (2.64)$$

$$= -\frac{5}{16}\tau_\alpha. \quad (2.65)$$

The derivation may be found in the appendix. Combining it with Eq. (2.59) one obtains a connection between the size of the charge sphere and the Hubbard parameter:

$$\tau_\alpha = \frac{16}{5}U_\alpha. \quad (2.66)$$

The Hubbard parameter for a spin-unpolarised atom can be calculated by [50, 53]

$$U_\alpha = \frac{\partial \epsilon_i}{\partial n_i}. \quad (2.67)$$

If this derivative is calculated with an *ab initio* method the exchange correlation part is included, leading to  $\gamma_{\alpha\beta}(R) = \gamma_{\alpha\beta}(U_\alpha, U_\beta, R)$  and the total energy in second order DFTB

$$E^{\text{TB}} = \sum_i^{\text{occ}} \langle \Psi_i | \hat{H}_0 | \Psi_i \rangle + \frac{1}{2} \sum_{\alpha\beta}^N \gamma_{\alpha\beta} \Delta q_\alpha \Delta q_\beta + E_{\text{rep}}. \quad (2.68)$$

The perturbation of the density expressed in these atomic centred charge fluctuations needs to be determined self-consistently. To this end, the single particle function  $\Psi_i$  is expanded into an set of (pseudo-) atomic orbitals.

$$\Psi_i(\vec{r}) = \sum_\nu c_{\nu i} \varphi_\nu(\vec{r}) \quad (2.69)$$

Generally, there would be other possibilities, but in the parametrisation used in this work confined Slater-type atomic orbitals are used. They are the solution of a Schrödinger equation for a free atom with a potential modified to (see section 2.4.4 for more details):

$$V(r) = V_{\text{nuc}}(r) + V_{\text{Hartree}}[\rho(r)] + V_{\text{xc}} + \left(\frac{r}{r_0}\right)^N \quad (2.70)$$

With this Eq. (2.68) gets

$$E^{\text{TB}} = \sum_i^{\text{occ}} \sum_{\nu\mu} c_{\nu i}^* c_{\mu i} H_{\nu\mu}^0 + \frac{1}{2} \sum_{\alpha\beta}^N \gamma_{\alpha\beta} \Delta q_\alpha \Delta q_\beta + E_{\text{rep}}. \quad (2.71)$$

Before deriving  $\Delta q_\alpha$  the charge localised on atom  $\alpha$  needs to be calculated [54]:

$$q_\alpha = \sum_i^{\text{occ}} \int_{V_\alpha} |\psi_i(\vec{r})| d\vec{r} = \sum_i^{\text{occ}} \sum_{\mu\nu} c_{vi}^* c_{\mu i} \int_{V_\alpha} \phi_\nu^*(\vec{r}) \phi_\nu(\vec{r}) d\vec{r} \quad (2.72)$$

This integral has to be evaluated on the volume  $V_\alpha$  assigned to atom  $\alpha$ . It is approximated as follows: All integrals with neither  $\mu$  nor  $\nu$  belonging to atom  $\alpha$  do not contribute to  $q_\alpha$ . If both belong to  $\alpha$  the integral is set to  $\delta_{\nu\mu}$ , because of the orthogonality on the same atom. For the case that only  $\nu$  belongs to  $\alpha$  the integral can be approximated by:

$$\int_{V_\alpha} |\psi_i(\vec{r})| d\vec{r} \approx \frac{1}{2} \int_V \phi_\mu^*(\vec{r}) \phi_\nu(\vec{r}) d\vec{r} = \frac{1}{2} S_{\mu\nu} = \frac{1}{2} \langle \phi_\mu | \phi_\nu \rangle. \quad (2.73)$$

This Mulliken population analysis [32] implies

$$q_\alpha = \sum_i^{\text{occ}} \sum_{\mu \in \alpha} \sum_\nu \frac{1}{2} \left( c_{vi}^* c_{\mu i} S_{\mu\nu} + c_{vi} c_{\mu i}^* S_{\nu\mu} \right). \quad (2.74)$$

Since in the reference structure the charge of an atom would be the number of valence electrons  $q_{0\alpha}$  the charge fluctuation is

$$\Delta q_\alpha = q_\alpha - q_{0\alpha} \quad (2.75)$$

By applying the variational principle on Eq. (2.71) one arrives at

$$\sum_\nu^M c_{vi} (H_{\mu\nu} - \varepsilon_i S_{\mu\nu}) = 0, \quad \forall \mu, i, \quad (2.76)$$

$$H_{\mu\nu} = H_{\mu\nu}^0 + \underbrace{\frac{1}{2} S_{\mu\nu} \sum_\xi (\gamma_{\alpha\xi} + \gamma_{\beta\xi}) \Delta q_\xi}_{H_{\mu\nu}^1}, \quad \mu \in \alpha, \nu \in \beta. \quad (2.77)$$

In this way the deviation from the reference density can be described, incorporating the characteristics of the atom types. How this allows molecular dynamics simulation is shown in the next section.

### 2.4.2. Forces

To perform a molecular dynamics simulation the interatomic forces can be calculated by the gradient of the total energy. The force acting on atom  $\alpha$  is [42]

$$\begin{aligned}\vec{F}_\alpha &= -\frac{\partial E_0}{\partial \vec{R}_\alpha} \\ &= \sum_i^{\text{occ}} \sum_v \sum_\mu c_{vi} c_{\mu i} \left[ \frac{\partial H_{\mu\nu}^0}{\partial \vec{R}_\alpha} - \left( \epsilon_i - \frac{H_{\mu\nu}^1}{S_{\mu\nu}} \right) \frac{\partial S_{\mu\nu}}{\partial \vec{R}_\alpha} \right] \\ &\quad - \Delta q_\alpha \sum_{\beta \neq \alpha} \frac{\partial \gamma_{\alpha\beta}}{\partial \vec{R}_\alpha} \Delta q_\beta - \sum_{\beta \neq \alpha} \frac{\partial E_{\text{rep}}(|\vec{R}_\alpha - \vec{R}_\beta|)}{\partial \vec{R}_\alpha}.\end{aligned}\quad (2.78)$$

The derivative of  $\gamma_{\alpha\beta}$  can be done analytically while the other gradients have to be performed via interpolation.

### 2.4.3. Time-dependent DFTB

To calculate excited states the time-dependent extension of DFTB [43] is used. It is derived analogously to the time-dependent form of DFT (TD-DFT) where excited states can be calculated by linear response to a time-dependent perturbation. One possibility to achieve this goal in TD-DFT as well as in TD-DFTB is the frequency domain response. After a ground state SCC-DFTB calculation one obtains the Kohn-Sham-orbitals with the coupling matrix  $K$  in adiabatic approximation [55]:

$$K_{ij\sigma,kl\tau} = \iint \psi_i(\vec{r}) \psi_j(\vec{r}) \left( \frac{1}{|\vec{r} - \vec{r}'|} + \frac{\partial^2 E_{\text{xc}}}{\partial \rho_\sigma(\vec{r}) \partial \rho_\tau(\vec{r}')} \right) \psi_k(\vec{r}') \psi_l(\vec{r}') d\vec{r} d\vec{r}' \quad (2.79)$$

In this representation the exchange energy  $E_{\text{xc}}$  is derived with the spin densities  $n_\sigma(\vec{r})$  and  $n_\tau(\vec{r})$ . This will lead to an eigenvalue problem of the dimension  $N_{\text{occ}} \times N_{\text{virt}}$  where  $N_{\text{occ}}$  denotes the number of occupied Kohn-Sham orbitals (with indices  $i,j,..$ ) and  $N_{\text{virt}}$  the number of unoccupied Kohn-Sham orbitals ( $k,l,..$ ) for a closed-shell system [56]:

$$\sum_{j,b,\sigma} \left[ \omega_{ia}^2 \delta_{ij} \delta_{ab} \delta_{\sigma\tau} + 2\sqrt{\omega_{ia}} K_{ia\sigma,jb\tau} \sqrt{\omega_{jb}} \right] F_{jb\sigma}^I = \omega_I^2 F_{ia\tau}^I. \quad (2.80)$$

Where  $\omega_{ia} = \epsilon_i - \epsilon_a$  and  $\omega_I$  is the sought excitation energy for the excitation  $I$  and  $F^I$  its corresponding excitation vector. Correct up to this point, the coupling matrix needs to be

approximated next. To be consistent to the DFTB ground state formalism with its density fluctuations the transition density  $\rho_{ij}$  is decomposed into atomic contributions:

$$\rho_{ij}(\vec{r}) = \psi_i(\vec{r})\psi_j^*(\vec{r}) = \sum_{\alpha} \rho_{ij}^{\alpha}(\vec{r}) \quad (2.81)$$

Staying within the DFTB scheme, these atomic centred parts are approximated as monopols

$$\rho_{ij}^{\alpha}(\vec{r}) = q_{ij}^{\alpha} F_{\alpha}(\vec{r}), \quad (2.82)$$

which defines the Mulliken atomic transition charges:

$$q_{ij}^{\alpha} = \frac{1}{2} \sum_{\mu \in \alpha} \sum_{\nu} \left( c_{\mu i} c_{\nu j} S_{\mu\nu} + c_{\nu i} c_{\mu j} S_{\nu\mu} \right). \quad (2.83)$$

The derivative of the exchange-correlation energy in Eq. (2.79) can be split into one part differentiate  $E_{xc}$  with respect to the total charge density  $\rho(\vec{r}) = \rho_{\uparrow}(\vec{r}) + \rho_{\downarrow}(\vec{r})$  and one part with respect to the spin-density  $m(\vec{r}) = \rho_{\uparrow}(\vec{r}) - \rho_{\downarrow}(\vec{r})$ :

$$\frac{\partial^2 E_{xc}}{\partial \rho_{\tau}(\vec{r}) \partial \rho_{\tau}(\vec{r}')} = \frac{\partial^2 E_{xc}}{\partial \rho(\vec{r}) \partial \rho(\vec{r}')} + (2\delta_{\sigma\tau} - 1) \frac{\partial^2 E_{xc}}{\partial m(\vec{r}) \partial m(\vec{r}')} \quad (2.84)$$

This leads to the approximated coupling matrix

$$K_{ij\sigma,kl\tau} = \sum_{\alpha\beta} q_{ij}^{\alpha} q_{kl}^{\beta} \left[ \tilde{\gamma}_{\alpha\beta} + (2\delta_{\sigma\tau} - 1) m_{\alpha\beta} \right] \quad (2.85)$$

with

$$\tilde{\gamma}_{\alpha\beta} = \iint \left( \frac{1}{|\vec{r} - \vec{r}'|} + \frac{\partial^2 E_{xc}}{\partial \rho(\vec{r}) \partial \rho(\vec{r}')} \Bigg|_{\rho} \right) F_{\alpha}(\vec{r}) F_{\beta}(\vec{r}') d\vec{r} d\vec{r}' \quad \text{and} \quad (2.86)$$

$$m_{\alpha\beta} = \iint \frac{\partial^2 E_{xc}}{\partial m(\vec{r}) \partial m(\vec{r}')} \Bigg|_{\rho} F_{\alpha}(\vec{r}) F_{\beta}(\vec{r}') d\vec{r} d\vec{r}'. \quad (2.87)$$

The slight difference between  $\gamma$  and  $\tilde{\gamma}$  is the density at which the derivative is evaluated. This difference is found to be small and is usually neglected [43]. Because of its short range character the second term  $m_{\alpha\beta}$  is set to zero for all off-site terms ( $\alpha \neq \beta$ ). The



on-site terms are given by

$$m_{\alpha\alpha} = \frac{1}{2} \left( \frac{\partial \varepsilon_{\uparrow}^{\text{Homo}}}{\partial n_{\uparrow}} - \frac{\partial \varepsilon_{\uparrow}^{\text{Homo}}}{\partial n_{\downarrow}} \right). \quad (2.88)$$

This Hubbard-like parameter is obtained from atomic DFT calculations of a neutral atom. The short range character has its reasons in the absence of the Coulomb part (compared to  $\tilde{\gamma}_{\alpha\beta}$ ). The oscillator strengths of a transition  $I$  can be calculated with

$$f^I = \frac{2}{3} \omega_I \sum_{k=x,y,z} \left| \sum_{ij} \langle \psi_i | \vec{r}_k | \psi_j \rangle \sqrt{\frac{\omega_{ij}}{\omega_I}} (F_{ji\uparrow}^I + F_{ji\downarrow}^I) \right|^2. \quad (2.89)$$

#### 2.4.4. Parametrisation

As mentioned above many calculations can be done before a DFTB run, no integrals have to be evaluated within it. These parametrisation includes the Hubbard parameters  $U_{\alpha}$ , the matrix elements  $H_{\mu\nu}$ ,  $E_{\text{rep}}$  and other values. All these were included in the so called Slater-Koster files. For this work the mio-1-1 package is used [42]. Starting with the pseudoatomic wave function in terms of Slater-type orbitals and spherical harmonics [41]

$$\phi_{\nu}(\vec{r}) = \sum_{n,\kappa,l_{\nu},m_{\nu}} a_{n\kappa} r^{l_{\nu}+n} e^{-\kappa r} Y_{l_{\nu},m_{\nu}} \left( \frac{\vec{r}}{r} \right) \quad (2.90)$$

a sufficient large basis with different values for  $\kappa$  and  $n$  needs to be found. In [41] these were 5 different values for  $\kappa$  and  $n = 0, 1, 2, 3$  which were found to be sufficient enough for a convergence of all atoms in the first three rows. With this ansatz a self consistent solution of the atomic Kohn-Sham equation

$$[\hat{T} + V(r)] \phi_{\nu}(\vec{r}) = \varepsilon_{\nu} \phi_{\nu}(\vec{r}) \quad (2.91)$$

is performed with a modified potential as given in Eq. (2.70). The last term causes an artificial confinement and leads to bound electrons whose wave functions are not as diffuse as pure atomic orbitals. For the used parameter set,  $N_{\nu}$  was set to 2 and  $r_0$  to the covalent radius of the respective element.

The next step is to calculate the overlap matrix  $S_{\mu\nu}$ . It is possible to decompose any overlap integral for a given interatomic distance  $R$  in a linear combination of orthogonal configurations of atomic basis functions with the same  $R$  [57]. For example the overlap

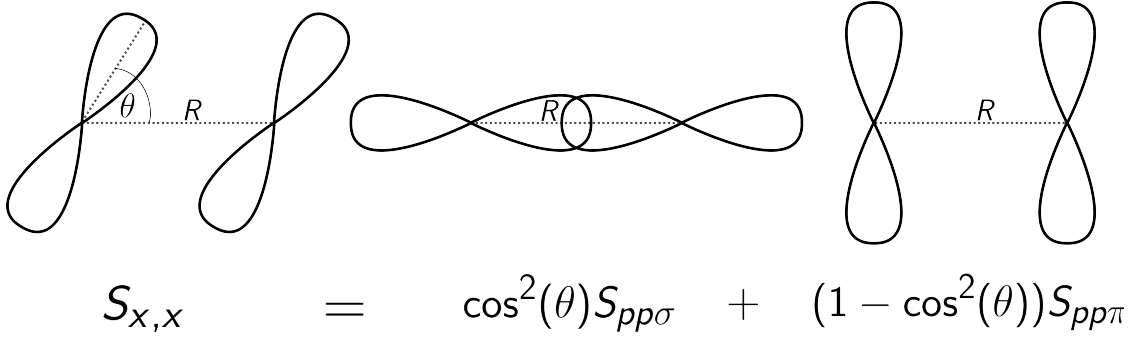


Figure 2.4.: Slater-Koster overlap integral of two p-orbitals

integral between two p-orbitals can be decomposed into

$$S_{x,x}(R) = \cos^2(\theta)S_{pp\sigma}(R) + (1 - \cos^2(\theta))S_{pp\pi}(R). \quad (2.92)$$

As illustrated in figure 2.4  $S_{pp\sigma}(R)$  is the overlap of two p-orbitals in  $\sigma$  configuration and  $S_{pp\pi}$  the same in  $\pi$  configuration. According to the angle  $\theta$  between the p-orbitals they contribute to the overlap integral.

In a Slater-Koster file all necessary integrals are stored for discrete values of  $R$ . The grid distance in the mio-1-1 package is 0.02. Between these configurations the values are interpolated. The diagonal elements of  $H_{\mu\nu}^0$  are the eigenvalues of Eq. (2.91). The non-diagonal elements are calculated in the two-center approximation

$$H_{\mu\nu}^0 = \langle \varphi_\mu | \hat{T} + V_0^\alpha + V_0^\beta | \varphi_\nu \rangle \quad (2.93)$$

$$= \langle \varphi_\mu | \hat{T} + V_{\text{eff}}[\rho_\alpha^0 + \rho_\beta^0] | \varphi_\nu \rangle, \mu \in \alpha, \nu \in \beta, \quad (2.94)$$

assuming a negligible contribution of third atoms. The integrals are stored in the same manner as the overlap integrals.

The most difficult part of the parametrisation is the repulsive potential. The first approximation is to consider  $E_{\text{rep}}$  as a sum of diatomic contributions. It is defined as

$$E_{\text{rep}}(R) = \left[ E_{\text{DFT}}^{\text{SCF}}(R) - \left( \sum_i^{\text{occ}} \langle \Psi_i | \hat{H}_0 | \Psi_i \rangle + \frac{1}{2} \sum_{\alpha\beta}^N \gamma_{\alpha\beta} \Delta q_\alpha \Delta q_\beta \right) \right] \Big|_{\text{reference structure}}. \quad (2.95)$$

The fitting process is very complex and can be done via minimising for example forces or energy differences. It is the most laborious work in the developing of a Slater-Koster package.

All current Slater-Koster files are parametrised with the functional of Perdew, Burke and

Ernzerhof (PBE) [58]. Using these parameters the DFTB method can not outperform a conventional DFT calculation using this functional. Quite the opposite, it will inherit the deficits of this functional which are typical for a generalised gradient approximation (GGA) functional. They include the overestimation of polarisabilities and delocalisation of excess charges in conjugated systems [59], the local exchange kernel leads to problems of CT states [60]. This comes along with a not reproduced  $1/r$  asymptotic description for separated charges what is based on the self-interaction error [61]. Additionally, no dispersion interactions are included. Like in DFT calculation most implementations of DFTB include the possibility to add an empirically corrected van-der-Waals interaction. It is either embedded via the Slater-Kirkwood polarisable atomic model [62] or via a Lennard-Jones potential [63] with parameters from the Universal Force Field (UFF) [64] like it is done in this work.

## 2.5. Coulomb Coupling within the DFTB-Scheme

In this section a method is presented, enabling the calculation of the Coulomb coupling from the electronic transition of the monomers obtained by a TD-DFTB calculation. It is derived in two ways. Firstly, the derivation starts with the expression for the Coulomb coupling defined in Section 2.2 and formulates the quantities by TD-DFTB representations (Mulliken transition charges). The second way formulates the TD-DFTB in a Frenkel exciton way.

### 2.5.1. Coulomb Coupling by Mulliken Transition Charges

The intermolecular Coulomb coupling for the transition  $a \rightarrow b$  in molecule  $m$  and the transition  $c \rightarrow d$  in molecule  $n$  splits up into different contributions (see Eq. (2.18)). The coupling between two transitions ( $a \neq b \wedge c \neq d$ ) is described by

$$J_{mn}(ab, cd) = \int d\vec{r} d\vec{r}' \varphi_{ma}^*(\vec{r}) \varphi_{nb}^*(\vec{r}') V_{mn}^{(\text{el-el})} \varphi_{nc}(\vec{r}') \varphi_{md}(\vec{r}). \quad (2.96)$$

It contains the transition charge  $\rho_{ad}$  which can be expressed in the TD-DFTB scheme by the Mulliken transition charges  $q_{\alpha}^{ad}$ :

$$\rho_{ad}^{(m)}(\vec{r}) = \varphi_{ma}^*(\vec{r}) \varphi_{md}(\vec{r}) \approx \sum_{\alpha \in m} q_{\alpha}^{ad} F_{\alpha}(|\vec{r} - \vec{R}_{\alpha}|) \quad (2.97)$$

For a pure Coulomb coupling the interaction potential is

$$V_{mn}^{(\text{el-el})} = \frac{1}{|\vec{r} - \vec{r}'|}. \quad (2.98)$$

With this the coupling becomes

$$J_{mn}(ab, cd) = \sum_{\alpha \in m} \sum_{\beta \in n} q_{\alpha}^{ad} q_{\beta}^{bc} \underbrace{\int \int d\vec{r} d\vec{r}' \left( \frac{1}{|\vec{r} - \vec{r}'|} \right) F_{\alpha}(|\vec{r} - \vec{R}_{\alpha}|) F_{\beta}(|\vec{r}' - \vec{R}_{\beta}|)}_{\zeta_{\alpha\beta}(|\vec{R}_{\alpha} - \vec{R}_{\beta}|)}, \quad (2.99)$$

where the integral  $\zeta_{\alpha\beta}(R)$  can be calculated analogously to  $\gamma_{\alpha\beta}(R)$  as described in Section 2.4.1. It is likewise dependent on the species of the two atoms and the distance  $R$  between them. To accommodate the different potentials (only Coulomb and no exchange-correlation potential) to a pure Coulomb interaction, a changed Hubbard parameter is used which is calculated without exchange interaction. The Mulliken transition charges  $q_{\alpha}^{ad}$  for every atomic site can be calculated by summing up all Kohn-Sham Mulliken transition charges

$$q_{\alpha}^{ad} = \sum_{ij} c_{ij\sigma}^I q_{ij}^{ij}, \quad (2.100)$$

weighted by the coefficients [65]

$$c_{ij\sigma}^I = \sqrt{\frac{\omega_{ij}}{\omega_I}} F_{ij\sigma}^I \quad (2.101)$$

with the transition vector  $F^I$  for the transition  $I = \{ad\}$  respectively  $\{cb\}$ . The index  $\sigma$  indicates the spin of the transition. It is specified by the type of transition  $I$ .

All other terms of the coupling matrix in Eq. (2.18) have to be treated together since a nucleus including its associated electrons has the total charge  $\Delta q_{\alpha}$ . The molecular transition charge density as defined in Eq. (2.20) is expressed in TD-DFTB as

$$n_{g,a}^{(m)}(\vec{r}) = \sum_{\alpha \in m} q_{\alpha}^{ad} F_{\alpha}(|\vec{r} - \vec{R}_{\alpha}|) + \delta_{g,a} \sum_{\alpha \in m} \Delta q_{\alpha}^{(g)} F_{\alpha}(|\vec{r} - \vec{R}_{\alpha}|) \quad (2.102)$$

for a transition from the ground state  $g$  to an arbitrary state  $a$  (which could be likewise the  $g$ ). Here  $q_{\alpha}^{ad}$  are the Mulliken transition charges on monomer  $m$  while  $\Delta q_{\alpha}^{(g)}$  are the net atomic charges, on monomer  $n$ , as defined in Eq. (2.75). With the same argumentation as above, the Coulomb coupling between a transition on monomer  $m$  and charges of the

ground state  $g$  on monomer  $n$  is given as

$$\begin{aligned} J_{mn}(ag, gd) &= \int d\vec{r} d\vec{r}' \frac{n_{a,d}^{(m)}(\vec{r}) n_{g,g}^{(n)}(\vec{r}')}{|\vec{r} - \vec{r}'|} \\ &= \sum_{\alpha \in m} \sum_{\beta \in n} q_{\alpha}^{ad} \Delta q_{\beta}^{(g)} \zeta_{\alpha\beta}(|\vec{R}_{\alpha} - \vec{R}_{\beta}|). \end{aligned} \quad (2.103)$$

The coupling between two ground states including all terms of Eq. (2.18) can be expressed by

$$\begin{aligned} J_{mn}(gg, gg) &= \int d\vec{r} d\vec{r}' \frac{n_{g,g}^{(m)}(\vec{r}) n_{g,g}^{(n)}(\vec{r}')}{|\vec{r} - \vec{r}'|} \\ &= \sum_{\alpha \in m} \sum_{\beta \in n} \Delta q_{\alpha}^{(g)} \Delta q_{\beta}^{(g)} \zeta_{\alpha\beta}(|\vec{R}_{\alpha} - \vec{R}_{\beta}|). \end{aligned} \quad (2.104)$$

An interaction with the charge distribution of an excited state  $e$  is not defined in the present formulation of TD-DFTB as a linear response.

## 2.5.2. Coupled System Formulation

Alternatively the coupling can be derived by considering two subsystems and their interaction. Reviewing Eq. (2.80)

$$\sum_{j,b,\sigma} \left[ \omega_{ia}^2 \delta_{ij} \delta_{ab} \delta_{\sigma\tau} + 2\sqrt{\omega_{ia}} K_{ia\sigma, jb\tau} \sqrt{\omega_{jb}} \right] F_{jb\sigma}^I = \omega_I^2 F_{ia\tau}^I, \quad (2.105)$$

which is adapted to the problem of two subsystems A and B (w.l.o.g with the same number of electrons). Assuming that the sets of Kohn-Sham orbitals are known for A and B and stay separated (postulates a sufficient large separation and no second order effects)  $F_{ij\sigma}^I$  can be sectioned into

$$F_{ij\sigma}^I = \begin{cases} F_{ij\sigma}^{I(AA)}, & \text{for } i, j \in A \\ F_{ij\sigma}^{I(AB)}, & \text{for } i \in A \wedge j \in B \\ F_{ij\sigma}^{I(BA)}, & \text{for } i \in B \wedge j \in A \\ F_{ij\sigma}^{I(BB)}, & \text{for } i, j \in B, \end{cases} \quad (2.106)$$

whereas the dimension of  $F_{ij\sigma}^I$  grows by a factor of 4. Introducing  $X$  and  $Y$  as new variables ( $X, Y \in \{(AA), (AB), (BA), (BB)\}$ ) Eq. (2.105) will be

$$\sum_{j,b,\sigma,X} \left[ \omega_{ia}^2 \delta_{ij} \delta_{ab} \delta_{\sigma\tau} \delta_{XY} + 2\sqrt{\omega_{ia}} K_{ia\sigma, jb\tau}^{XY} \sqrt{\omega_{jb}} \right] F_{jb\sigma}^{IX} = \omega_I^2 F_{ia\tau}^{IY}. \quad (2.107)$$

$K^{(AA,AA)}$  and  $K^{(BB,BB)}$  stay unchanged, whereby it should be noted that the summation over all atoms has to be performed within the corresponding molecule.  $K^{(AA,BB)}$  and  $K^{(BB,AA)}$  are the couplings between two Kohn-Sham transitions, one on molecule A and one on molecule B:

$$K_{ij\sigma, kl\tau}^{(AA,BB)} = \sum_{\alpha \in A} \sum_{\beta \in B} q_{\alpha}^{ij} q_{\beta}^{kl} \left[ \tilde{\gamma}_{\alpha\beta} + (2\delta_{\sigma\tau} - 1)m_{\alpha\beta} \right] \quad (2.108)$$

This describes the interaction of the Mulliken transition charges on molecule  $\alpha$  ( $q_{\alpha}^{ij}$ ) with those on molecule  $\beta$ .

Terms like  $K_{ij\sigma, kl\tau}^{(AA,AB)}$  describe a coupling between a local excitation and a charge transfer which is excluded in the Frenkel exciton picture. Therefore they are neglected. This holds true for  $K_{ij\sigma, kl\tau}^{(AB,AB)}$ ,  $K_{ij\sigma, kl\tau}^{(BA,BA)}$ ,  $K_{ij\sigma, kl\tau}^{(AB,BA)}$  and  $K_{ij\sigma, kl\tau}^{(BA,AB)}$  describing a 2-electron CT. Neglecting the sections  $F_{ij\sigma}^{I(AB)}$  and  $F_{ij\sigma}^{I(BA)}$  of the transition vector is justified by the same argument. In this way the dimension of the eigenvalue problem is reduced by the factor 2 and can be written as

$$\begin{pmatrix} M_{AA} & C_{AB} \\ C_{BA} & M_{BB} \end{pmatrix} \begin{pmatrix} F^{I(AA)} \\ F^{I(BB)} \end{pmatrix} = \omega_D^2 \begin{pmatrix} F^{I(AA)} \\ F^{I(BB)} \end{pmatrix} \quad (2.109)$$

where  $M_{AA}$   $M_{BB}$  are the matrices from Eq. (2.80) for monomer A resp. B.  $C_{AB}$  describes the interaction and is given by

$$C_{AB, ij\sigma, kl\tau} = 2\sqrt{\omega_{ij}} K_{ij\sigma, kl\tau}^{(AA,BB)} \sqrt{\omega_{kl}}. \quad (2.110)$$

The formulation of treating this is consistent to Ref. [66]. The transitions for the isolated monomers can be found by solving  $M_{AA} F^{I(AA)} = \omega_I^2 F^{I(AA)}$  and the equation corresponding to monomer B. To calculate the coupling between a pair of resonant transitions (transition frequency  $\omega_0$  and eigenvector  $F_A$  as solution for monomer A,  $\omega_B$  and  $F_B$  for monomer B) the interaction will be considered as a perturbation. The solution are two transition

frequencies  $\omega_+$  and  $\omega_-$ . The zeroth order eigenvector is

$$F_{D\pm}^I = \frac{1}{\sqrt{2}} \begin{pmatrix} F_A \\ \pm F_B \end{pmatrix} \quad (2.111)$$

with the modified transition frequencies

$$\omega_{\pm}^2 = \frac{(F_A^T, \pm F_B^T) \begin{pmatrix} M_{AA} & C_{AB} \\ C_{BA} & M_{BB} \end{pmatrix} \begin{pmatrix} F_A \\ \pm F_B \end{pmatrix}}{(F_A^T, \pm F_B^T) \begin{pmatrix} F_A \\ \pm F_B \end{pmatrix}}. \quad (2.112)$$

Since

$$\omega_{\pm} = \omega_0 \pm J, \quad (2.113)$$

it follows that

$$\begin{aligned} J &= \frac{\omega_+^2 - \omega_-^2}{4\omega_0} \\ &= \frac{1}{2\omega_0} F_A^T C_{AB} F_B \\ &= \frac{1}{2\omega_0} \sum_{i,j \in A} \sum_{k,l \in B} F_{ij\sigma}^A 2\sqrt{\omega_{ij}} K_{ij\sigma,kl\tau} \sqrt{\omega_{kl}} F_{kl\tau}^B \\ &= \sum_{i,j,\alpha \in A} \sum_{k,l,\beta \in B} F_{ij\sigma}^A \sqrt{\frac{\omega_{ij}}{\omega_0}} F_{kl\tau}^B \sqrt{\frac{\omega_{kl}}{\omega_0}} q_{\alpha}^{ij} q_{\beta}^{kl} \left[ \tilde{\gamma}_{\alpha\beta} + (2\delta_{\sigma\tau} - 1)m_{\alpha\beta} \right]. \end{aligned} \quad (2.114)$$

With Eq. (2.100) the coupling is derived as

$$J = \sum_{\alpha \in A} \sum_{\beta \in B} q_{\alpha}^{ad} q_{\beta}^{cb} \left[ \tilde{\gamma}_{\alpha\beta} + (2\delta_{\sigma\tau} - 1)m_{\alpha\beta} \right]. \quad (2.115)$$

Since  $m_{\alpha\beta}$  is only non zero on the diagonal it reduces to

$$J = \sum_{\alpha \in A} \sum_{\beta \in B} q_{\alpha}^{ad} q_{\beta}^{cb} \tilde{\gamma}_{\alpha\beta}(R). \quad (2.116)$$

The definition the Coupling by half of the energy gap (Eq. (2.113)) includes the exchange interaction. This can be subsequently corrected by replacing  $\tilde{\gamma}_{\alpha\beta}(R)$  with  $\zeta_{\alpha\beta}(R)$ . The result

is the same equation as derived earlier (Eq. (2.99)):

$$J_{mn}^{(\text{el-el})}(ab, cd) = \sum_{\alpha \in m} \sum_{\beta \in n} q_{\alpha}^{ad} q_{\beta}^{cb} \zeta_{\alpha\beta}(R) \quad (2.117)$$

Both ways of establishing an expression result in the same equation for the Coulomb coupling. The principle assumption in both ways is that the transition is set up by local transitions which follows from the definition of a Frenkel exciton. These local transitions are the same as they are in the separated monomer. This assumption is either formulated in expressing the transition density by the Mulliken transition charges of a monomer transition (Eq. (2.97)) or by defining the eigenvector for a transition of the dimer as a combination of the monomer transition vectors (Eq. (2.111)).

Without further assumptions the presented method has not the ability to determine more than the absolute value of the Coulomb coupling since the sign of  $F_A^I$  is arbitrary. Therefore the sign of  $J$  can only be concluded by a comparison to the dipole-dipole approximation, to a supermolecular calculation or to similar configurations.

The TD-DFTB formulation of a Frenkel exciton Hamiltonian, labelled with the acronym TBFE, is applied on two different dimers in the next chapter. It is as well compared to other methods calculating the Coulomb coupling, as they are described above.

## 2.6. Computational Details

For (TD-)DFTB calculations of the monomers, supermolecules and geometry optimisations the unpublished package **TDDFTB<sup>+</sup>** by Th. Niehaus (University of Regensburg) is used. It originates from the **DFTB<sup>+</sup>** program package [42, 62, 67]. Back-end of the Mulliken transition density calculation is the NG branch of the **DFTB<sup>+</sup>** program package in version 1.4. The subroutine, responsible to calculate the electronic transition, is taken from a development version provided by Th. Niehaus. To achieve a better performance the diagonalisation algorithm for the transition matrix, originally used in this development version, is substituted by the implicitly restarted Arnoldi iteration as implemented in the ARPACK package [68]. Further change is the implementation of the Mulliken transition charges calculation according to Eq. (2.100). This change is done to be able to calculate the Coulomb coupling as proposed.

All parameters are taken from the mio-1-1 Slater-Koster files [42]. The function  $\zeta_{\alpha\beta}(R)$  is calculated analogously to  $\gamma_{\alpha\beta}(R)$ . The difference is the use of modified Hubbard parameters  $\tilde{U}$  which are derived without exchange correlation interaction. The utilised values are



[69]:

$$\tilde{U}_H = 0.57962094$$

$$\tilde{U}_C = 0.51864556$$

$$\tilde{U}_N = 0.63092682$$

$$\tilde{U}_O = 0.74161363.$$

DFT calculations are performed with TURBOMOLE [70, 71, 72] by using a 6-311G\*\* basis set with the functionals B3LYP [73, 74], PBE [58, 75] and PBE0 [76]. The electronic coupling matrix elements are calculated by the pre-release version of the "intact" module of TURBOMOLE implemented by A. Köhn (University of Mainz).

# Chapter 3.

## Results

### 3.1. Formaldehyde Oxime Dimer

The aim of this chapter is to test the method, introduced above and to compare it with other methods. For this purpose a formaldehyde oxime (Figure 3.1) dimer is used as a model. The dimer is build up by two monomers, whereas one is shifted with respect to the other perpendicular to the monomer's symmetry plane. This initial configuration is not the equilibrium of the dimer. It is chosen because of its symmetry of the transition dipole moments. The conformation of the dimer is varied by the distance  $X$  between the monomers (Figure 3.2) and by the tilt angle (Figure 3.3).

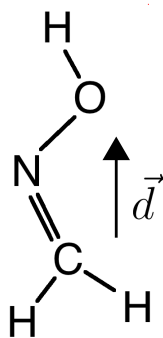


**Figure 3.1.:** Formaldehyde oxime monomer (N-methylidenehydroxylamine, CAS number: 75-17-2 ) and the orientation of the transition dipole vector  $\vec{d}$

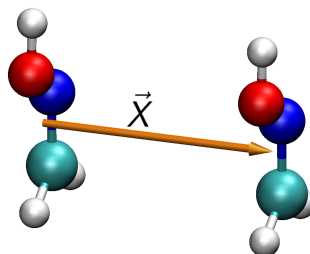


Figure 3.2.: Varying the distance (orthogonal to transition dipole moment)

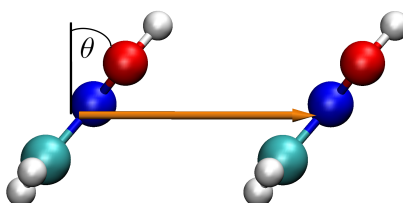
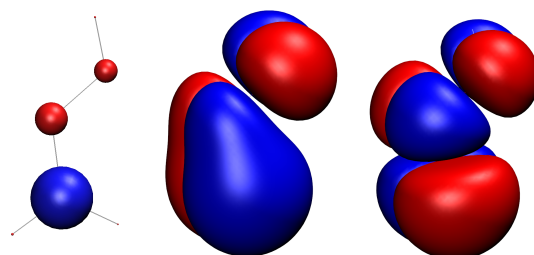


Figure 3.3.: Varying the tilt angle  $\theta$  (tilt axis perpendicular to transition dipole moment, the distance between the monomer in the calculation is larger compared to the distance indicated in this picture)

### 3.1.1. Dependence of the Coupling Strength on the Distance

In order to test the presented coupling-calculating method the TBFE is compared with the following calculations explained in detail in Section 2.3:

- **Supermolecular TD-DFTB:** The dimer is calculated as a supermolecule with TD-DFTB. Among the resulting transitions the two representing the coupled  $S_0 \rightarrow S_1$  excitation are identified by comparing the structure of the Kohn-Sham orbitals involved in the leading transitions. The coupling strength is obtained by the half energy split which includes additionally to  $J$  also  $K$ .
- **Dipole Approximation:** The transition dipole moments  $\vec{d}_m$  are calculated via TD-DFTB (TD-DFT respectively). The coupling is estimated by Eq. (2.27)
- **Supermolecular DFT:** It follows the same procedure as the supermolecular TD-DFTB ansatz. Details including the used functionals are mentioned in Chapter 2.6.
- **Electronic Coupling Matrix Elements:** Alternatively the transition charges of the monomers can be calculated in independent calculations. They are used to estimate the coupling strength by the Electronic Coupling Matrix Analysis.



**Figure 3.4.:** From left to right: 1) Mulliken Transition charges for the  $S_0 \rightarrow S_1$  transition; the colors indicate the sign and the radii the absolute value of  $q_\alpha^{0,1}$  2) HOMO-1 3) LUMO; the HOMO-1 $\rightarrow$ LUMO is the main contribution to the  $S_0 \rightarrow S_1$  transition

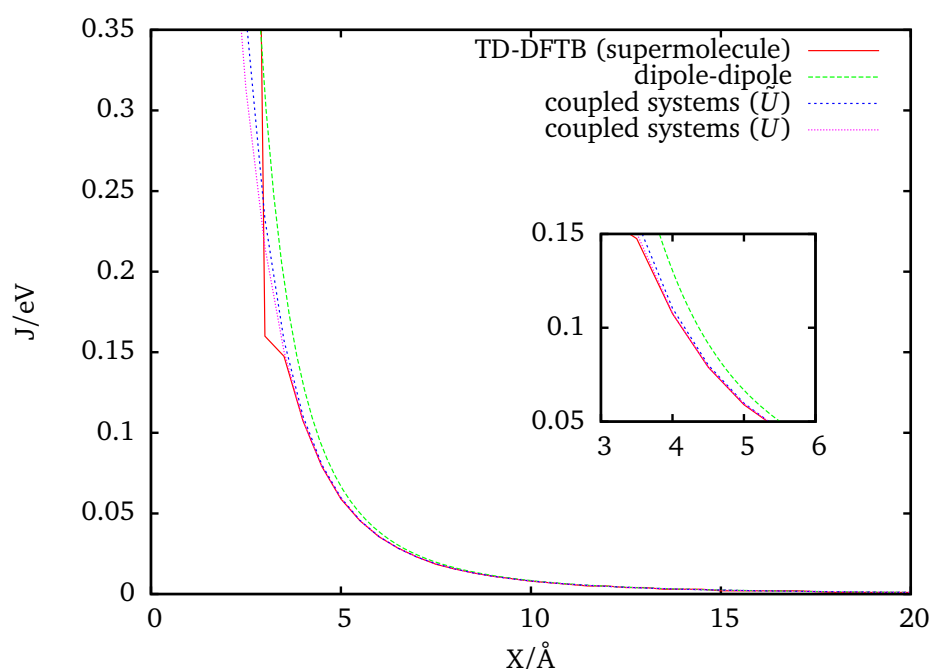


**Figure 3.5.:** TD-DFTB based methods to calculate the coupling strength of the formaldehyde oxime (values are calculated with a stepsize of  $0.5 \text{ \AA}$ , for a better viewing the lines result from a fitting procedure)

The Mulliken transition charges of the monomer are pictured in Figure 3.4. For a parallel orientation the distance  $X$  between the two monomers is varied from  $0.5 \text{ \AA}$  to  $20.5 \text{ \AA}$ . The values of  $J$  obtained by the different methods mentioned above are compared.

Before the tight-binding procedure is compared to results based on common DFT, the TBFE method is classified in the context of the other TD-DFTB based methods like the supermolecule calculation and the dipole-dipole approximation (with  $\vec{d}$  calculated by TD-DFTB). Additionally to that, Figure 3.5 shows the TBFE coupling calculated with the original Hubbard derivatives  $U$ .

For large distances the supermolecular calculation, the subsystem-TD-DFTB and the dipole-dipole approximation, which has a  $1/X^3$  dependency, show good agreement. For intermediate distances the three tight-binding methods fall below the most simple approximation. This is congruent with the fact that in a parallel transition dipole orientation the next best approximation, the extended dipole approximation, is always below the point dipole-dipole approximation which can be shown.

At 3 Å the supermolecular calculation shows a salient point and differs from the TBFE calculation for smaller distance. A detailed analysis of the contributing Kohn-Sham transitions revealed that there are two CT transition with energies below the coupled  $S_0 \rightarrow S_1$  for larger distances. For approaching monomers these energies are increasing. At 3 Å they reached the lowest non-CT transition, leading to a mixing of CT and non-CT transitions. Such CT transition are excluded in TBFE and therefore it deviates from the supermolecular calculation below this distance.

The deviation resulting for the coupled system method according the choice of  $U$  or  $\tilde{U}$  indicates the contribution of exchange part to the coupling. The magnified detail in Figure 3.5 shows that TBFE, which includes the full coupling, is practically not distinguishable from the supermolecular calculations. Neglecting this contribution which is approximatively equivalent to use  $\tilde{U}$ , in the calculation of  $\zeta_{\alpha\beta}(R)$  provides slightly larger coupling strengths. It can be gathered that the Coulomb part is dominant in the total coupling for the distance as presented here.

The comparison with DFT based methods starts with the calculation of the transition dipole moments  $d$  of the monomer by the different methods:

$$\text{TD-DFTB} : d = 1.44$$

$$\text{TD-DFT(B3LYP)} : d = 1.08$$

$$\text{TD-DFT(PBE)} : d = 0.92.$$

While the spatial orientation is nearly the same, the absolute values differ clearly and can be explained by the TD-DFTB faults discussed in Section 2.4.4. This is a first indication of a difference between the methods, at least for large intermolecular distances, where the coupling strength should converge to the dipole-dipole approximation.

The comparison of the coupling strength to conventional DFT based methods is shown in Figure 3.6. For large distances they are all smaller than the TBFE method, like it has been expected from the transition dipole calculations. The DFTB(PBE) supermolecule calculation shows a non-monotonic behaviour for distance larger than 9 Å. For distances smaller than 5 Å it is not possible to identify the transitions in both supermolecular

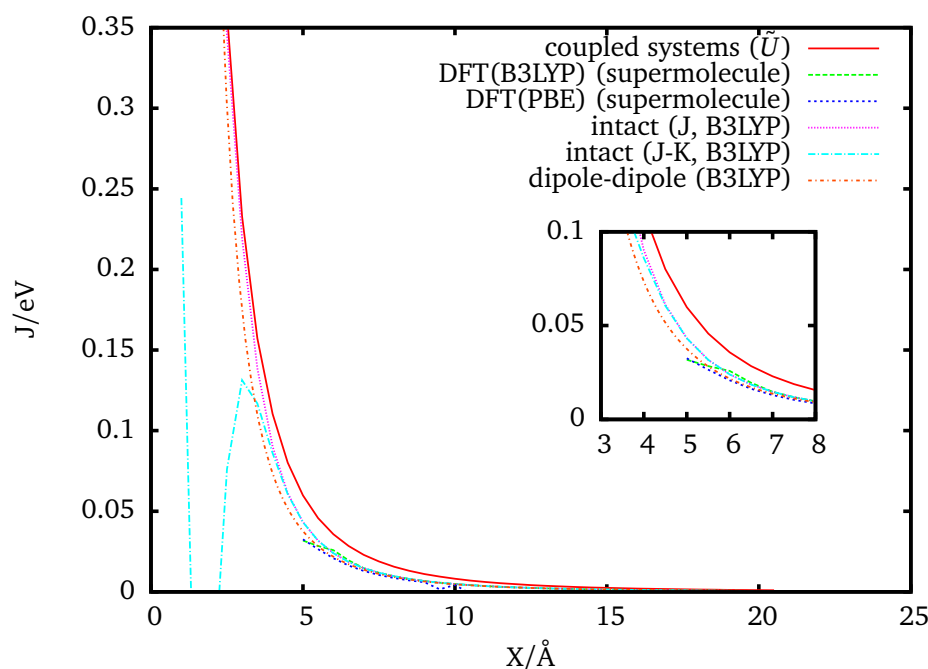


**Figure 3.6.:** TBE compared to various DFT based methods (values are calculated with a stepsize of  $0.5 \text{ \AA}$ , for a better viewing the lines result from a fitting procedure)

DFT calculation. These behaviours indicate the suffering from fractional charge errors. At certain configurations a CT transition with an underestimated transition energy may fall below the transition which represents a local excitation and modifies the results for the coupling strengths by a transition mixing [77]. Such problems are excluded in the calculations with the intact program. In contrast to the statements above its results are above the point-dipole-dipole coupling strength. For distances below  $4 \text{ \AA}$  the exchange part is dominating, indicating that the spatial overlap between the molecular orbitals is not negligible.

### 3.1.2. Dependence of the Coupling Strength on the Angle

With a center of mass distance fixed at  $5 \text{ \AA}$  both molecules are tilted in a sense that the transition dipole moment is slanted towards  $\vec{X}$  as indicated in Figure 3.3. The progression of the coupling for TD-DFTB based methods may be found in Figure 3.7.

Again, the sub-system like formulation of the coupling strength gives results in accordance to the supermolecular TD-DFTB. For small angles both are below the dipole-dipole approximation, which is analysed above. An equivalent explanation can be used for tilt angles close to  $90^\circ$ . For these angles it can be shown that any extended dipole approximation

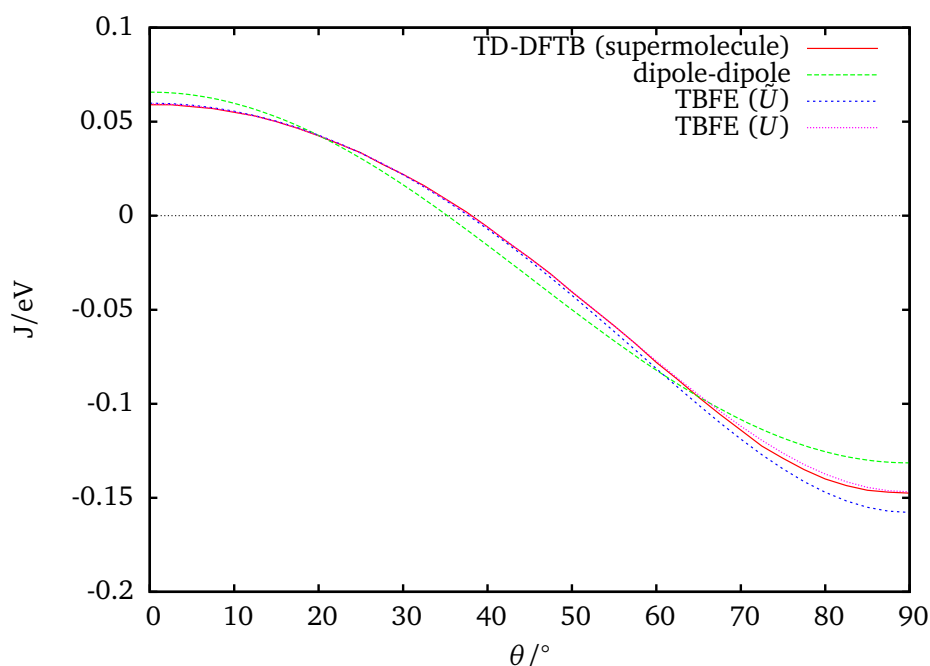


**Figure 3.7.:** TD-DFTB based methods to calculate the coupling of the formaldehyde oxime for different tilt angles  $\theta$  (values are calculated with a stepsize of  $2.5^\circ$ , for a better viewing the lines result from a fitting procedure)

leads to a stronger coupling than the point dipole-dipole approximation. In this range the deviation between the two differently parametrised TBFE calculations grows significantly, since the extension of the molecule is not negligible compared to the displacement. This means the overlap between the orbitals of the different molecules contributes to the results.

Unfortunately, the TBFE results cannot be reproduced by the supermolecular TD-DFT calculations (B3LYP as well as PBE and PBE0, both not shown) as it is illustrated in Figure 3.8. They do not produce a dipole-approximation-like behaviour and the coupling strengths differ strongly for close tilt angles. The reasons may be found in the fractioned charge. The intact calculations reproduce qualitatively the dipole-dipole behaviour. Comparing the Coulomb interaction ( $J$ ) with the full coupling ( $J - K$ ), the difference is much smaller than the TD-DFTB calculations would indicate. Since the transition dipole moment is larger calculated by TD-DFTB than by TBFE predicts a stronger coupling than the electronic coupling matrix calculation based on DFT does, without being able to say which is closer to experimental results.

These two geometry manipulations have shown that the TBFE method is consistent with supermolecular TD-DFTB calculations. Differences to TD-DFT calculations are related

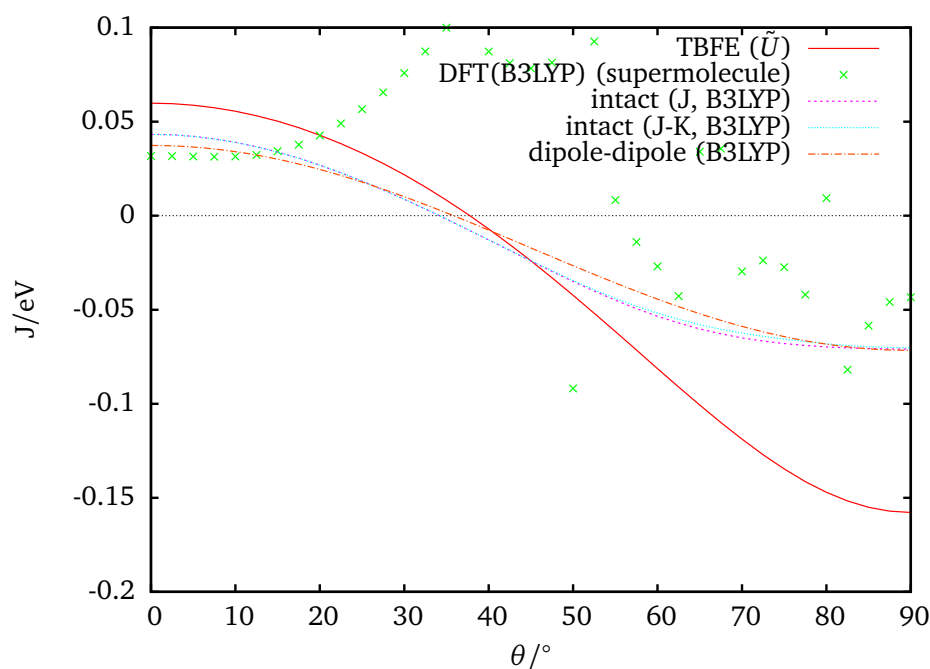


**Figure 3.8.:** TBFE compared to various DFT based methods for different tilt angles  $\theta$  (values are calculated with a stepsize of  $0.5 \text{ \AA}$ , for a better viewing the lines result from a fitting procedure)

to the differences of transition dipoles. The case of tilted monomers shows that TD-DFT calculations for separated systems cannot be used as a benchmark for the proposed method.

## 3.2. Perylene Bisimide Dye

As the coupled-system TD-DFTB method has been tested on the formaldehyde oxime dimer as a model, it is now applied to a system of larger chromophores. Perylene Bisimide has an extensive set of derivatives composing to different forms of aggregates [78]. Those arranging to J-aggregates are of special interest since they offer a high fluorescence. PBI-1 (N,N'-di(N-(2-aminoethyl)-benzamide)-1,6,7,12-tetra(4-*tert*-butylphenoxy)-3,4:9,10-perylenbiscarboximide) (see Figure 3.9) is one of these dyes with spectra pointing to a J-aggregate-like characteristic [79]. It is synthesised by imidisation of *tert*-butyl-phenoxy perylene tetracarboxylic acid bisanhydride with aminoethyl-tris(dodecyloxy)benzamide in quinoline using  $\text{Zn}(\text{OAc})_2$  as catalyst [80]. Its aggregation structure itself is still unclear.



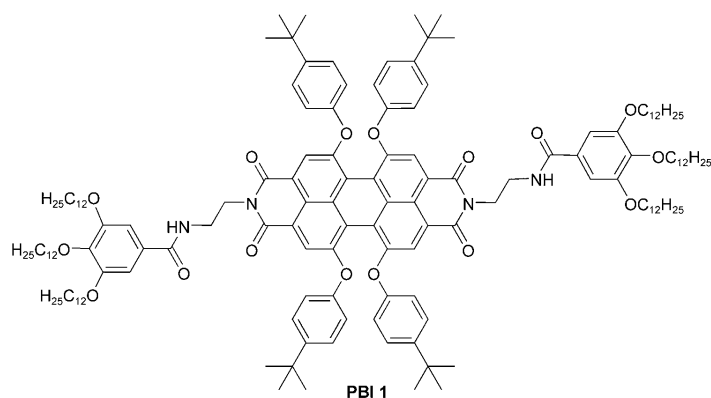


Figure 3.9.: Molecular structure of PBI-1[80]

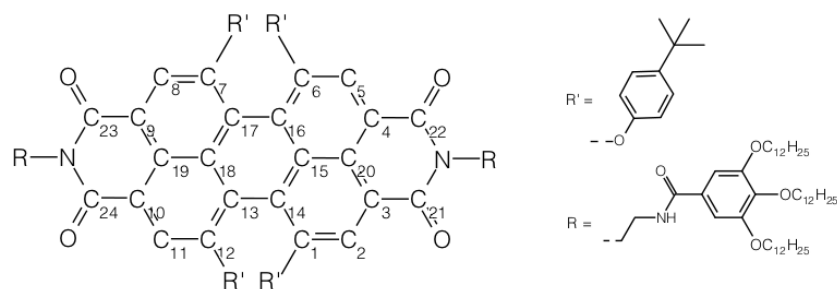


Figure 3.10.: Molecular structure in its dissected form [81], the groups R and R' are replace by H

### 3.2.1. Geometry of Monomer and Dimer

A DFT(B3LYP) geometry optimisation as it has been described and published in [81] is used for further calculation and comparison. This monomer structure as well as the dimer structure [82] have been optimised for a reduced molecule (see Figure 3.10). The *tert*-butyl groups on the phenoxy groups as well as the six dodecyloxy groups are replaced by a hydrogen atom. Various tests have shown that a geometry for this structure can be well reproduced by a DFTB geometry optimisation as shown in Figure 3.11. The root mean square distance between the atomic sites predicted by the two methods is for the PBI-core (as shown in Figure 3.10 without rests) 0.21 Å.

### 3.2.2. Electronic Structure of the PBI Monomer

To exclude effects of different structures and to allow a comparison with the DFT(B3LYP) results all calculations are carried out by the geometries obtained with the DFTB geometry optimisation. DFT calculations are performed with different functionals (B3LYP, PBE and

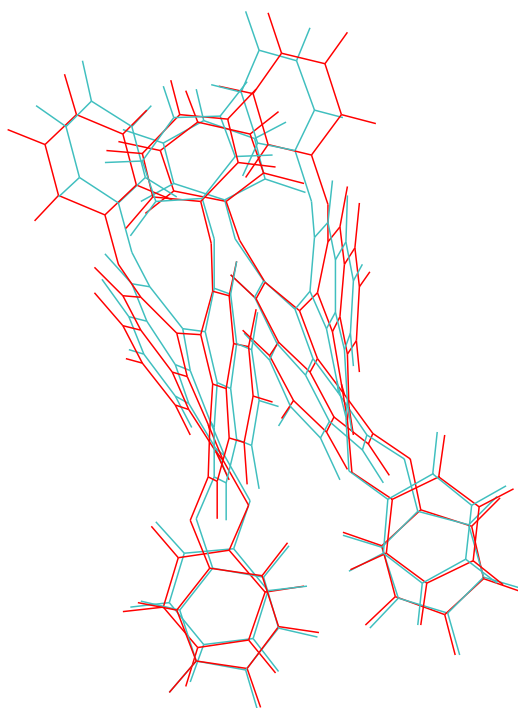


**Figure 3.11.:** Geometry optimisation with DFTB (blue) and DFT/B3LYP (red)

PBE0). Using the B3LYP functional the  $S_0 \rightarrow S_1$  excitation energy results in 2.11 eV, the hybrid functional PBE0 results in 2.18 eV for this transition. The PBE functional offers several transitions which can be identified as CT transition by their oscillator strength close to zero. In contrast to other transitions they are typically composed of only one Kohn-Sham transition. A third criterion is that the two involved orbitals are located in different regions of the molecule. The first non-CT transition is for a calculation using a PBE functional at 1.82 eV. By comparing the Kohn-Sham orbitals of the leading transitions qualitatively it is possible to connect the transition between the different methods. Table 3.1 summarises the transitions. Since PBE0 is a hybrid functional it is not susceptible to problems connected to CT states in the present case.

In the TD-DFTB scheme it is as well possible to calculate the molecular orbitals and as the electronic transitions of the PBI monomer. The TD-DFTB calculations (the input may be found in Appendix C) suffer from the CT-excitation like DFT(PBE) does. Figure 3.12 shows a qualitatively good agreement of the HOMO and LUMO for TD-DFTB and DFT computations.

This facilitates the possibility to assign the transitions obtained by the different methods listed in Table 3.1. Similar to DFT(PBE) TD-DFTB provides CT transitions below the first excitation offered by DFT(B3LYP). They are easily identified as described above.

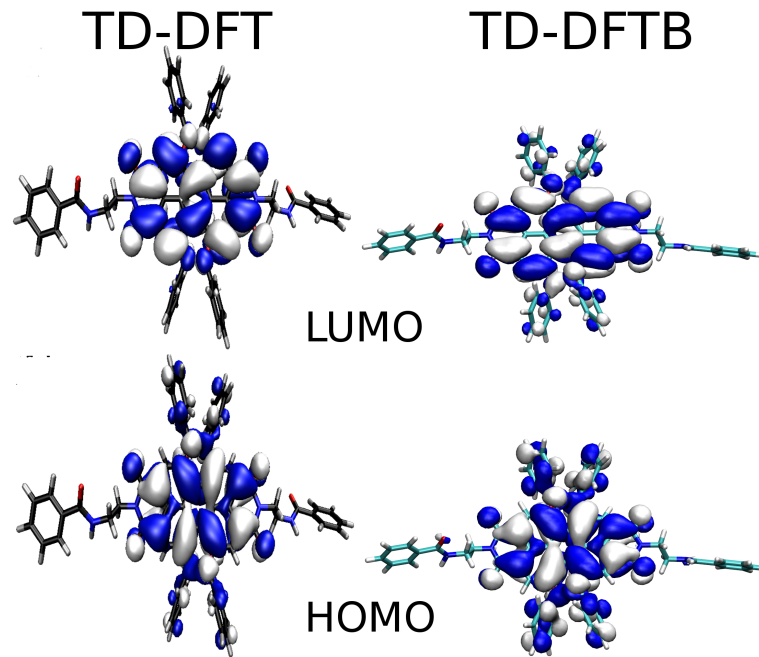


Figure 3.12.: HOMO and LUMO obtained by TD-DFT and TD-DFTB

B3LYP			PBE			PBE0			TDDFTB		
Leading	f	E/eV	Leading	f	E/eV	Leading	f	E/eV	Leading	f	E/eV
			272-275	0.02	0.65						
			271-275	0.01	1.76						
									193-195	0.00	1.47
									192-195	0.00	1.47
274-275	0.58	2.11	274-275	0.38	1.82	274-275	0.61	2.18	194-195	0.40	1.81
									187-195	0.03	2.04
273-275	0.24	2.39	273-275	0.19	1.85	273-275	0.26	2.52	191-195	0.16	2.11
272-275	0.10	2.67				272-275	0.01	2.80			
271-275	0.00	2.68				271-275	0.00	2.84			

Table 3.1.: Assignment of the transition obtained by the different methods, one line signifies transition including same orbitals in the leading transition; the  $S_0 \rightarrow S_1$  excitation ( $\pi \rightarrow \pi^*$ ) is highlighted in colour

The transition dipole moments according to TD-DFT(PBE) and TD-DFTB for the  $S_0 \rightarrow S_1$  excitation are

$$\vec{d}_{\text{PBE}} = \begin{pmatrix} 2.83 \\ 0.59 \\ 0.47 \end{pmatrix} \quad \vec{d}_{\text{TB}} = \begin{pmatrix} 2.91 \\ 0.62 \\ 0.50 \end{pmatrix}$$

which results in a deviation of the absolute values of 3% and of  $0.41^\circ$  in orientation

$$\Delta d = 0.03 \cdot d_{\text{TB}}, \Theta = 0.41^\circ.$$

Together with the structure of the HOMO and the LUMO orbitals this leads to the assumption TD-DFTB can reproduce the DFT(PBE) results of the  $S_0 \rightarrow S_1$  transition. With this identification the electronic structure of the dimer is calculated to evaluate the coupling strength.

### 3.2.3. Electronic Structure of the PBI Dimer

Knowing that the TD-DFTB calculation for the PBI-1 monomer can reproduce at least the DFT(PBE) results, it is applied to the PBI-1 dimer in the following. Starting from a dimer geometry realised in [81] the structure is optimised in DFTB with a Slater-Koster dispersion correction. Since the size of the system is much larger than in the monomer, the dimer with its two conjugated systems is more prone to CT transitions. Due to a distinct mixing of the local excitation, it is more difficult to identify the excitation originating from the local  $S_0 \rightarrow S_1$  transition. In the end the following numbers are found:

E/eV	Osc. strength	lead. transit.	weight	2 <sup>nd</sup> transition	weight
1.711	0.0176388	385-390	0.846	386-389	0.470
1.866	0.4162492	386-390	0.723	385-389	0.571

These transitions are presented in Figure 3.13. Since the blue-shifted transition is brighter, this dimer has H-aggregate character. By the difference of the transition it results that the coupling strength is 0.078 eV. Additionally the Coulomb coupling strength is calculated by TBFE which results in 0.073 eV. For a pure Coulomb coupling,  $\tilde{U}$  values are used instead of the Hubbard parameters.

### 3.2.4. Coupling Strength in Dependence on the Dimer Configuration

The result ascribing an H-aggregate character to the PBI-1 dimers at first glance disagrees to the spectroscopic observation suggesting a J-aggregate [79]. This contradiction can be resolved either with another dimer configuration or with an aggregate structure which is not a sequel of dimers. To form pure J-aggregates a dimer structure bringing forth a

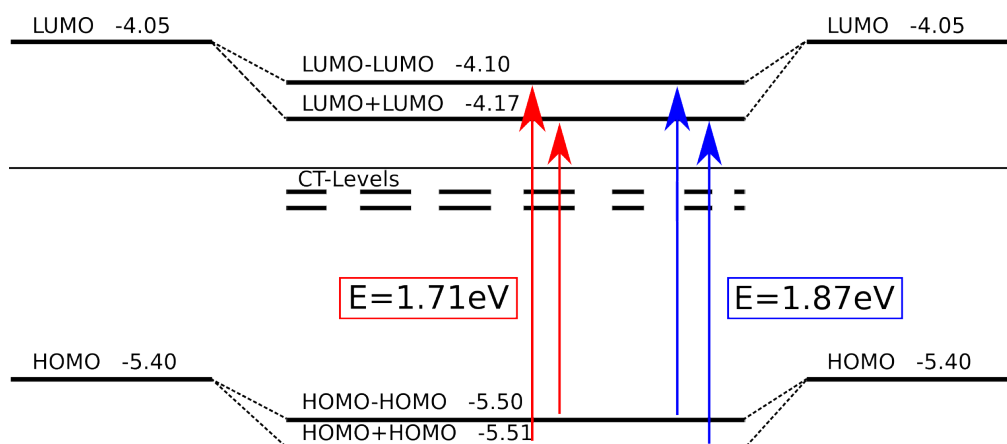


**Figure 3.13.:** Excitation scheme for a PBI-1 dimer (TD-DFTB supermolecule calculation), energies in eV

negative coupling is needed for both cases.

As Figure 3.12 shows at least the  $S_0 \rightarrow S_1$  transition is mainly connected to a charge redistribution on the PBI-core. To purify the coupling to its contribution by these cores a dimer of PBI-cores is regarded for different configurations. Despite removing the side groups the monomers themselves are not modified. This diminishment is not motivated in the numerical effort of the coupling calculation which is a relatively fast process. Keeping the phenoxy and the peptide group would require a geometry optimisation for these groups since the molecule could not be translated as freely as without.

The starting geometry is the dimer optimised with DFT(B3LYP) [82] where all side groups are replaced by hydrogens. In a following geometry optimisation only the position of these added hydrogen atoms are changed. The axes are defined by the principle axes of inertia of monomer one where the x-axis is the long axis. The y-axis is likewise in the PBI-plane and the z-axis is pointing from monomer one to monomer two (see also Figure 3.14).

The configurations are scanned by displacing the second monomer along the three axes and by turning it with the angle  $\phi$  around the z-axis. The calculations are performed in a supermolecule manner with TD-DFTB. Output quantities are the total energy, the gap for the lowest (non CT) excitation, the  $S_1$  energy and the coupling strength.

The first scan is presented in Figure 3.15 for x- and y-direction. On the x-y surface there are four unfavourable areas, where two of the oxygen atoms being originally part of the phenoxy groups come close. The  $S_1$ -level is mainly influenced by this effect. Both in the gap and in the coupling presentation a fine structure is expressed on top of the basis structure. This pattern is existent in both transitions. In these local minima the description of the Kohn-Sham composition of the transition given above and summarised in Figure 3.13 stays true. In the local maxima the Kohn-Sham transition, contributing normally to the lower

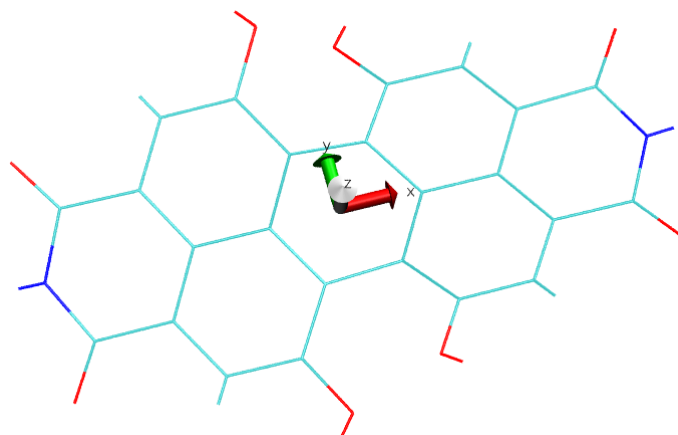


**Figure 3.14.:** PBI-core with axes

and electronic transition, are present in the bright electronic transition. Neglecting the areas which are energetically inaccessible the coupling switches to negative values, in simple terms, by a translation of more than 7 Å in x-direction.

This is still the case for an increased intermolecular distance  $z$ . These scans are shown in Figure 3.16 for  $z = 1$  Å and in Figure 3.17 for  $z = 2$  Å. Here, if not before, it becomes clear that the coupling reaches the lowest values if the monomer is shifted in y-direction as well. The dependency of the coupling on  $z$  is shown in Figure 3.18. Again areas with close oxygen atoms show an extremely high energy. In this scan a negative coupling can again only be achieved for translation of  $\pm 7$  Å. It should be noted that a logarithmic plot is partially used in Figure 3.18.

Varying the twist of the dimer while scanning the translation in x-direction leads to the same results (see Figure 3.19). Again a negative coupling can only be achieved for a clear translation in x-direction.

### 3.2.5. Coulomb Coupling by the TBFE Approach

The TBFE approach provides a way to calculate the coupling in a more efficient way. At the same time any CT transition between the molecules, which make the Frenkel exciton picture not applicable, and a mix between different transitions is avoided. Preparing these calculations the Mulliken transition charges are determined for both molecules. The results for one monomer can be found in Figure 3.20. The resulting coupling for the scans are presented in Figure 3.21. All main features of the supermolecule calculation are reproduced, at least in the energetically accessible configurations. Only the fine patten

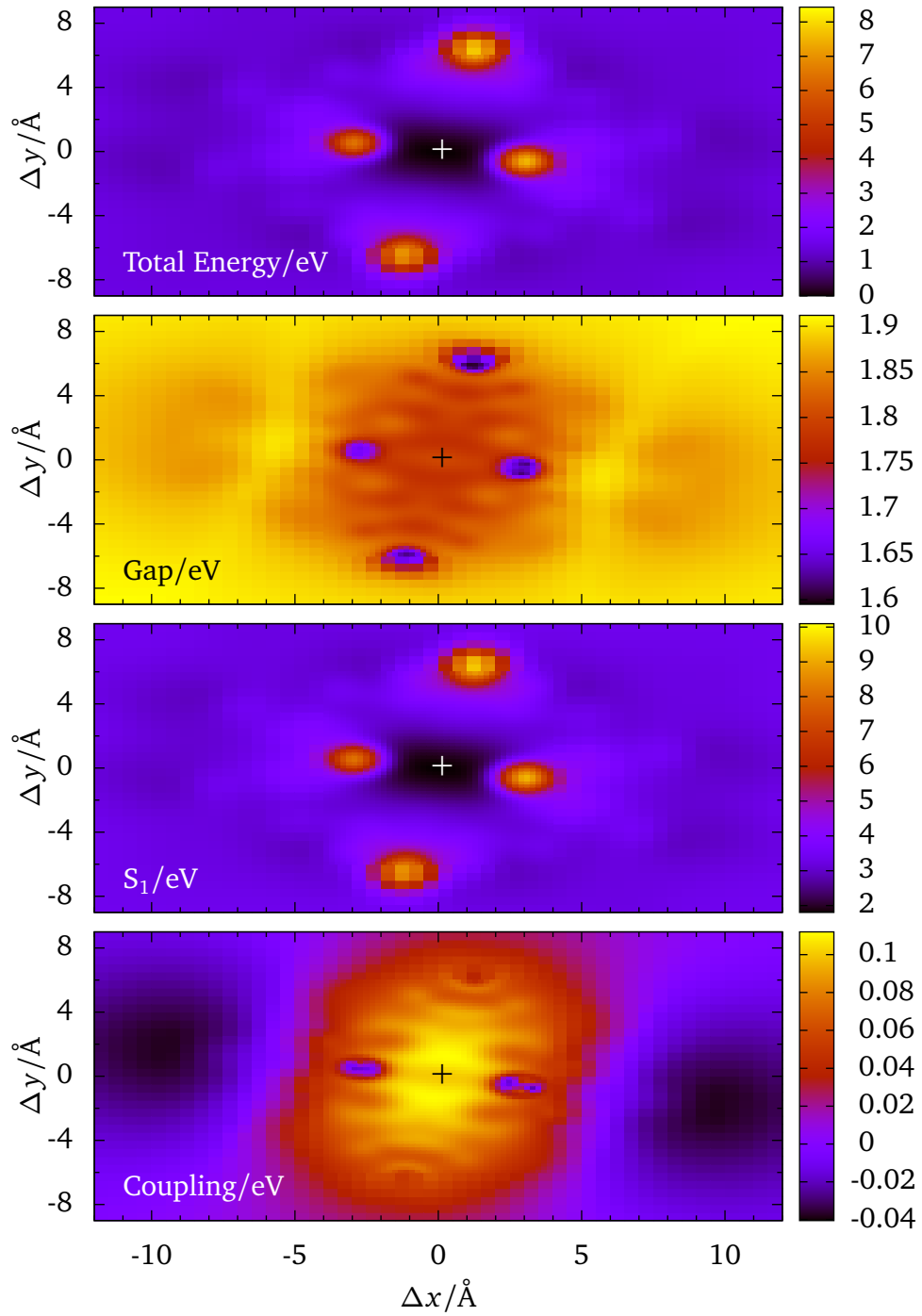


Figure 3.15.: Scan of the deformed dimer in x- and y-direction

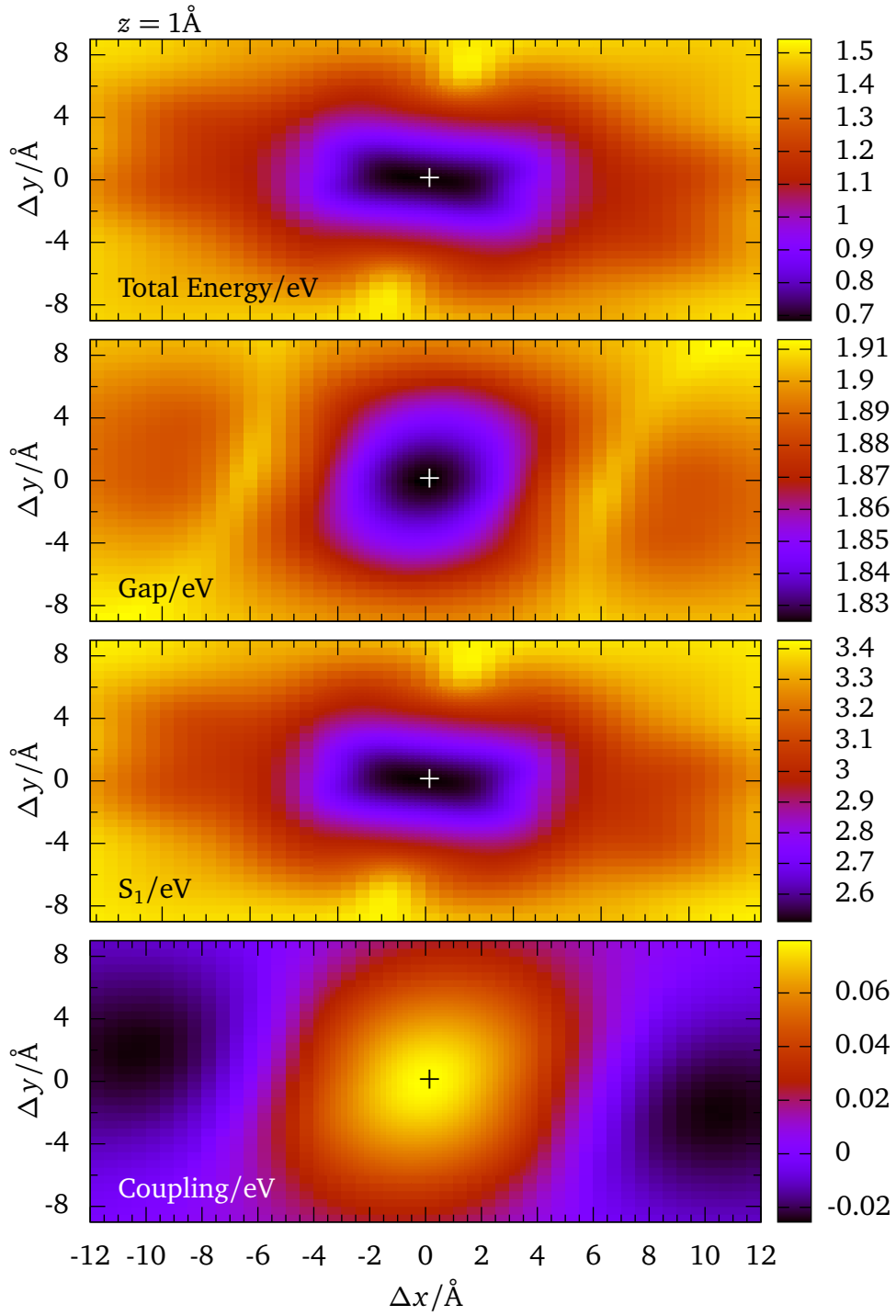


Figure 3.16.: Scan of the deformed dimer in x- and y-direction,  $z=1 \text{ \AA}$



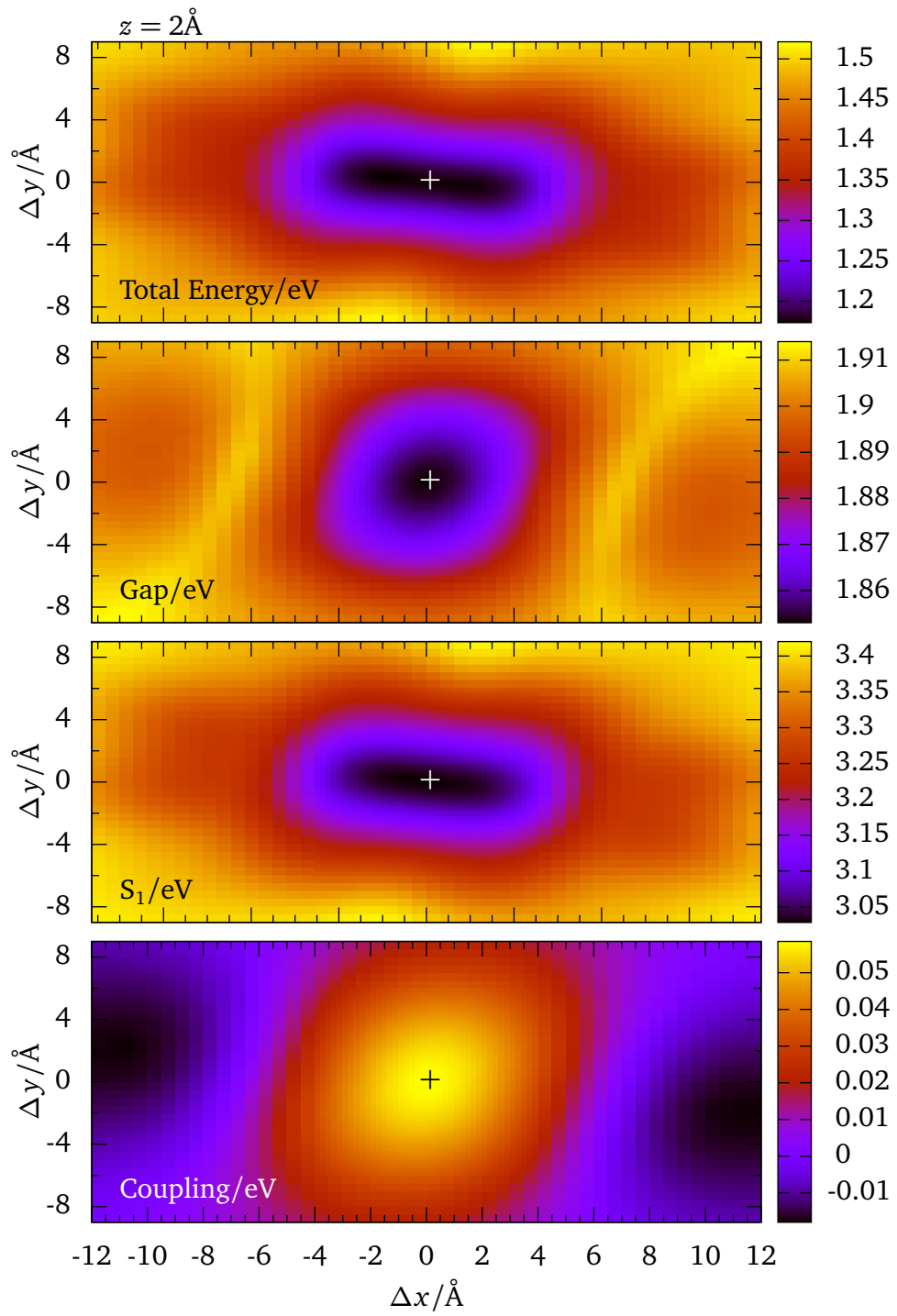


Figure 3.17.: Scan of the deformed dimer in x- and y-direction,  $z=2\text{\AA}$

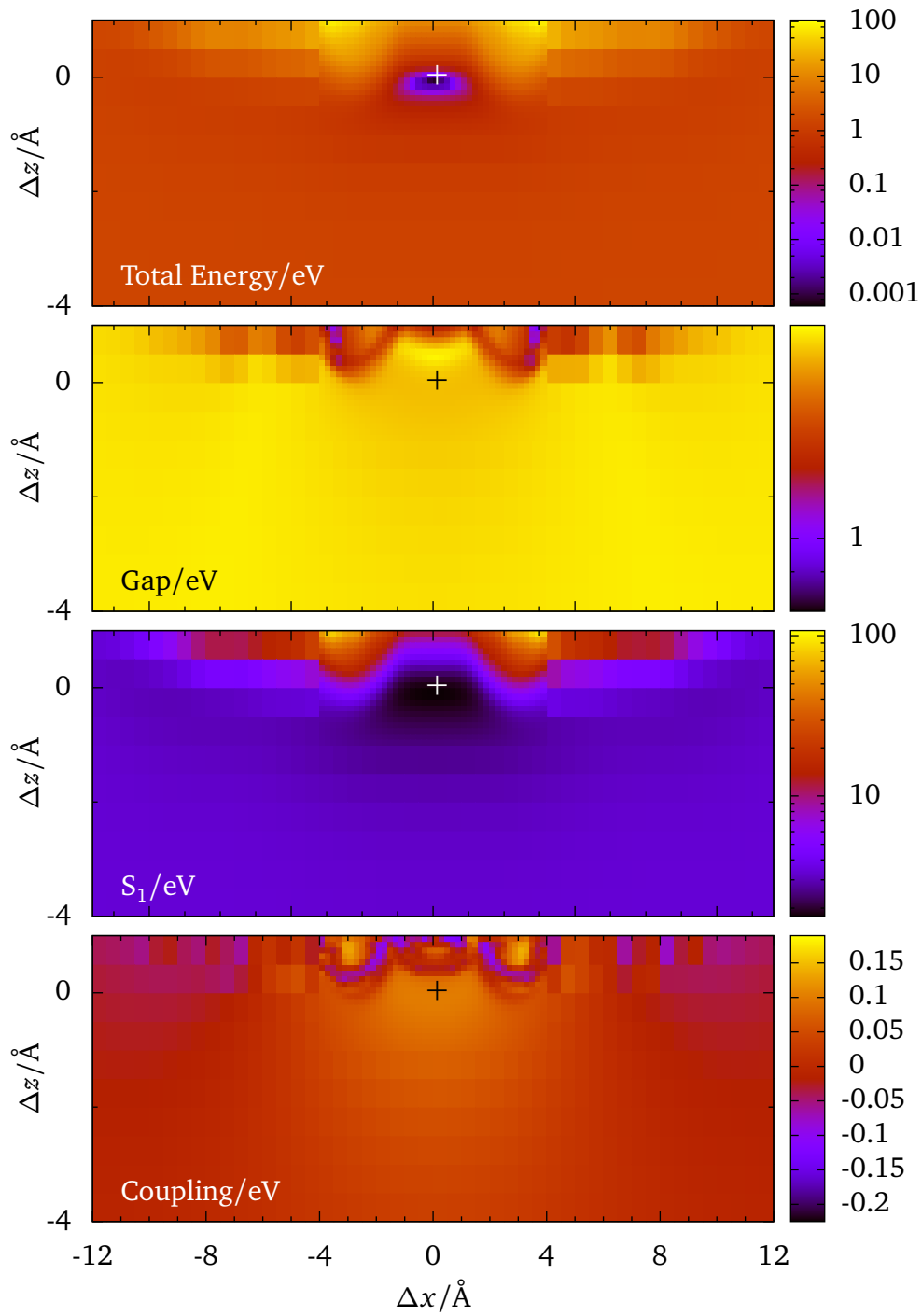


Figure 3.18.: Scan of the deformed dimer in x- and z-direction

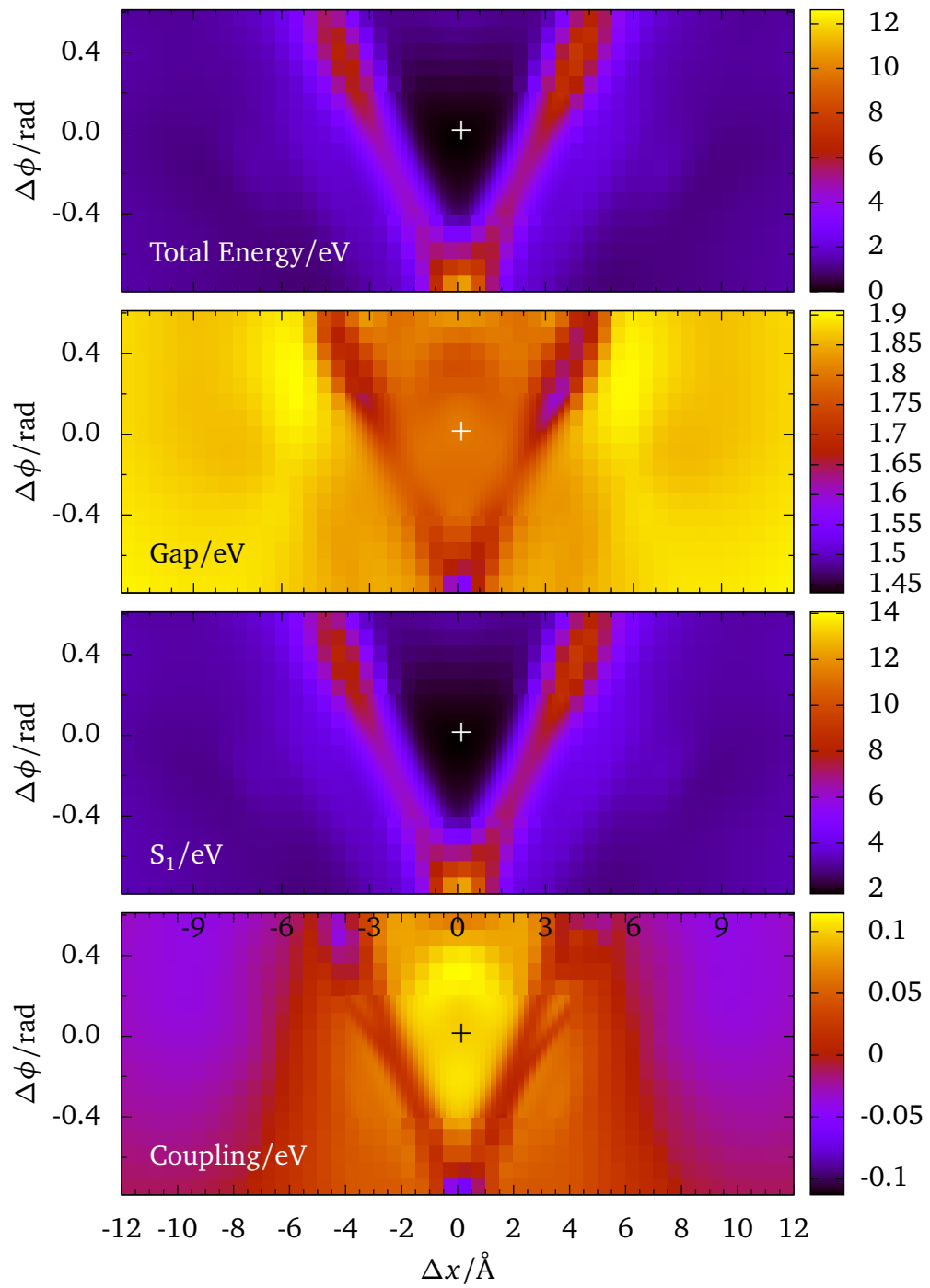
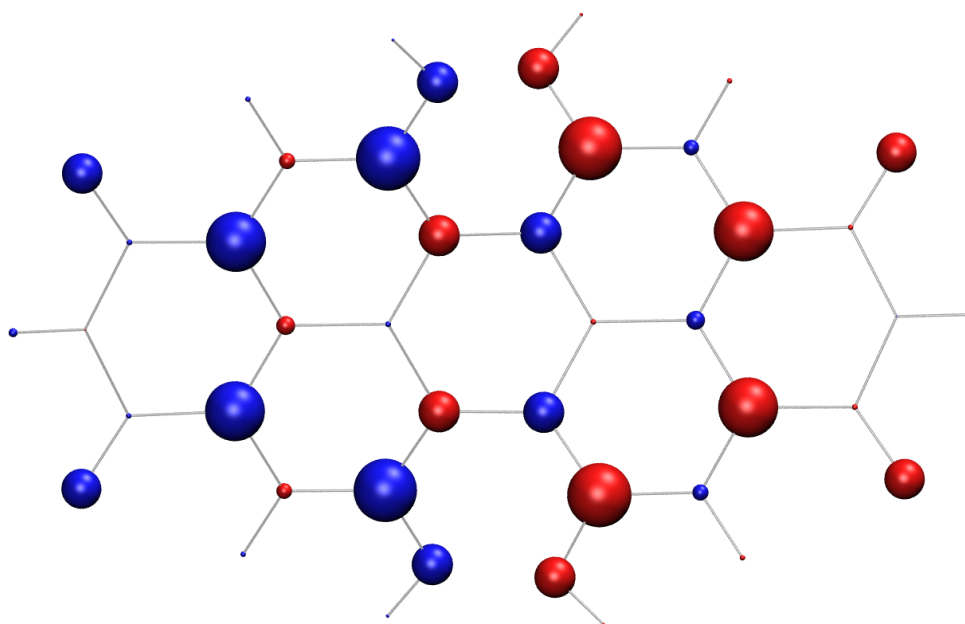


Figure 3.19.: Scan of the deformed dimer in x-direction and turning around the z-axis



**Figure 3.20.:** Mulliken transition charges of PBI-1 monomer, radii are proportional to the absolute value

of the x-y scan around the equilibrium geometry is not visible. Since this stems from the mixing of the transition, it is not visible in this formulation which strictly separates the transition by definition. The change between the values parametrised obtained by using  $U$  instead of  $\tilde{U}$  would be too small to cause a difference in this picture.

The current investigation has only examined the interaction between two transitions ( $J(eg, eg)$ ). All other terms like  $J(eg, ge)$  and  $J(gg, gg)$  and especially  $J(ee, eg)$  are excluded in this state of description. The deviations of the Mulliken charges in the ground state of a dimer compared to two non interacting monomers can only be an indication of the impact of these neglected contributions. In the basic configuration ( $\Delta x = \Delta y = \Delta z = \Delta \phi = 0$ ) the difference of the net atomic charges  $\Delta q_\alpha$  is up to 8% of the net charges in the monomers in the ground state. The main differences are found on the atomic sites which are close to the oxygen atoms of the neighboured molecule. The root mean square of this relative deviations is 0.28. Since the global distribution of the charge fluctuation is not appreciably changed in the dimer, the characteristics of the local transitions should be maintained, but an impact cannot be excluded in general.

The general pattern indicates, as well as the supermolecular calculation does, that there are configurations of the dimer with negative values of  $J$  which would result in J-aggregate characteristics. The necessary changes are rather huge and include a translation of one

monomer of  $\pm 7$  Å in x-direction. It is examined in the next section whether these structures are existent for the dimer and for the aggregate.

### 3.2.6. Aggregation Structure

The results of several works [78, 83, 84, 85] suggest that the actual aggregation structure depends to a great extent on minor changes of the side groups and not only on the  $\pi$ -stacking forces. Consequently, it is questionable for a geometry optimisation to crop the molecule. In contrast to this, the complete molecule would be too demanding for a common DFT based geometry optimisation. Even for a DFTB based optimisation the limits are reached. Nevertheless an annealing DFTB-MD as described in Section 2.4.2 may help finding possible aggregation structures.

Two configurations can be identified. One is found when starting from the cropped dimer configuration. After adding all tert-butyl and dodecyloxy groups an annealing MD with DFTB (for details see Appendix C) is performed and leads to an overlapping configuration shown in Figure 3.23.

This structure stays clearly in the scope of positive coupling constants as determined in the previous chapter. The extension to a tetramer would cause a problematic interlocking of the phenoxy groups including tert-butyl groups. In the dimer configuration the distance can be maximised by groups pointing out of the PBI-plane. This is not possible for longer aggregates which could hinder an aggregation to longer chains in this structure (schematically shown in Figure 3.22).

Alternatively the initial structure is chosen to be a shifted dimer (both dimers may be found in Figure 3.23). One of the monomers is shifted by 10 Å in x-direction. For this configuration an annealing DFTB-MD shows a local minimum for the total energy (see Figure 3.23). While the total energy minimum is of clearly higher value ( $+4$  eV<sup>1</sup>) than the total energy of the structure, described above, the phenoxy groups are not interlocked. That fact seems to allow for J-aggregate formation which is in agreement with the spectroscopic observations. The structure can be found for a tetramer in Figure 3.24, which is calculated in a similar annealing DFTB-MD. The starting point has been two shifted dimers, as obtained in the previous calculation, set together respectively to the translation within the shifted dimer.

These two configurations are candidates for the dimer model proposed by S. Lochbrunner (University Rostock) et al. They observe a change in the absorption/emission spectrum

---

<sup>1</sup>This value should be viewed with caution, since it strongly depends on the starting configuration of the dodecyloxy groups.

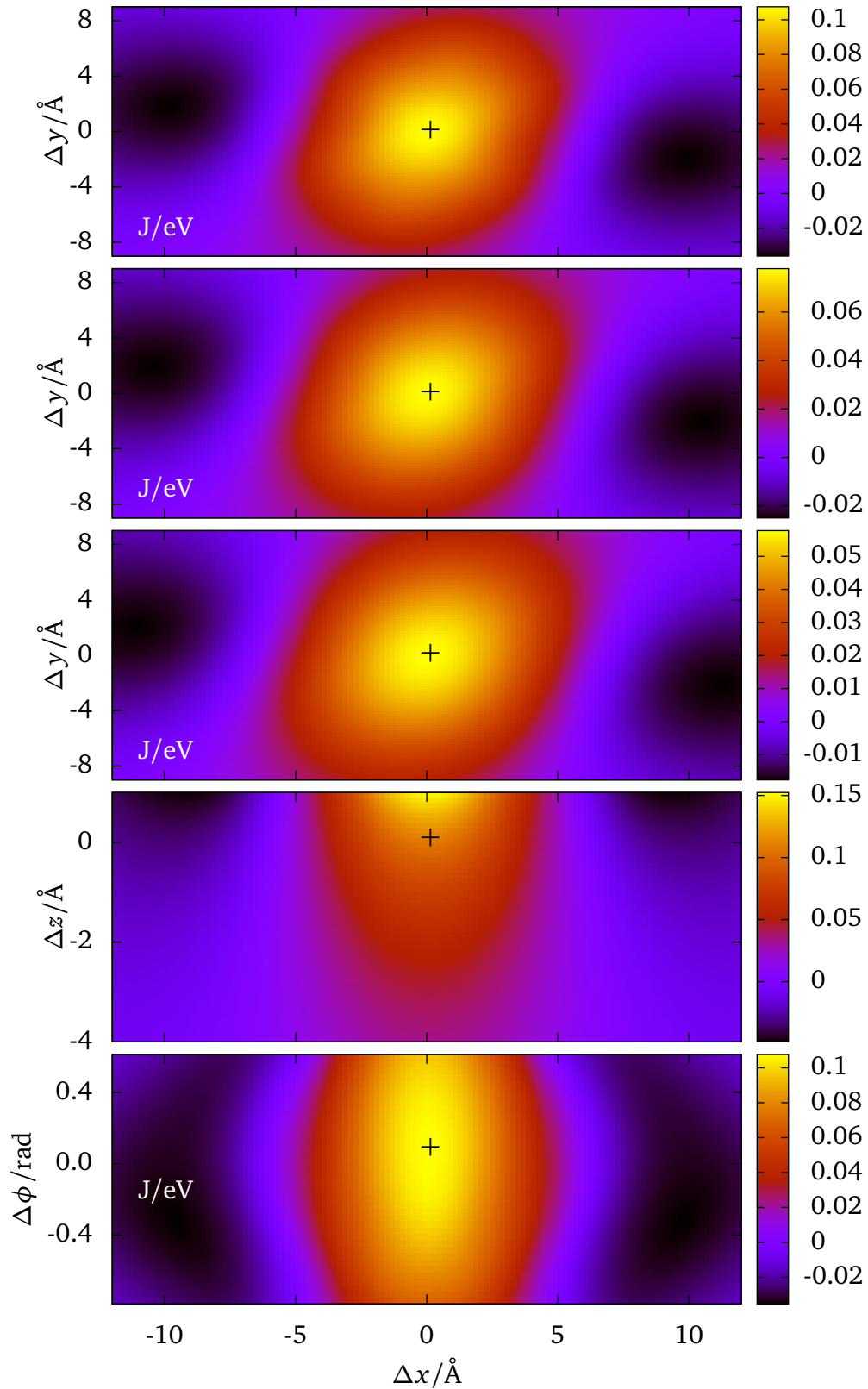


**Figure 3.21.:** Scan of the deformed dimer, coupled-system method, from top to bottom: 1) scan in x- and y-direction 2) same as before with  $z = 1 \text{ \AA}$  3) same as before with  $z = 1 \text{ \AA}$  4) scan in x- and z-direction 5) scan in x-direction and turning around the z-axis

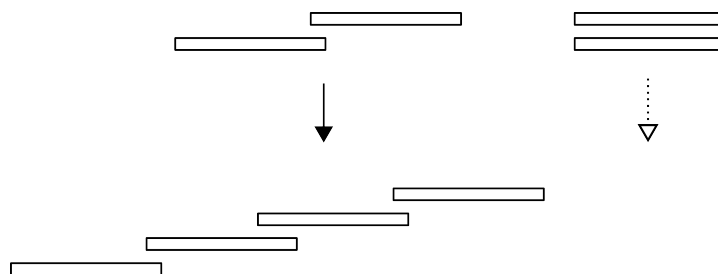


**Figure 3.22.:** Illustration of the different types of PBI-1 dimers; the shifted dimer (left) is the basic component of the aggregate; the planar dimer (right) energetically preferred but cannot form longer chains

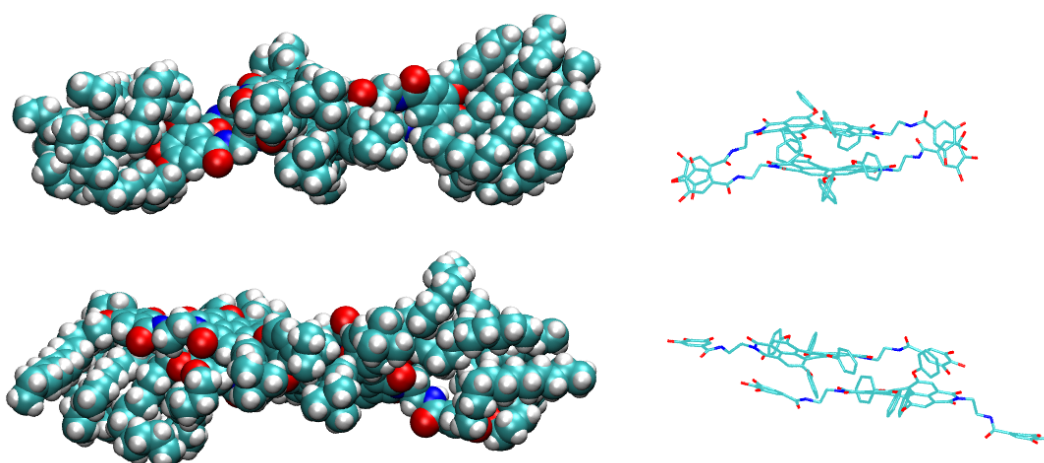


**Figure 3.23.:** Top: planar dimer; bottom: shifted dimer; left: complete structure; right: framework without side groups

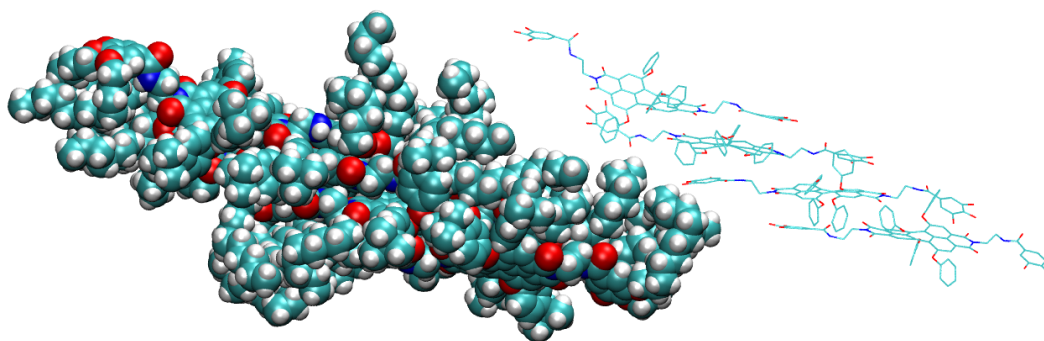


**Figure 3.24.:** Tetramer structure; left: including all groups; right: framework without side groups

when rising the temperature of a PBI-1 solution. While at room temperature the absorption spectra have J-aggregate characteristics, upon raising the temperatures substantial changes appear (reduced fluorescence quantum yield) that are in accord with an H-type aggregation as it is calculated for a dimer in the overlapping case.



## Chapter 4.

### Conclusion

This thesis has considered the theoretical description of Frenkel excitons which are central for understanding excitation energy transfer (EET) in nanomaterials and biological light harvesting systems. The main parameter in the description of these processes is the Coulomb coupling between monomers' excitations. The aim of this work was to develop a new approach for its calculation within the TD-DFTB framework. It was successfully implemented and thus, it was shown that the new method is consistent with supermolecular calculations of conventional TD-DFTB.

TD-DFTB expresses the coupling between Kohn-Sham transitions by Mulliken transition charges. Using them to calculate the Frenkel exciton parameters was the first ansatz. The Coulomb coupling could be expressed by atomic centred transition charges which are a weighted summation of Mulliken transition charges. Since the latter are available from a monomer TD-DFTB calculation the numerical effort to calculate the Coulomb coupling is relatively low.

Alternatively, the Frenkel exciton TD-DFTB formulation starts from an extended formulation of the excitation vector and its corresponding coupling matrix. The dimer is separated into two sub-systems and the interaction between them is formulated. Fixing the allowed transitions to a superposition of the monomers' transitions, which is equivalent to local excitations as assumed in the Frenkel exciton definition, leads to the same expression as obtained with the first ansatz.

This formulation of the Coulomb coupling has been implemented in a TD-DFTB program package which has enabled the comparison to other methods. For this purpose a formaldehyde oxime dimer has been utilised. The geometry of the dimer has been manipulated by varying the distance between the monomers and by tilting them against the displacement vector. For each configuration the introduced method has been compared to other methods. The results of the supermolecular TD-DFTB calculations could be reproduced for large and

intermediate distances. Only for small distances, where the overlap between the orbitals of the monomers is not negligible, deviations are observed. Since common DFT-based methods generate smaller transition dipole moments, they produce lower coupling strengths for all distances. Especially for the tilted monomers the DFT calculations have suffered from known charge transfer problems.

In general, therefore, the proposed method provides the same results as TD-DFTB and is devoid of problems of separated systems. At the same time it is restricted to Frenkel excitons by construction. Above all, the identification of the combined electronic monomer transitions is feasible without limitation. The numerical effort allows for treatment of large systems.

The DFT calculations in a conventional formulation have shown that they are not a possible benchmark for interacting systems. Therefore, it is recommended that further research be undertaken to use other references like the subsystem TD-DFT [86]. Moreover, the reliability of the method developed in this work has to be further tested on a variety of systems.

The progressions in DFTB, like DFTB3 [87], a multipole development of the charge fluctuation [88] and the use of range separated functionals [89], may lead to a better performance of the DFTB ground state calculations and the calculations of the electronic transitions of the monomers.

This perception is encouraged by the results for the PBI-1 dimer. Although the electronic transition energies obtained by TD-DFTB differ from the DFT(B3LYP) transition energies, they are in accordance with the DFT(PBE) results. The coupling is calculated for a wide range of configurations and compared to supermolecular calculations. In general they match in their values and in their dependence of the displacement. Slight differences arise from the transition mixing in the supermolecular calculation which are excluded in the proposed method. Nevertheless, the latter is orders of magnitude faster and does not comprise any problem to identify the transitions.

Both methods show that the PBI-1 dimer in a planar configuration without offset between the PBI cores has a positive coupling. At first sight, this is in contradiction to the experimental results where PBI-1 aggregates show an absorption spectrum that indicates a J-aggregate characteristic. The necessary negative values of the Coulomb coupling can be found for a large displacement of one monomer against the other. This proposes a possible aggregation structure.

With this first application of the new method to calculate the Coulomb coupling consistent to TD-DFTB it may offer a possibility, surely after additional modification and further analysis as described above, to determine Frenkel exciton parameters along a MD trajectory.

In such an implementation the structural propagation is described by the DFTB forces. The electronic transitions of the separated monomers can be calculated for each step. Using these to obtain the Coulomb coupling in the described way would include all intra- and intermolecular vibrational effects and structural changes in the aggregate.

This procedure may help to achieve the long time goal having a efficient, flexible and broadly applicable method for Frenkel exciton simulations for a broad class of materials met in organic electronics and complex light harvesting systems.



# Appendix A.

## Derivations

### A.1. Coulomb Interactions of Two Slater-Type Orbitals

Starting from Eq. (2.62) the integrations over  $\vec{r}'$  is carried out. W.l.o.g the system is translated to  $\vec{R}_\alpha$ , the distance between the atomic sites is  $\vec{R} = \vec{R}_\alpha - \vec{R}_\beta$ .

$$\gamma_{\alpha\beta} = \iint \frac{1}{|\vec{r} - \vec{r}'|} \frac{\tau_\alpha^3}{8\pi} e^{-\tau_\alpha|\vec{r}'|} \frac{\tau_\beta^3}{8\pi} e^{-\tau_\beta|\vec{r}+\vec{R}|} d\vec{r}' d\vec{r} \quad (\text{A.1})$$

$$= \int \left[ \iiint \frac{r' 2 \sin \theta'}{\sqrt{r^2 + r'^2 - 2rr' \cos \theta'}} \frac{\tau_\alpha}{8\pi} e^{-\tau_\alpha r'} dr' d\theta' d\phi' \right] \frac{\tau_\beta^3}{8\pi} e^{-\tau_\beta|\vec{r}+\vec{R}|} d\vec{r} \quad (\text{A.2})$$

$$= \int \left[ \iint \frac{r'}{\sqrt{u} 2r} \frac{\tau_\alpha}{4} e^{-\tau_\alpha r'} dr' du \right] \frac{\tau_\beta^3}{8\pi} e^{-\tau_\beta|\vec{r}+\vec{R}|} d\vec{r} \quad (\text{A.3})$$

$$= \int \left[ \int \frac{r'}{r} \sqrt{u} \frac{r^2+r'^2+2rr'}{r^2+r'^2-2rr'} \frac{\tau_\alpha}{4} e^{-\tau_\alpha r'} dr' \right] \frac{\tau_\beta^3}{8\pi} e^{-\tau_\beta|\vec{r}+\vec{R}|} d\vec{r} \quad (\text{A.4})$$

$$= \int \left[ \int \frac{r'}{r} (|r+r'| - |r-r'|) \frac{\tau_\alpha}{4} e^{-\tau_\alpha r'} dr' \right] \frac{\tau_\beta^3}{8\pi} e^{-\tau_\beta|\vec{r}+\vec{R}|} d\vec{r} \quad (\text{A.5})$$

$$= \int \left[ \frac{\tau_\alpha}{4} \left( \int_0^r \frac{r'^2}{r} e^{-\tau_\alpha r'} dr' + \int_r^\infty r' e^{-\tau_\alpha r'} dr' \right) \right] \frac{\tau_\beta^3}{8\pi} e^{-\tau_\beta|\vec{r}+\vec{R}|} d\vec{r} \quad (\text{A.6})$$

$$= \int \left[ \frac{1}{|\vec{r}|} - \left( \frac{\tau_\alpha}{2} + \frac{1}{|\vec{r}|} \right) e^{-\tau_\alpha|\vec{r}|} \right] \frac{\tau_\beta^3}{8\pi} e^{-\tau_\beta|\vec{r}+\vec{R}|} d\vec{r} \quad (\text{A.7})$$

The integration over  $\vec{r}$  is performed by translating the system by  $\vec{R}/2$  and by introducing prolate spheroidal coordinates:

$$\xi = \frac{|\vec{r}| + |\vec{r} - \vec{R}|}{R} \quad (\text{A.8})$$

$$\eta = \frac{|\vec{r}| - |\vec{r} - \vec{R}|}{R} \quad (\text{A.9})$$

$$(\text{A.10})$$

Hence, from this definition it follows that

$$|\vec{r}| = \frac{R}{2}(\xi + \eta) \quad (\text{A.11})$$

$$|\vec{r} - \vec{R}| = \frac{R}{2}(\xi - \eta) \quad (\text{A.12})$$

$$d\vec{r} = \frac{1}{8}R^3(\eta^2 - \xi^2)d\eta d\xi d\phi \quad (\text{A.13})$$

With these  $\gamma_{\alpha\beta}$  becomes

$$\gamma_{\alpha\beta} = \int_0^{2\pi} \int_1^\infty \int_{-1}^1 \left[ \frac{2}{R(\xi + \eta)} - \left( \frac{\tau_\alpha}{2} + \frac{2}{R(\xi + \eta)} \right) e^{-\tau_\alpha \frac{R}{2}(\xi + \eta)} \right] \quad (\text{A.14})$$

$$\times \frac{\tau_\beta^3}{8\pi} e^{-\tau_\beta \frac{R}{2}(\xi - \eta)} \frac{1}{8} R^3 (\eta^2 - \xi^2) d\eta d\xi d\phi \quad (\text{A.15})$$

$$= \int_0^{2\pi} \int_1^\infty \int_{-1}^1 \left[ \frac{2}{R(\xi + \eta)} - \left( \frac{\tau_\alpha}{2} + \frac{2}{R(\xi + \eta)} \right) e^{-\tau_\alpha \frac{R}{2}(\xi + \eta)} \right] \quad (\text{A.16})$$

$$\times \frac{\tau_\beta^3}{32} e^{-\tau_\beta \frac{R}{2}(\xi - \eta)} R^3 (\eta^2 - \xi^2) d\eta d\xi \quad (\text{A.17})$$

$$= \frac{e^{-R\tau_\alpha}}{2R(\tau_\alpha^2 - \tau_\beta^2)^3} \left[ \tau_\alpha^2(6 + R\tau_\alpha)\tau_\beta^4 - (2 + R\tau_\alpha)\tau_\beta^6 - 2e^{R\tau_\alpha}(\tau_\alpha^2 - \tau_\beta^2)^3 \right] \quad (\text{A.18})$$

$$+ e^{R(\tau_\alpha - \tau_\beta)} \tau_\alpha^4 \left( \tau_\alpha^2(2 + R\tau_\beta) - \tau_\beta^2(6 + R\tau_\beta) \right) \quad (\text{A.19})$$

$$= \frac{1}{R} - \left[ e^{-\tau_\alpha R} \left( \frac{\tau_\beta^4 \tau_\alpha}{2(\tau_\alpha^2 - \tau_\beta^2)^2} - \frac{\tau_\beta^6 - 3\tau_\beta^4 \tau_\alpha^2}{(\tau_\alpha^2 - \tau_\beta^2)^3 R} \right) + e^{-\tau_\beta R} \left( \frac{\tau_\alpha^4 \tau_\beta}{2(\tau_\beta^2 - \tau_\alpha^2)^2} - \frac{\tau_\alpha^6 - 3\tau_\alpha^4 \tau_\beta^2}{(\tau_\beta^2 - \tau_\alpha^2)^3 R} \right) \right]. \quad (\text{A.20})$$

## A.2. Limit for $\gamma_{\alpha\alpha}$

For  $\tau_\beta = \tau_\alpha$  Eq. (A.14) is

$$\gamma(\tau_\alpha, \tau_\alpha, R) = e^{-R\tau_\alpha} \left( \frac{1}{R} + \frac{\tau_\alpha}{48} (33 + 9R\tau_\alpha + R^2\tau_\alpha^2) \right) - \frac{1}{R}. \quad (\text{A.21})$$

Its limits for  $R \rightarrow 0$  is derived by expanding the exponential term:

$$\gamma_{\alpha\alpha} = \lim_{R \rightarrow 0} (1 - R\tau_\alpha + \dots) \left( \frac{1}{R} + \frac{\tau_\alpha}{48} (33 + 9R\tau_\alpha + R^2\tau_\alpha^2) \right) - \frac{1}{R} \quad (\text{A.22})$$

$$= -\tau_\alpha + \frac{33}{48}\tau_\alpha \quad (\text{A.23})$$

$$= \frac{5}{16}\tau_\alpha \quad (\text{A.24})$$

# Appendix B.

## Program Source Code

### B.1. Extract of Modified Linear Response Calculation

This extract shows how the atomic centred Mulliken transition charges are extracted from a linear response calculation in TDDFTB<sup>+</sup>.

```
C      repmax:  Maximal size of response matrix
nexc:    Number of excitations
nmat:    Number of KS transitions
mxditr:  Number of maximal iterations
ido:     Status of diagonalisation
z:       Excitation vector
nn:      Number of atoms
idm:     List of all possible transitions
qovers:  Weighted sum of qover for transition
.....

C      diagonalizing response matrix
abstol = 2*dlamch('S')
do i=1,(repmax*(repmax+1))/2
enddo
ncv = 3*nexc
if(ncv.gt.nmat) ncv = nmat
lworkl = ncv*(ncv+8)
info = 0
ido = 0
```



```

    iparam(1) = 1
    iparam(3) = mxditr
    iparam(7) = 1
102  continue

    call dsaupd (ido, 'I', nmat, 'SM', nexc, tol, resid, ncv,
& z, repmax, iparam, ipntr, workd, workl, lworkl, info)
    if (ido .eq. -1 .or. ido .eq. 1) then
C      The matrix-vector product (TDDFT or RPA Casida)
    call omegatvec(workd(ipntr(1)),workd(ipntr(2)),wij,nmat,nn,
&          'S' ,win,nocc,nhel,ndim,ind,stimc,c,qij,gamma)
    go to 102
    end if
    if ( info .lt. 0 ) then
        print *, 'Error with dsaupd, info = ', info
        stop
    else
        rvec = .true.
        call dseupd ( rvec, 'All', select, w, z, repmax, sigma,
&          'I', nmat, 'SM', nexc, abstol, resid, ncv, z, repmax,
&          iparam, ipntr, workd, workl, lworkl, ierr )
        if ( ierr .ne. 0) then
            print *, 'Error with dseupd, info = ', ierr
            stop
        endif
        if ( info .eq. 1) then
            print *, 'Maximum number of iterations reached.'
            print *, 'Increase # of excited states to solve for.'
            stop
        endif
    end if
    if(info.ne.0) then
        print *, 'Eigenvalue-solver not converged!'
        stop
    endif

```

.....

*C calculate osz. strength*

```
do i = 1,nexc
  sym(i) = 'S'
  osz(i) = 0.0d0
  do l = 1,3
    rfoo = 0.0d0
    do indm = 1,nmat
      rfoo = rfoo +
&      transd(indm,l)*dsqrt(wij(indm))*z(indm,i)
    enddo
    osz(i) = osz(i) + 2.0d0*twothi*rfoo*rfoo
  enddo
enddo
```

*c calculate transition-dipole-moments*

```
do i = 1,nexc
  do l = 1,3
    transdip(i,l) = 0.0d0
    do indm = 1,nmat
      transdip(i,l)=transdip(i,l)+transd(indm,l)*
&      dsqrt(wij(indm))*z(indm,i)*dsqrt(2/dsqrt(w(i)))
    enddo
  enddo
enddo
```

.....

*c Calculation of the atomic centred Mulliken transition charges*

```
do transition = 1,3
  write(filename,1234)transition
1234  FORMAT('QS',I2.2,'.DAT')
  write(*,*)filename
  open(46,FILE=filename)
  write(46,'(1x,a,□4x,□a,□10x,□a,□10x,□a,□10x,□a)') 'Atom','x',
```

```

& 'y','z', 'q10', 'in_au'

rsqw = 1.0d0/dsqrt(w(transition))
do i=1,nn
    qovers(transition,i)=0.0d0
    do j = 1,nmat
        qovers(transition,i)=qovers(transition,i)
& +qover(j,i)*z(j,transition)*dsqrt(wij(j)*rsqw*2)
        enddo
        write(46,'(1x,i3,4f11.5)') i, rat(1,i), rat(2,i),
& rat(3,i),qovers(transition,i)
    enddo
c transition dipol moment by M. trans. charges. to check calc.
do l=1,3
    transtest(1)=0.0d0
    do k=1,nn
        transtest(1)=transtest(1)+
& rat(1,k)*qovers(transition,k)
        enddo
    enddo
    write(46,'(3f10.3)') transtest(1), transtest(2),
& transtest(3)
    close(46)
enddo

```

## B.2. Calculating the Coupling Strength

The following code displays the program to calculate the coupling strength within the TD-DFTB scheme. For a detailed description see Section 2.6.

```

c max number of atoms per monomer, maximal types
integer maxat, maxtype
parameter (maxat=200)
c to do: automatically same in subroutine

```

```
        parameter (MAXTYPE=4)
c names of read files
        character*65 transqm1, transqm2, geom1, geom2
c temp strings
        character*20 st1, st2, st3, st4, st5
c number of atoms in monomers
        integer natoms(2), sumatoms
c elements in monomers
        character type(2,4)
        integer element(2*MAXAT)
c position of atom
        real*8 pos(2,3,MAXAT), rat(3,2*MAXAT)
c transition charge
        real*8 charge(2,MAXAT)
c loop vars
        integer i,m,j, k
c strength of coupling, distance of pair,
c coulombian part (point-point), full Coulomb
        real*8 coupling, r, coulomb, coulombfull
c Uhubb of atom, inputs, of types
        real*8 uhubb(8), uhubbH, ubhubbC, uhubbN,Uhubb0
c Achtung: Bisher alles Us, noch zu klaeren
        parameter (uhubbH=0.4195d0, uhubbC=0.3647d0, uhubbN=0.4309d0,
&                Uhubb0=0.4954d0)
c Uhubb ohne XC
        real*8 uhubbCoul(8), uhubbHCoul, ubhubbCCoul, uhubbNCoul,
&            Uhubb0Coul
        parameter (uhubbHCoul=0.57962094d0, uhubbCCoul=0.51864556d0,
&            uhubbNCoul=0.63092682d0, Uhubb0Coul=0.74161363d0)
c gammamatrix
        real*8 gamma(2*MAXAT,2*MAXAT)
c gammatrix for Coulomb case
        real*8 gammaCoul(2*MAXAT,2*MAXAT)
C conversion hartree -> eV
        real*8 conv
        parameter (conv = 27.21139908d0)
```

```
write(*,*) 'Daten_werden_gelesen'
read *, transqm1, transqm2, geom1, geom2
open(1,file=transqm1, status='old')
open(2,file=transqm2, status='old')
open(3,file=geom1, status='old')
open(4,file=geom2, status='old')
sumatoms=0
k=0
do m=1,2
  read(m+2,*) natoms(m), st1
  if(natoms(m).gt.MAXAT) then
    write(*,*) 'Monomer_zu_gross,_MAXAT_anpassen'
  endif
  read(m+2,*) type(m,1), type(m,2), type(m,3), type(m,4)
c Uhubb: has to be built like in gettab.r (later)
  do i=1,4
    if(type(m,i).EQ.'H') then
      uhubb(i+4*(m-1))=uhubbH
      uhubbCoul(i+4*(m-1))=uhubbHCoul
    else if(type(m,i).EQ.'C') then
      uhubb(i+4*(m-1))=uhubbC
      uhubbCoul(i+4*(m-1))=uhubbCCoul
    else if(type(m,i).EQ.'N') then
      uhubb(i+4*(m-1))=uhubbN
      uhubbCoul(i+4*(m-1))=uhubbNCoul
    else if(type(m,i).EQ.'O') then
      uhubb(i+4*(m-1))=uhubbO
      uhubbCoul(i+4*(m-1))=uhubbOCoul
    else
      write(*,*) 'Element_not_in_list'
    endif
  enddo

  read(m,*)
  read(m,*)
```

```

do i=1,natoms(m)
    k=k+1
    read(m+2,*) st1, element(k)
    element(k)=element(k)+(m-1)*4
    read(m,*) st1, pos(m,1,i), pos(m,2,i), pos(m,3,i),
&        charge(m,i)
    rat(1,k)=pos(m,1,i)
    rat(2,k)=pos(m,2,i)
    rat(3,k)=pos(m,3,i)
enddo
sumatoms=sumatoms+natoms(m)
enddo

c   write(*,*) element(126), pos(2,1,2), pos(2,2,2), pos(2,3,2),
c   & charge(2,2)
c   write(*,*) element(126), rat(1,126), rat(2,126), rat(3,126),
c   & charge(2,2)
do i=1,124
c   write(*,*) pos(2,1,i), rat(1,i+124)
enddo

C   build up gamma matrix
call gammatrixc(sumatoms, rat, element, uhubb, gamma, tr)
C   build up gamma matrix for Coulomb case
call gammatrixc(sumatoms, rat, element, uhubbCoul, gammaCoul, tr)

do k=1, sumatoms
    do j=k+1, sumatoms
        gamma(k,j) = gamma(j,k)
        gammaCoul(k,j) = gammaCoul(j,k)
        tr(k,j)=tr(j,k)
    enddo
enddo

c loop over monomer1
coupling=0.0d0

```

```

        coulomb=0.0d0
        coulombfull=0.0d0
        do i=1,natoms(1)
c loop over monomer2
            do j=1,natoms(2)
                r=dsqrt((pos(1,1,i)-pos(2,1,j))**2+(pos(1,2,i)-pos(2,2,j))
&                    +(pos(1,3,i)-pos(2,3,j))**2)
                coulomb=coulomb+charge(1,i)*charge(2,j)/r
                coupling=coupling+charge(1,i)*charge(2,j)*
&                    gamma(i,natoms(1)+j)
                coulombfull=coulombfull+charge(1,i)*charge(2,j)*
&                    gammaCoul(i,natoms(1)+j)
            enddo
        enddo

        write(*,*) coupling, '□=□', coupling*conv, 'eV'
        write(*,*) coulomb, '□=□', coulomb*conv, 'eV□(pp-Coulomb)'
        write(*,*) coulombfull, '□=□', coulombfull*conv, 'eV
□□□□□&□□□□□(Full-Coulomb)'
        end

c=====
c Build lower triangular matrix containing Ewald potentials + short
c range terms
c VERSION for CLUSTER !!!!
c
c INPUT Parameter:
c INTEGER nat          number of atoms
c REAL*8 rat(3,*)     position of atoms
c REAL*8 u(*)          hubbard parameters

c
c OUTPUT:
c REAL*8 gammamat(*,*) matrix containing the values of the ew pot
c                    in the upper triangular part
c !!! NOTE THAT phi(ri - rj) = phi(rj - ri) !!!

```

```

c      !!! NOTE THAT shortrange(ri - rj) = shortrange(rj - ri) !!!
c
c=====

      SUBROUTINE gammatrixc(nat, rat, atomtype, u, gammamat, testr)
      IMPLICIT NONE
      INTEGER nat
      integer maxat
      parameter (maxat=200)
      REAL*8 rat(3,*), u(8), gammamat(2*MAXAT, 2*MAXAT)
      REAL*8 testr(2*MAXAT, 2*MAXAT)
      INTEGER i, j, atomtype(*)
      REAL*8 r(3)
      REAL*8 gval, norm

      do i=1, nat
         do j=1, i
            r(1)=rat(1, i)-rat(1, j)
            r(2)=rat(2, i)-rat(2, j)
            r(3)=rat(3, i)-rat(3, j)

            norm = sqrt(r(1)**2+r(2)**2+r(3)**2)

c      get value for Gamma
            CALL GAM12(norm, u(atomtype(i)), u(atomtype(j)), gval)
            gammamat(i, j)=gval
         END DO
      END DO

      END

c=====
c
c      gamma resulting from exact Coulomb interaction of normalized
c      exp(-a*r) charge distribution
c      Attention: subroutine gamsub needed

```



```

c
c      input:  r:      distance
c             uhub1: Hubbard parameter orbital 1
c             uhub2: Hubbard parameter orbital 2
c      output: gval:  gamma12 function value
c
c=====

      subroutine gam12(r,uhub1,uhub2,gval)
      IMPLICIT NONE
      REAL*8 zero
      parameter(zero=1.0d-4)
      REAL*8 gval,a1,a2,src,avg,uhub1,uhub2,rrc,rrc3
      REAL*8 val12,val21,drv12,drv21,r,fac,fac2,efac
c      neu fuer H-bonds
      real*8 fhbond,uhubh
      real*8 kl1
c      open(111,file='switch')
c      read(111,*) kl1
c      close(111)
      kl1 = 4.0
      uhubh= 0.4195007d0
      fhbond = 1.0
c      if((uhub1.eq.uhubh).and.(uhub2.ne.uhubh)) then
c      write(*,*) 'uhubh, gamma on',uhubh,uhub1,uhub2
      if ((uhub1.eq.uhubh).or.(uhub2.eq.uhubh)) then
      fhbond= exp(-(((uhub1+uhub2)/2)**kl1)*r**2)
      endif
c      if (uhub2.eq.uhubh) then
c      if((uhub2.eq.uhubh).and.(uhub1.ne.uhubh)) then
c      fhbond= exp(-(((uhub1+uhub2)/2)**kl1)*r**2)
c      endif
c      end neu hbond
c gamma besteht aus einem 1/r Term, und etwas,
c was fuer r=0 gegen Hubbard geht:
c multipliziere einfach den zweiten Term mit fhbond!

```

```

gval= 0.0
a1= 3.2*uhub1
a2= 3.2*uhub2
IF (a1+a2 .lt. zero) THEN
  RETURN
ENDIF
src= 1.0/(a1+a2)
fac= a1*a2*src
avg= 1.6*(fac+fac*fac*src)
IF (r .lt. zero) THEN
  gval= 0.3125*avg
ELSE
  rrc= 1.0/r
  rrc3= rrc*rrc*rrc
  IF (abs(a1-a2) .lt. 1.0d-5) THEN
    fac= avg*r
    fac2= fac*fac
    efac= exp(-fac)/48.0
    gval= (1.0-fhbond*(48.0+33*fac+fac2*(9.0+fac))*efac)*rrc
  ELSE
    call gamsub(a1,a2,r,rrc,val12,drv12)
    call gamsub(a2,a1,r,rrc,val21,drv21)
    gval= rrc-fhbond*val12-fhbond*val21
  ENDIF
ENDIF
RETURN
END

```

```

c=====
c      auxiliary routine needed by gam12 and gam121
c
c      input      a:      alpha1
c                  b:      alpha2
c                  r:      distance
c                  rrc:    1/distance
c      output:  gval:  function value

```

```
c          gdrv: function derivative
c
c=====
      subroutine gamsub(a,b,r,rrc,gval,gdrv)
      IMPLICIT NONE
      REAL*8 a,a2,b,b2,b4,b6,drc,drc2,r,efac,rrc,fac,gval,gdrv
      a2= a*a
      b2= b*b
      b4= b2*b2
      b6= b4*b2
      drc= 1.0/(a2-b2)
      drc2=drc*drc
      efac= exp(-a*r)
      fac= (b6-3*a2*b4)*drc2*drc*rrc
      gval= efac*(0.5*a*b4*drc2-fac)
      gdrv= -a*gval+efac*fac*rrc
      RETURN
      END
```

# Appendix C.

## TDDFTB<sup>+</sup> Inputs

### C.1. Electronic Transitions

The following input calculates the electronic transitions in the PBI monomer:

```
Geometry = GenFormat {<<<geom.out.gen}
Driver = {}
Hamiltonian = DFTB {
  SCC = Yes
  SCCTolerance = 1.0E-008
  MaxSCCIterations = 1000
  Mixer = Anderson {
    MixingParameter = 5.00E-002
    Generations = 8 }
  MaxAngularMomentum = {
    O = "p"
    N = "p"
    C = "p"
    H = "s" }
  Charge = 0.00E+000
  SpinPolarisation = {}
  Eigensolver = Standard {}
  Filling = Fermi {
    Temperature [Kelvin] = 0.000 }
SlaterKosterFiles = Type2FileNames {
  Prefix = "/usr/local/Slater-Koster-Lib/mio-1-1/"
```

```
Separator = "-"
Suffix = ".skf" }
Dispersion = {}
ReadInitialCharges = Yes
LinearResponse = {
  NrOfExcitations = 10
  StateOfInterest = 0
  Symmetry = singlet
  HubbardDerivatives{
    #   G_up,up G_up,down
    N = 0.57770 0.62370
    O = 0.68464 0.73464
    H = 0.34710 0.49190
    C = 0.341975 0.387425
  }
  WriteTransitions = Yes } }
Options = {
  WriteAutotestTag = No
  WriteDetailedXML = No
  WriteEigenvectors = No }
ParserOptions = {
  ParserVersion = 4}
```

## C.2. Annealing MD

This is an example for the annealing procedure used to obtain geometries of the PBI-1 dimers and tetramers.

```
Geometry = GenFormat {
  <<<geom_start.gen}
Driver = VelocityVerlet{
  MovedAtoms = 1:-1
  KeepStationary = Yes
  Timestep[fs] = 0.25 # 0.25
  OutputPrefix = "geom_end"
```

```
MDRestartFrequency = 5
ConvergentForcesOnly = Yes
Thermostat = Berendsen{
    Temperature[Kelvin]= TemperatureProfile {
        constant 4000 400 # 4000 steps at T=400K
        exponential 4000 100 # Exp. decreasing in 4000 st
        constant 4000 100
    }
    Timescale[fs]=50}
}

Hamiltonian = DFTB {
    SCC = Yes
    SCCTolerance =1.0E-003 # 1.0E-008 # Extremely small!
    MaxSCCIterations = 1000
    Mixer = Anderson {
        MixingParameter = 5.0000000000000000E-002
        Generations = 8
    }
    MaxAngularMomentum = {
        O = "p"
        N = "p"
        C = "p"
        H = "s"
    }
    Charge = 0.0000000000000000E+000
    SpinPolarisation = {}
    Eigensolver = Standard {}
    Filling = Fermi {
        Temperature [Kelvin] = 300.0
    }
    SlaterKosterFiles = Type2FileNames {
        Prefix ="/usr/local/Slater-Koster-Lib/mio-1-1/"
        Separator = "-"
        Suffix = ".skf"
    }
}
```

```
Dispersion = LennardJones {
    Parameters = UFFParameters {}
}
ReadInitialCharges = No
}

Options = {
    WriteAutotestTag = No
}

ParserOptions = {
    ParserVersion = 4
}
```

### C.3. NG-Branch Input

Calculation of electronic transition of a separated monomer and their atomic centred Mulliken transition charges are base on the NG-branch of TDDFTB<sup>+</sup>. An example input is given here. It is structured as followed:

- 1: mode max-force scc-on scttol read-charges dispersion external-field-charges
- 2: 'structure.gen' # geometry in .gen format
- 3: charge
- 4: constraints # redundant for single point calculation
- 5: nb-excited-states ex-state-of-interest trans output
- 6: 'output.gen'
- 7: L1 L2 .. LN # basis set size for atoms 1...N, 1 for H, 2 for C, O, N, 3 for S, P, Zn
- 8...M: Slater-Koster-Files
- M+1: stepsize atomic-temperature electronic-temperatur scalfactor number-of-steps

```
10 0.0001 T 0.000001 F F 'NO' T
'mono1.gen'
0
0
10 3 'S' T
```

```
'out'  
 2 2 1 2  
'/usr/local/Slater-Koster-Lib/mio-1-1/C-C.skf'  
'/usr/local/Slater-Koster-Lib/mio-1-1/C-N.skf'  
'/usr/local/Slater-Koster-Lib/mio-1-1/C-H.skf'  
'/usr/local/Slater-Koster-Lib/mio-1-1/C-O.skf'  
'/usr/local/Slater-Koster-Lib/mio-1-1/N-C.skf'  
'/usr/local/Slater-Koster-Lib/mio-1-1/N-N.skf'  
'/usr/local/Slater-Koster-Lib/mio-1-1/N-H.skf'  
'/usr/local/Slater-Koster-Lib/mio-1-1/N-O.skf'  
'/usr/local/Slater-Koster-Lib/mio-1-1/H-C.skf'  
'/usr/local/Slater-Koster-Lib/mio-1-1/H-N.skf'  
'/usr/local/Slater-Koster-Lib/mio-1-1/H-H.skf'  
'/usr/local/Slater-Koster-Lib/mio-1-1/H-O.skf'  
'/usr/local/Slater-Koster-Lib/mio-1-1/O-C.skf'  
'/usr/local/Slater-Koster-Lib/mio-1-1/O-N.skf'  
'/usr/local/Slater-Koster-Lib/mio-1-1/O-H.skf'  
'/usr/local/Slater-Koster-Lib/mio-1-1/O-O.skf'  
0 0.0 0.0 0.0 2000
```



# Bibliography

- [1] Yohei Ishida, Tetsuya Shimada, and Shinsuke Takagi. Artificial Light-Harvesting Model in a Self-Assembly Composed of Cationic Dyes and Inorganic Nanosheet. *The Journal of Physical Chemistry C*, 117(18):9154–9163, 2013.
- [2] Krishna K Niyogi and Thuy B Truong. Evolution of flexible non-photochemical quenching mechanisms that regulate light harvesting in oxygenic photosynthesis. *Current Opinion in Plant Biology*, 16(3):307 – 314, 2013.
- [3] Thomas Renger, Volkhard May, and Oliver Kühn. Ultrafast excitation energy transfer dynamics in photosynthetic pigment-protein complexes. *Physics Reports*, 343(3):137 – 254, 2001.
- [4] Gregory S. Orf and Robert E. Blankenship. Chlorosome antenna complexes from green photosynthetic bacteria. *Photosynthesis Research*, pages 1–17, 2013.
- [5] Eunwoo Lee, Chanhoi Kim, and Jyongsik Jang. High-Performance Förster Resonance Energy Transfer (FRET)-Based Dye-Sensitized Solar Cells: Rational Design of Quantum Dots for Wide Solar-Spectrum Utilization. *Chemistry – A European Journal*, 19(31):10280–10286, 2013.
- [6] Urartu Ozgur Safak Seker, Evren Mutlugun, Pedro Ludwig Hernandez-Martinez, Vijay K. Sharma, Vladimir Lesnyak, Nikolai Gaponik, Alexander Eychmuller, and Hilmi Volkan Demir. Bio-nanohybrids of quantum dots and photoproteins facilitating strong nonradiative energy transfer. *Nanoscale*, 5:7034–7040, 2013.
- [7] R. Smith, B. Liu, J. Bai, and T. Wang. Hybrid III-Nitride/Organic Semiconductor Nanostructure with High Efficiency Nonradiative Energy Transfer for White Light Emitters. *Nano Letters*, 13(7):3042–3047, 2013.
- [8] Organic Electronics for a Better Tomorrow: Innovation, Accessibility, Sustainability. A White Paper from the Chemical Science and Society Summit (CS3), September 2012.

- [9] G. Grancini, M. Maiuri, D. Fazzi, A. Petrozza, H.-J. Egelhaaf, D. Brida, Cerullo G., and Lanzani G. Hot exciton dissociation in polymer solar cells. *Nature Materials*, 12:29–33, 2013.
- [10] Jelley. Spectral Absorption and Fluorescence of Dyes in the Molecular State. *Nature*, pages 1009–1010, 1936.
- [11] G. Scheibe. VII. Fachgebiet Photochemie und Photographische Chemie. *Angewandte Chemie*, 49(31):563, 1936.
- [12] G. Scheibe. Über die Veränderlichkeit der Absorptionsspektren in Lösungen und die Nebenvalenzen als ihre Ursache. *Angewandte Chemie*, 50(11):212–219, 1937.
- [13] James Franck and Edward Teller. Migration and Photochemical Action of Excitation Energy in Crystals. *The Journal of Chemical Physics*, 6(12):861–872, 1938.
- [14] Frank C. Spano, Stefan C. J. Meskers, Emanuelle Hennebicq, and David Beljonne. Probing Excitation Delocalization in Supramolecular Chiral Stacks by Means of Circularly Polarized Light: Experiment and Modeling. *Journal of the American Chemical Society*, 129(22):7044–7054, 2007. PMID: 17497856.
- [15] Motoichi Ohtsu, T. Kawazoe, Takashi Yatsui, and M. Naruse. Nanophotonics: Application of Dressed Photons to Novel Photonic Devices and Systems. *Selected Topics in Quantum Electronics, IEEE Journal of*, 14(6):1404–1417, 2008.
- [16] Dobrinka Dotcheva, Markus Klapper, and Klaus Müllen. Soluble polyimides containing perylene units. *Macromolecular Chemistry and Physics*, 195(6):1905–1911, 1994.
- [17] Frank Würthner. Perylene bisimide dyes as versatile building blocks for functional supramolecular architectures. *Chem. Commun.*, pages 1564–1579, 2004.
- [18] Henning Marciniak, Xue-Qing Li, Frank Würthner, and Stefan Lochbrunner. One-Dimensional Exciton Diffusion in Perylene Bisimide Aggregates. *The Journal of Physical Chemistry A*, 115(5):648–654, 2011.
- [19] Th. Förster. Zwischenmolekulare Energiewanderung und Fluoreszenz. *Annalen der Physik*, 437(1-2):55–75, 1948.
- [20] IUPAC. Compendium of Chemical Terminology, 2nd ed. (the "Gold Book"). Compiled by A. D. McNaught and A. Wilkinson. Blackwell Scientific Publications, Oxford (1997). XML on-line corrected version: <http://goldbook.iupac.org> (2006-) created by M. Nic, J. Jirat, B. Kosata; updates compiled by A. Jenkins. ISBN 0-9678550-9-8.

doi:10.1351/goldbook.

- [21] D. L. Dexter. A Theory of Sensitized Luminescence in Solids. *The Journal of Chemical Physics*, 21(5):836–850, 1953.
- [22] Mitio Inokuti and Fumio Hirayama. Influence of Energy Transfer by the Exchange Mechanism on Donor Luminescence. *The Journal of Chemical Physics*, 43(6):1978–1989, 1965.
- [23] V. May and O. Kühn. *Charge and Energy Transfer Dynamics in Molecular Systems*. John Wiley & Sons, 2004.
- [24] Hiroyuki Asanuma, Taiga Fujii, Tomohiro Kato, and Hiromu Kashida. Coherent interactions of dyes assembled on DNA. *Journal of Photochemistry and Photobiology C: Photochemistry Reviews*, 13(2):124 – 135, 2012.
- [25] Ana Damjanović, Thorsten Ritz, and Klaus Schulten. Energy transfer between carotenoids and bacteriochlorophylls in light-harvesting complex II of purple bacteria. *Phys. Rev. E*, 59:3293–3311, Mar 1999.
- [26] Prashant K. Jain, Susie Eustis, and Mostafa A. El-Sayed. Plasmon Coupling in Nanorod Assemblies: Optical Absorption, Discrete Dipole Approximation Simulation, and Exciton-Coupling Model. *The Journal of Physical Chemistry B*, 110(37):18243–18253, 2006. PMID: 16970442.
- [27] Alexander O. Govorov, Garnett W. Bryant, Wei Zhang, Timur Skeini, Jaebeom Lee, Nicholas A. Kotov, Joseph M. Slocik, and Rajesh R. Naik. Exciton-Plasmon Interaction and Hybrid Excitons in Semiconductor-Metal Nanoparticle Assemblies. *Nano Letters*, 6(5):984–994, 2006.
- [28] V. Czikkely, H.D. Forsterling, and H. Kuhn. Extended dipole model for aggregates of dye molecules. *Chemical Physics Letters*, 6(3):207 – 210, 1970.
- [29] I. A. Howard, F. Zutterman, G. Deroover, D. Lamoen, and C. Van Alsenoy. Approaches to Calculation of Exciton Interaction Energies for a Molecular Dimer. *The Journal of Physical Chemistry B*, 108(50):19155–19162, 2004.
- [30] Kurt A. Kistler, Francis C. Spano, and Spiridoula Matsika. A Benchmark of Excitonic Couplings Derived from Atomic Transition Charges. *The Journal of Physical Chemistry B*, 117(7):2032–2044, 2013.

- [31] Sameer Patwardhan, Sanchita Sengupta, Frank Würthner, Laurens D. A. Siebbeles, and Ferdinand Grozema. Theoretical Study of the Optical Properties of Artificial Self-Assembled Zinc Chlorins. *The Journal of Physical Chemistry C*, 114(48):20834–20842, 2010.
- [32] R. S. Mulliken. Electronic Population Analysis on LCAO[Single Bond]MO Molecular Wave Functions. I. *The Journal of Chemical Physics*, 23(10):1833–1840, 1955.
- [33] F.L. Hirshfeld. Bonded-atom fragments for describing molecular charge densities. *Theoretica chimica acta*, 44(2):129–138, 1977.
- [34] M. E. Madjet, A. Abdurahman, and T. Renger. *The Journal of Physical Chemistry B*, 110(34):17268–17281, 2006. PMID: 16928026.
- [35] Brent P. Krueger, Gregory D. Scholes, and Graham R. Fleming. Calculation of Couplings and Energy-Transfer Pathways between the Pigments of LH2 by the ab Initio Transition Density Cube Method. *The Journal of Physical Chemistry B*, 102(27):5378–5386, 1998.
- [36] Arkadiusz Czader and Eric R. Bittner. Calculations of the exciton coupling elements between the DNA bases using the transition density cube method. *The Journal of Chemical Physics*, 128(3):035101, 2008.
- [37] Burkhard Fockel, Andreas Kohn, Michael E. Harding, Gregor Diezemann, Gerald Hinze, Thomas Basche, and Jurgen Gauss. Theoretical investigation of electronic excitation energy transfer in bichromophoric assemblies. *The Journal of Chemical Physics*, 128(7):074505, 2008.
- [38] Aron J. Cohen, Paula Mori-Sánchez, and Weitao Yang. Insights into Current Limitations of Density Functional Theory. *Science*, 321(5890):792–794, 2008.
- [39] Johannes Neugebauer, Oleg Gritsenko, and Evert Jan Baerends. Assessment of a simple correction for the long-range charge-transfer problem in time-dependent density-functional theory. *The Journal of Chemical Physics*, 124(21):214102, 2006.
- [40] Johannes Neugebauer. Couplings between electronic transitions in a subsystem formulation of time-dependent density functional theory. *The Journal of Chemical Physics*, 126(13):134116, 2007.
- [41] D. Porezag, Th. Frauenheim, Th. Köhler, G. Seifert, and R. Kaschner. Construction of tight-binding-like potentials on the basis of density-functional theory: Application to

- carbon. *Phys. Rev. B*, 51:12947–12957, May 1995.
- [42] M. Elstner, D. Porezag, G. Jungnickel, J. Elsner, M. Haugk, Th. Frauenheim, S. Suhai, and G. Seifert. Self-consistent-charge density-functional tight-binding method for simulations of complex materials properties. *Phys. Rev. B*, 58:7260–7268, Sep 1998.
- [43] T. A. Niehaus, S. Suhai, F. Della Sala, P. Lugli, M. Elstner, G. Seifert, and Th. Frauenheim. Tight-binding approach to time-dependent density-functional response theory. *Phys. Rev. B*, 63:085108, Feb 2001.
- [44] Yang, Haibo Yu, Darrin York, Qiang Cui, and Marcus Elstner. Extension of the Self-Consistent-Charge Density-Functional Tight-Binding Method: Third-Order Expansion of the Density Functional Theory Total Energy and Introduction of a Modified Effective Coulomb Interaction. *The Journal of Physical Chemistry A*, 111(42):10861–10873, 2007. PMID: 17914769.
- [45] Jeffrey R. Reimers, Gemma C. Solomon, Alessio Gagliardi, Ante Bilić, Noel S. Hush, Thomas Frauenheim, Aldo Di Carlo, and Alessandro Pecchia. The Green’s Function Density Functional Tight-Binding (gDFTB) Method for Molecular Electronic Conduction. *The Journal of Physical Chemistry A*, 111(26):5692–5702, 2007. PMID: 17530826.
- [46] Hao Hu, Zhenyu Lu, Marcus Elstner, Jan Hermans, and Weitao Yang. Simulating Water with the Self-Consistent-Charge Density Functional Tight Binding Method: From Molecular Clusters to the Liquid State. *The Journal of Physical Chemistry A*, 111(26):5685–5691, 2007. PMID: 17474727.
- [47] Supriya Saha and Pranab Sarker. Electronic structure of ZnO/ZnS core/shell quantum dots. *Chemical Physics Letters*, 555(0):191 – 195, 2013.
- [48] W. Matthew C. Foulkes and Roger Haydock. Tight-binding models and density-functional theory. *Phys. Rev. B*, 39:12520–12536, Jun 1989.
- [49] Rudolph Pariser. Theory of the Electronic Spectra and Structure of the Polyacenes and of Alternant Hydrocarbons. *The Journal of Chemical Physics*, 24(2):250–268, 1956.
- [50] Robert G. Parr and Ralph G. Pearson. Absolute hardness: companion parameter to absolute electronegativity. *Journal of the American Chemical Society*, 105(26):7512–7516, 1983.

- [51] G. Klopman. A Semiempirical Treatment of molecular Structures. II. Molecular Terms and Application to diatomic Molecules. *Journal of the American Chemical Society*, 86(21):4550–4557, 1964.
- [52] Kimio Ohno. Some remarks on the Pariser-Parr-Pople method. *Theoretica chimica acta*, 2:219–227, 1964.
- [53] J. F. Janak. Proof that  $\frac{\partial E}{\partial n_i} = \epsilon$  in density-functional theory. *Phys. Rev. B*, 18:7165–7168, Dec 1978.
- [54] Pekka Koskinen and Ville Mäkinen. Density-functional tight-binding for beginners. *Computational Materials Science*, 47(1):237 – 253, 2009.
- [55] Gotthard Seifert and Jan-Ole Joswig. Density-functional tight binding—an approximate density-functional theory method. *Wiley Interdisciplinary Reviews: Computational Molecular Science*, 2(3):456–465, 2012.
- [56] T.A. Niehaus. Approximate time-dependent density functional theory. *Journal of Molecular Structure: THEOCHEM*, 914:38 – 49, 2009.
- [57] J. C. Slater and G. F. Koster. Simplified LCAO Method for the Periodic Potential Problem. *Phys. Rev.*, 94:1498–1524, Jun 1954.
- [58] John P Perdew, Kieron Burke, and Matthias Ernzerhof. Generalized Gradient Approximation Made Simple. *Phys. Rev. Lett.*, 77:3865–3868, Oct 1996.
- [59] Marius Wanko, Michael Hoffmann, Thomas Frauenheim, and Marcus Elstner. Computational photochemistry of retinal proteins. *Journal of Computer-Aided Molecular Design*, 20(7-8):511–518, 2006.
- [60] M. Wanko, M. Hoffmann, P. Strodel, A. Koslowski, W. Thiel, F. Neese, T. Frauenheim, and M. Elstner. Calculating Absorption Shifts for Retinal Proteins-Computational Challenges. *The Journal of Physical Chemistry B*, 109(8):3606–3615, 2005. PMID: 16851399.
- [61] Andreas Dreuw and Martin Head-Gordon. Failure of Time-Dependent Density Functional Theory for Long-Range Charge-Transfer Excited States - The Zincbacteriochlorin - Bacteriochlorin and Bacteriochlorophyll,àSpheroidene Complexes. *Journal of the American Chemical Society*, 126(12):4007–4016, 2004. PMID: 15038755.
- [62] Marcus Elstner, Pavel Hobza, Thomas Frauenheim, Sándor Suhai, and Efthimios Kaxiras. Hydrogen bonding and stacking interactions of nucleic acid base pairs: A density-

- functional-theory based treatment. *The Journal of Chemical Physics*, 114(12):5149–5155, 2001.
- [63] Lyuben Zhechkov, Thomas Heine, Serguei Patchkovskii, Gotthard Seifert, and Helio A. Duarte. An Efficient a Posteriori Treatment for Dispersion Interaction in Density-Functional-Based Tight Binding. *Journal of Chemical Theory and Computation*, 1(5):841–847, 2005.
- [64] A. K. Rappe, C. J. Casewit, K. S. Colwell, W. A. Goddard, and W. M. Skiff. UFF, a full periodic table force field for molecular mechanics and molecular dynamics simulations. *Journal of the American Chemical Society*, 114(25):10024–10035, 1992.
- [65] M.E. Casida. Time-Dependent Density Functional Response Theory for Molecules. In D.P. Chong, editor, *Recent Advances in Density Functional Methods*, volume 1, page 155. World Scientific, 1995.
- [66] Chao-Ping Hsu, Graham R. Fleming, Martin Head-Gordon, and Teresa Head-Gordon. Excitation energy transfer in condensed media. *The Journal of Chemical Physics*, 114(7):3065–3072, 2001.
- [67] B. Aradi, B. Hourahine, and Th. Frauenheim. DFTB+, a Sparse Matrix-Based Implementation of the DFTB Method,. *The Journal of Physical Chemistry A*, 111(26):5678–5684, 2007. PMID: 17567110.
- [68] R. B. Lehoucq, D. C. Sorensen, and C. Yang. ARPACK Users Guide: Solution of Large Scale Eigenvalue Problems by Implicitly Restarted Arnoldi Methods., 1997.
- [69] T. A. Niehaus. Hubbard parameters for pure coulomb interaction. personal communication, May 2013.
- [70] TURBOMOLE V6.4, a development of University of Karlsruhe and Forschungszentrum Karlsruhe GmbH, 1989-2007, TURBOMOLE GmbH, since 2007; available from <http://www.turbomole.com>.
- [71] Oliver Treutler and Reinhart Ahlrichs. Efficient molecular numerical integration schemes. *The Journal of Chemical Physics*, 102(1):346–354, 1995.
- [72] Rüdiger Bauernschmitt and Reinhart Ahlrichs. Treatment of electronic excitations within the adiabatic approximation of time dependent density functional theory. *Chemical Physics Letters*, 256(4-5):454 – 464, 1996.

- [73] Axel D. Becke. Density-functional thermochemistry. III. The role of exact exchange. *The Journal of Chemical Physics*, 98(7):5648–5652, 1993.
- [74] P. J. Stephens, F. J. Devlin, C. F. Chabalowski, and M. J. Frisch. Ab Initio Calculation of Vibrational Absorption and Circular Dichroism Spectra Using Density Functional Force Fields. *The Journal of Physical Chemistry*, 98(45):11623–11627, 1994.
- [75] John P. Perdew, Kieron Burke, and Matthias Ernzerhof. Generalized Gradient Approximation Made Simple [Phys. Rev. Lett. 77, 3865 (1996)]. *Phys. Rev. Lett.*, 78:1396–1396, Feb 1997.
- [76] Carlo Adamo and Vincenzo Barone. Toward reliable density functional methods without adjustable parameters: The PBE0 model. *The Journal of Chemical Physics*, 110(13):6158–6170, 1999.
- [77] Andrzej L. Sobolewski and Wolfgang Domcke. Ab initio study of the excited-state coupled electron-proton-transfer process in the 2-aminopyridine dimer. *Chemical Physics*, 294(1):73 – 83, 2003.
- [78] Suhrit Ghosh, Xue-Qing Li, Vladimir Stepanenko, and Frank Würthner. Control of H- and J-Type  $\pi$  Stacking by Peripheral Alkyl Chains and Self-Sorting Phenomena in Perylene Bisimide Homo- and Heteroaggregates. *Chemistry – A European Journal*, 14(36):11343–11357, 2008.
- [79] David Ambrosek, Henning Marciniak, Stefan Lochbrunner, Jorg Tatchen, Xue-Qing Li, Frank Würthner, and Oliver Kuhn. Photophysical and quantum chemical study on a J-aggregate forming perylene bisimide monomer. *Phys. Chem. Chem. Phys.*, 13:17649–17657, 2011.
- [80] Xue-Qing Li, Xin Zhang, Suhrit Ghosh, and Frank Würthner. Highly Fluorescent Lyotropic Mesophases and Organogels Based on J-Aggregates of Core-Twisted Perylene Bisimide Dyes. *Chemistry – A European Journal*, 14(27):8074–8078, 2008.
- [81] D. Ambrosek, A. Köhn, J. Schulze, and O. Kühn. Quantum Chemical Parametrization and Spectroscopic Characterization of the Frenkel Exciton Hamiltonian for a J-Aggregate Forming Perylene Bisimide Dye. *The Journal of Physical Chemistry A*, 116(46):11451–11458, 2012.
- [82] S. Bokarev. personal communication, April 2013.



- [83] Virgil Percec, Mihai Peterca, Timur Tadjiev, Xiangbing Zeng, Goran Ungar, Pawaret Leowanawat, Emad Aqad, Mohammad R. Imam, Brad M. Rosen, Umit Akbey, Robert Graf, Sivakumar Sekharan, Daniel Sebastiani, Hans W. Spiess, Paul A. Heiney, and Steven D. Hudson. Self-Assembly of Dendronized Perylene Bisimides into Complex Helical Columns. *Journal of the American Chemical Society*, 133(31):12197–12219, 2011.
- [84] Joseph K. Gallaher, Emma J. Aitken, Robert A. Keyzers, and Justin M. Hodgkiss. Controlled aggregation of peptide-substituted perylene-bisimides. *Chem. Commun.*, 48:7961–7963, 2012.
- [85] Zhijian Chen, Andreas Lohr, Chantu R. Saha-Moller, and Frank Wurthner. Self-assembled [small pi]-stacks of functional dyes in solution: structural and thermodynamic features. *Chem. Soc. Rev.*, 38:564–584, 2009.
- [86] Johannes Neugebauer, Carles Curutchet, Aurora Muñoz-Losa, and Benedetta Mennucci. A Subsystem TDDFT Approach for Solvent Screening Effects on Excitation Energy Transfer Couplings. *Journal of Chemical Theory and Computation*, 6(6):1843–1851, 2010.
- [87] Michael Gaus, Albrecht Goetz, and Marcus Elstner. Parametrization and Benchmark of DFTB3 for Organic Molecules. *Journal of Chemical Theory and Computation*, 9(1):338–354, 2013.
- [88] Zoltán Bodrog and Bálint Aradi. Possible improvements to the self-consistent-charges density-functional tight-binding method within the second order. *physica status solidi (b)*, 249(2):259–269, 2012.
- [89] Thomas A. Niehaus and Fabio Della Sala. Range separated functionals in the density functional based tight-binding method: Formalism. *physica status solidi (b)*, 249(2):237–244, 2012.

# Danksagung

An dieser Stelle möchte ich mich bei der AG „Molekulare Quantendynamik“ für Unterstützung und Rechenzeit bedanken. Insbesondere gilt mein Dank meinem Betreuer Prof. Oliver Kühn für die intensive Betreuung und konstruktive Hilfestellung. Auch danke ich Prof. Thomas Niehaus und seiner Arbeitsgruppe für die Unterstützung und die Programmbereitstellung.

# **Selbständigkeitserklärung**

Ich versichere hiermit an Eides statt, dass ich die vorliegende Arbeit selbstständig angefertigt und ohne fremde Hilfe verfasst habe, keine außer den von mir angegebenen Hilfsmitteln und Quellen dazu verwendet habe und die den benutzten Werken inhaltlich und wörtlich entnommenen Stellen als solche kenntlich gemacht habe.

Rostock, 26.8.2013